Research Report
Research Project Agreement No.T1803, Task 15
AWV Instrumentation

SEISMIC INSTRUMENTATION FOR THE ALASKAN WAY VIADUCT

by

Steven L. Kramer
Professor

Allen L. Jones
Research Assistant

Marc O. Eberhard
Associate Professor

Pedro Arduino
Assistant Professor

Department of Civil and Environmental Engineering
University of Washington, Bx 352700
Seattle, Washington

Washington State Transportation Center (TRAC)
University of Washington, Box 354802
University District Building
1107 NE 45th Street, Suite 535
Seattle, Washington 98105-4631

Washington State Department of Transportation
Technical Monitor
Jugesh Kapur
Bridge Design Engineer

Prepared for

Washington State Transportation Commission
Department of Transportation
and in cooperation with
U.S. Department of Transportation
Federal Highway Administration

June 2002

TECHNICAL REPORT STANDARD TITLE PAGE

1. REPORT NO.	2. GOVERNMENT ACCESSION NO.	3. RECIPIENT'S CATALOG NO.
WA-RD 520.1		

4. TITLE AND SUBTITLE	5. REPORT DATE
Seismic Instrumentation for the Alaskan Way Viaduct	June 2002
	6. PERFORMING ORGANIZATION CODE

7. AUTHOR(S)	8. PERFORMING ORGANIZATION REPORT NO.
Steven L. Kramer, Allen L. Jones, Pedro Arduino, Marc O. Eberhard	

9. PERFORMING ORGANIZATION NAME AND ADDRESS	10. WORK UNIT NO.
Washington State Transportation Center (TRAC) University of Washington, Box 354802 University District Building; 1107 NE 45th Street, Suite 535 Seattle, Washington 98105-4631	11. CONTRACT OR GRANT NO. Agreement T1803, Task 15

12. SPONSORING AGENCY NAME AND ADDRESS	13. TYPE OF REPORT AND PERIOD COVERED
Research Office Washington State Department of Transportation Transportation Building, MS 47370 Olympia, Washington 98504-7370 Keith Anderson, Project Manager, 360-709-5405	Research report
	14. SPONSORING AGENCY CODE

15. SUPPLEMENTARY NOTES

This study was conducted in cooperation with the U.S. Department of Transportation, Federal Highway Administration.

16. ABSTRACT

The Alaskan Way Viaduct, which runs along the Seattle waterfront, is highly susceptible to damage during earthquakes. Previous studies have shown that extensive soil liquefaction could cause collapse of sections of the Viaduct through a complex mechanism that involves the seismic performance of a nearby seawall. Occurrence of such collapse events would be expected to occur at some time after the initiation of earthquake shaking, thereby providing some period of time in which motorists could potentially be kept from entering the Viaduct. The purpose of this project was to evaluate the feasibility of instrumenting the Viaduct to (a) provide warning of potentially unsafe situations, and (b) reduce post-earthquake closure times by speeding the process of evaluating the condition of the Viaduct following earthquake shaking.

Because of the numerous and significant sources of uncertainty in the prediction of collapse, a probabilistic approach to the warning system problem was adopted. This procedure accounted for, to the extent possible given available information, uncertainties in ground shaking characteristics, uncertainties in soil properties, uncertainties in seawall behavior, uncertainties in Viaduct foundation behavior, and uncertainties in structural response. The results are expressed in estimated collapse probabilities for various warning system triggering levels. Selection of triggering levels will require balancing the costs and benefits of successful and unsuccessful collapse predictions.

Structural analyses of specific sections of the Viaduct were used to develop recommendations for performance monitoring instrumentation. Proposed response levels for inspection and inspection/closure are also presented.

17. KEY WORDS	18. DISTRIBUTION STATEMENT
Seismic instrumentation, liquefaction, structural analysis	No restrictions. This document is available to the public through the National Technical Information Service, Springfield, VA 22616

19. SECURITY CLASSIF. (of this report)	20. SECURITY CLASSIF. (of this page)	21. NO. OF PAGES	22. PRICE
None	None		

DISCLAIMER

The contents of this report reflect the views of the authors, who are responsible for the facts and the accuracy of the data presented herein. The contents do not necessarily reflect the official views or policies of the Washington State Transportation Commission, Department of Transportation, or the Federal Highway Administration. This report does not constitute a standard, specification, or regulation.

TABLE OF CONTENTS

Section	Page
EXECUTIVE SUMMARY	**xi**
CHAPTER 1. INTRODUCTION	**1**
Background	2
Foundation Vulnerabilities	2
Structural Vulnerabilities	3
Objectives	4
Organization of Report	4
CHAPTER 2. EARTHQUAKE WARNING SYSTEMS	**5**
Regional Warning Systems	6
Local Warning Systems	7
Structure-Specific Warning Systems	9
Components	10
Summary	13
CHAPTER 3. SEISMIC VULNERABILITY OF THE ALASKAN WAY VIADUCT	**14**
Geologic Setting	14
Viaduct Construction	15
Performance of the Alaskan Way Viaduct	17
Comparison with Oakland and San Francisco Viaducts	20
Seismic Vulnerability Evaluation	20
Design-Level Ground Motion	20
Ground Response	21
Liquefaction Hazards	21
Effects of Liquefaction	22
Structural Performance	23
Peer Review	24
Conclusions	25
CHAPTER 4. EVALUATION OF LIQUEFACTION HAZARDS	**26**
Soil Liquefaction	26
Liquefaction Hazard Evaluation	27
Susceptibility	28
Initiation of Liquefaction	30
Cyclic Stress Approach	30
Energy Approach	33

TABLE OF CONTENTS (Continued)

Section	Page
Effects of Liquefaction	36
Effects on Site Response	36
Settlement	38
Flow Slides	39
Lateral Spreading	40
Foundation Failure	42
Summary	44
CHAPTER 5. A WARNING ALGORITHM FOR LIQUEFACTION-INDUCED FAILURE	**46**
Sequence of Liquefaction-Induced Failure	46
Framework for Warning Criterion	48
Uncertainties in Evaluating Liquefaction-Induced Failure Potential	50
Subsurface Soil Conditions	51
Ground Motions	52
Residual Strength of Liquefied Soil	57
Uncertainty in Lateral Soil Displacement	59
Uncertainty in Total Pile Displacement	61
Uncertainty in Relative Pile Displacement	63
Uncertainty in Structural Failure	65
Results of Probabilistic Analysis	70
True-Positive Outcomes	71
False-Negative Outcomes	73
Discussion	75
Liquefaction Warning System Instrumentation Plan	77
Trigger Criteria	77
CHAPTER 6. STRUCTURAL INSTRUMENTATION	**80**
Structural Behavior for Transverse Loads and for Support Displacements	80
Structural Displacements at the Onset of Structural Damage	83
Structural Damage Warning-System Instrumentation Plan	85
Trigger Criteria	86
Distributed Bridge Instrumentation Network	88
Exploratory Study	88
Implementation Considerations	91
CHAPTER 7. SUMMARY AND CONCLUSIONS	**92**
Warning Criteria for Liquefaction-Induced Collapse	93
Criteria for Structural Inspection and Closure	94
Instrumentation	95
REFERENCES	**96**

TABLE OF CONTENTS (Continued)

Section	Page
APPENDIX A. INPUT MOTIONS	A.1
APPENDIX B. WAVE	B.1

LIST OF FIGURES

Figure		Page
3.1	Longitudinal elevation of WSDOT typical unit	15
3.2	Interior transverse frame for WSDOT typical unit	16
3.3	Damage to bent 100 knee joint immediately after the 2001 earthquake	19
3.4	Damage to bent 100 knee joint of Alaskan Way Viaduct one month after the 2001 earthquake	19
4.1	Three basic types of response observed by Castro (1969) in static triaxial tests	29
4.2	Steady state line	29
4.3	Number of equivalent cycles of loading to evaluation liquefaction potential	31
4.4	Relationship between cyclic stress ratio and $(N_1)_{60}$ for Mw=7.5 earthquakes	32
4.5	Magnitude scaling factors	32
4.6	I_h for 50^{th} percentile earthquake response plotted as a function of surface distance to fault rupture, r; moment magnitude, M; and site material properties of rock, alluvium, and soft soil, based on 10 km earthquake focal depth	34
4.7	Relationship between SPT resistance and Arias intensity required to trigger liquefaction	35
4.8	I_{hb} versus q_c	35
4.9	Time history of ground surface acceleration from Niigata, Japan	37
4.10	Coastal flooding due to liquefaction-induced subsidence in Golcuk	39
4.11	Structural failure due to liquefaction-induced settlement of isolated footing at Port of Taichung	39
4.12	Examples of the effects of lateral spreading on bridges and wharf structures	41
4.13	Liquefaction-induced bearing capacity failure in Adapazari, Turkey	42
4.14	Damage to Monterey Bay Aquarium Research Institute following 1989 Loma Prieta earthquake	43
4.15	Pile damage due to lateral spreading beneath the NHK Building in Niigata, Japan	43
4.16	Failure of Showa River bridge in Niigata, Japan, due to lateral spreading	44
4.17	Pile damage due to lateral spreading in Kobe, Japan	44
5.1	Sequence of events leading to potential liquefaction-induced collapse of Alaskan Way Viaduct	47
5.2	Variation of ground motion intensity with time relative to a particular trigger criterion	50
5.3	SPT profiles used for analysis	52
5.4	Response spectra for all input motions	53
5.5	Arias intensity for the first 40 seconds of the base motions	54
5.6	Variation of average pore pressure with time	56

LIST OF FIGURES (Continued)

Figure		Page
5.7	Variation of I_a with time	56
5.8	Liquefaction probability distribution	58
5.9	Residual strength probability density function	58
5.10	Free field soil displacement related to soil strength	60
5.11	Probability density function of seawall displacement	60
5.12	Relation between pile and soil displacements	62
5.13	Probability density function for soil and pile displacements	63
5.14	Probability distribution function for ratio of soil displacement to pile displacement	64
5.15	Probability density functions for relative pile displacement given displacement of the soil	65
5.16	Flowchart for calculating structural vulnerability to pile-cap displacements	69
5.17	Variation of column shear resistance with displacement ductility	70
5.18	Structural fragility curves for SED typical unit	70
5.19	Probability of collapse (true positive) considering sources of uncertainty	72
5.20	Uniform probability curves for collapse (true positive)	73
5.21	Probability of unpredicted collapse (false negative)	74
5.22	Conceptual benefit-cost analysis for a given value of t^*	76
5.23	Proposed flow chart for a potential warning algorithm	79
6.1	Results of pushover analysis for SED exterior frame	81
6.2	Results of support-displacement analysis for SED exterior frame	82
6.3	Base shear-top displacement relationships for SED transverse frames	84
6.4	Column shear-support displacement relationships for SED transverse frames	85
6.5	Proposed locations for structural seismic instrumentation	86
6.6	ShakeMap for spectral acceleration at period of 0.3s	89
6.7	Correlation between damage likelihood and spectral acceleration at 0.3 sec.	90

LIST OF TABLES

Table		Page
5.1	Soil density values	51
5.2	Parameter variation for calculating structural fragility curves	68
5.3	Tabulated collapse probabilities for true positive events	73
5.4	Tabulated collapse probabilities for false negatives	75
6.1	Characteristics of units to be monitored	86
6.2	Spectral acceleration for triggering events	87

Executive Summary

This report presents the results of an investigation into the feasibility and preliminary design of a system intended to warn of potential collapse of the Alaskan Way Viaduct following earthquake shaking. Such a system would also help WSDOT decide when to inspect the Viaduct and would aid in post-earthquake evaluation.

Most of the Alaskan Way Viaduct is located in an area that was originally within the waters of Elliott Bay. As a result, these portions of the Viaduct are located on filled ground. The filling operations that produced the current topography of the Seattle waterfront area were accomplished with techniques that were common at that time. These techniques are now known, however, to produce liquefiable soil deposits. As part of the process of developing the Seattle waterfront, a seawall was constructed in the 1930s; this seawall retains the liquefiable soils that surround the Viaduct's foundations, but it was not designed to retain liquefied soils.

Previous studies of the seismic vulnerability of the Alaskan Way Viaduct have identified liquefaction and the resulting lateral movement of the liquefied soil as an important threat to the integrity of the structure. Liquefaction could lead to collapse of portions of the Viaduct through a series of related events – liquefaction of soil beneath the Viaduct and behind the Seattle seawall, lateral movement of the seawall with consequent movement of the soil behind it, lateral movement of the Viaduct's pile foundations, and excessive differential movements of the columns of the Viaduct. The most critical portions of the Viaduct, with respect to this potential collapse mechanism,

are expected to be between University and Madison streets and between Washington and Columbia streets. The studies described in this report have focused on the conditions that exist in those areas, although they should not be considered the only areas with potential for severe damage and/or collapse.

The seismic performance of the Viaduct is extremely complex and will be influenced by many known and unknown factors that relate to the above- and below-ground portions of the Viaduct, the soils that support the Viaduct, and the performance of nearby structures such as the Seattle seawall. Furthermore, the Viaduct is now approximately 50 years old; its current condition is undoubtedly influenced by its sustained and heavy use. The Viaduct was subjected to moderate shaking in 1965 and 2001, the effects of which are not known entirely. The investigators have attempted to consider all reasonable, known conditions, and have used available information to identify the most critical conditions relative to potential collapse of the structure. It should be recognized, however, that unknown and/or differing conditions might exist and lead to different seismic vulnerabilities and/or unanticipated mechanisms of failure or collapse.

Warning Criteria for Liquefaction-Induced Collapse

The cyclic stresses induced by earthquake shaking cause the incremental buildup of porewater pressure in liquefiable soils. This process takes some time to occur, and many case histories of liquefaction-induced failures have shown that some degree of pore pressure redistribution accompanies the development of large soil deformations. Therefore, liquefaction-induced failures often occur some time after earthquake shaking has ended. Although the amount of the time delay cannot be predicted reliably by

available procedures, experience offers some hope that early warning of liquefaction will provide a period of time before failure in which defensive measures can be taken.

In recognition of the numerous and significant uncertainties in most of the series of events that are expected to lead to liquefaction-induced collapse, the warning system triggering criterion was developed probabilistically. This approach required identification of a suitable ground motion parameter for predicting liquefaction, evaluation of the probability of liquefaction for given values of that parameter, evaluation of the probability of various levels of liquefied soil displacement, evaluation of the probability of various levels of foundation movement, and evaluation of the probability of collapse for different levels of foundation movement. Arias intensity, an integral ground motion parameter that has been used to predict liquefaction potential, was used to formulate the warning criterion. The various probability distributions required to formulate the probabilistic analyses were determined from data when available or estimated when data were not available.

A collapse warning system should desirably provide warning early enough to allow defensive measures to be taken, but not so early that the warning is unreliable. To allow WSDOT to weigh the various trade-offs between early and later warning, triggering criteria were evaluated for a range of different triggering levels. Estimated probabilities of collapse for different combinations of trigger level-trigger time are presented. By using cost-benefit analysis, techniques these probabilities can be helpful, along with estimates of the costs and benefits of successful and unsuccessful warning, to select desired triggering criteria.

Criteria for Structural Inspection and Closure

Previous studies have shown that structural damage could occur in the Viaduct for relatively low levels of ductility demands. To confirm that the Viaduct is not damaged by earthquake shaking, structural inspections are conducted following most earthquakes that are felt in the Seattle area. To provide a rational basis for determining whether such inspections are advisable, the results of push-over analyses and support-displacement analyses for the Seattle Engineering Department (SED) typical three-span unit were used to develop a criterion for initiating post-earthquake structural inspections. This criterion is based on a condition in which structural displacements exceed one-half the displacement at the expected onset of significant nonlinear behavior. For a structural period of 1.0 sec, this displacement corresponds to a spectral acceleration of 0.13g for the SED.

Stronger earthquake motions may cause sufficient damage to warrant closure of the Viaduct until its safety can be established. A criterion for closure of the Viaduct is based on the condition in which structural displacements reach the level at which significant nonlinear behavior is expected to occur. For a structural period of 1.0 sec, this displacement corresponds to a spectral acceleration of 0.22g for the SED.

Instrumentation

Implementation of the warning systems described in this report will require the design, installation, and operation of an instrumentation/warning system. The instrumentation system will include transducers, cables, and a data acquisition system. The warning system will include a computer connected to the data acquisition system, cables, relays, and warning devices (e.g., red lights, electronic signs, gates, horns). To enable WSDOT to verify that the system is functioning properly and to help with post-

earthquake recovery, the instrumentation will need to be monitored continuously. One option for ensuring such monitoring would be to connect the AWV instruments to the Advanced National Seismic System.

Chapter 1
Introduction

The Alaskan Way Viaduct, which carries nearly 100,000 vehicles per day, is one of only two north-south highways through downtown Seattle. The 3.5-km long structure was designed and constructed in two sections. The first section, which extends from near the Battery Street Tunnel in the north to approximately Dearborn Street in the south, was designed by the City of Seattle in the late 1940s and constructed in 1950. The second section, which runs from the south end of the first section to the current southern end of the Viaduct, was designed by WSDOT in the early 1950s and completed in 1956. The Viaduct is a double-deck structure over most of its length, but it transitions to side-by-side single deck structures near its northern and southern ends.

The existence and continuing operation of the Viaduct is vital to the economic health of Seattle and the greater Puget Sound region. Substantial economic costs would be incurred by private and public entities if the Viaduct were closed. The Alaskan Way Viaduct also affects the physical well-being of Washington residents. If all of the vehicular traffic happened to be spread evenly over a 24-hr day at an average speed of 80 km/hr, approximately 185 vehicles would be on the Viaduct at any particular instant in time. At any time, therefore, the condition of the Alaskan Way Viaduct directly affects the safety of well over 200 people; during commute hours, thousands of people can be on the Viaduct.

Recent studies sponsored by the Washington State Department of Transportation (WSDOT) indicated that the Alaskan Way Viaduct is expected to incur severe damage and partial collapse if an earthquake produces strong ground shaking at the site. Given the high traffic volume of this structure, a large number of casualties might occur. To date, sufficient funds to repair or replace the Viaduct have not been available. Until such funds become available and repair/replacement work is completed, the seismic vulnerability of the Alaskan Way Viaduct will continue to threaten the economic and physical well-being of Washington State residents. To reduce this threat, development of an instrumented monitoring system was investigated in this study. The monitoring

system would be designed (1) to warn of at least one mechanism of impending Viaduct collapse and (2) to minimize Viaduct closure time following significant earthquakes by providing post-earthquake inspectors with quantitative information on bridge response and damage.

BACKGROUND

Following the 1989 Loma Prieta earthquake, which caused collapse of the Cypress structure in Oakland, California, WSDOT initiated a series of studies of the seismic vulnerability of the Alaskan Way Viaduct (Dodson et al., 1990; Brown et al., 1992; Eberhard et al., 1995; Knaebel et al., 1995; Kramer et al., 1995). These studies showed that the Alaskan Way Viaduct is vulnerable to extensive damage and partial collapse during and/or shortly after strong earthquake shaking. The vulnerabilities are associated with deficiencies in the above-ground structure and in the foundations. The foundation problems are exacerbated by the existence of highly liquefiable soils beneath the Viaduct, and by the seismic vulnerability of the Seattle seawall that is located immediately west of the Viaduct.

Foundation Vulnerabilities

Liquefaction is a phenomenon in which rapidly applied stresses, such as those induced in soil deposits by strong earthquake shaking, cause a buildup of porewater pressure that markedly reduces the strength and stiffness of the soil. At sites where initial shear stresses exist, such as those with sloping ground surfaces or those adjacent to retaining structures, liquefaction can lead to permanent lateral soil movements. Such movements can damage structures, particularly pile-supported structures whose foundations were not designed with proper consideration of liquefaction effects.

The effects of liquefaction are frequently observed near or even after the end of strong ground shaking. There are two reasons for this behavior: (1) liquefaction is a cumulative damage process in which porewater pressure develops incrementally as more and more stress reversals occur, and (2) liquefaction-induced ground movements may result from the redistribution of porewater pressure that occurs during and after strong ground shaking; porewater pressures may increase in critically stressed areas to produce

failures after shaking has ended. As a result, it may be possible to develop instrumentation systems that provide a short warning period before occurrence of the most damaging effects of liquefaction.

Previous investigations have found that sections of the Alaskan Way Viaduct are expected to collapse following strong ground shaking. This collapse is expected to result from excessive total and differential lateral movement of the soil surrounding the pile foundations that support the Viaduct. The lateral soil movement would result from anticipated excessive seaward displacement of portions of the seawall that runs along the Seattle waterfront.

Structural Vulnerabilities

Earthquake engineering has evolved greatly since the 1950s, when the Alaskan Way Viaduct was constructed. Older reinforced concrete bridges tend to have much less confinement (transverse) reinforcement than new bridges, and consequently, older bridges are usually more brittle than new ones. The Alaskan Way Viaduct is no exception. Previous investigations have found that the Viaduct's lap splices are too short, inadequately confined, and poorly located. The beam-to-column joints might also be vulnerable because they have no confinement reinforcement. In some columns, the potential for catastrophic shear failure exists.

Given the uncertainties associated with predictions of ground-shaking intensity, site response, liquefaction, and structural vulnerability, it is difficult to accurately predict levels of structural damage. It is particularly challenging to make damage estimates for the Viaduct, because liquefaction-induced vertical and lateral soil movements would exacerbate any damage caused by strong ground shaking.

The high potential for damage to the Alaskan Way Viaduct by strong ground motion means that the Viaduct will likely be closed for inspection following earthquakes that produce moderate to strong shaking in Seattle. This was the case following the 2001 Nisqually earthquake. Depending on the level of shaking and soil deformation, WSDOT might be able to return the Viaduct to service quickly, or the Viaduct might have to be closed until repairs can be completed. To make decisions on the closing and re-opening

of the Viaduct after an earthquake, reliable and timely information about the Viaduct's structural response and damage is needed.

OBJECTIVES

This research project had two primary objectives: (1) to develop design characteristics for an instrumentation system that would detect the onset of soil liquefaction and provide input to a collapse warning system, and (2) to develop design requirements for a structural instrumentation system that would reduce durations of Viaduct closures by speeding the process of evaluating the post-earthquake condition of the structure. The first objective was directed toward life safety, the second toward reduction of economic impacts. Detailed design and specification development for the instrumentation was beyond the scope of this project.

ORGANIZATION OF REPORT

This report is organized into six additional chapters. Chapter 2 describes earthquake warning systems. Chapter 3 reviews the seismic vulnerability of the Viaduct. Chapter 4 presents background information on methods for evaluating liquefaction hazards. The development of an algorithm for warning of impending Viaduct collapse is described in detail in Chapter 5. Chapter 6 describes an instrumentation scheme for improved evaluation of structural performance. Finally, the results of the research are summarized and conclusions drawn in Chapter 7.

Chapter 2
Earthquake Warning Systems

Systems for the detection of earthquake have been available for many centuries. Detectors invented and used in China as early as the second century B.C. used a series of balls that would be jostled out of holders by significant earthquake shaking. By looking at the positions of the balls that fell from their holders, the direction of strongest shaking could also be estimated. A variety of early and relatively crude mechanical detectors, called seismoscopes, were developed in later years. These devices generally provided after-the-fact confirmation that earthquake shaking had occurred, along with various levels of information about the characteristics of the shaking.

Some 150 years ago, ground motion recorders (seismometers or seismographs) were developed. Early seismographs typically involved some sort of sprung mass whose motion relative to its support could be recorded by a stylus on smoked glass, or a rotating drum, or by reflected light on a film. These analog devices, which generally required a triggering level of ground motion, were used effectively for many years. Modern seismographs typically use triaxial accelerometers (accelerometers capable of recording motion on three orthogonal axes) to obtain digital ground motion records. These motions can be transmitted to seismograph stations by telephone or internet systems, or in a wireless mode using radio, microwave, or cellular communications systems.

In recent years, instruments of various types have been used to develop earthquake warning systems. These systems are relatively new, and operate at different spatial scales. The remainder of this chapter provides a brief description of the primary types of earthquake warning systems that have been reported in the earthquake engineering literature and of the various components of those systems. Because these systems are new, involve rapidly changing technologies, and have different objectives, the characteristics of existing systems may not represent the optimum characteristics of a new system.

REGIONAL WARNING SYSTEMS

Some earthquake warning systems operate on a regional basis and attempt to provide a warning of impending ground motion that may range from seconds to minutes. The goals of such systems typically include provision of earthquake warnings, damage detection, and post-earthquake response deployment

The detection of distant earthquakes can provide a significant period of time in which residents of a particular area can take action to secure their own safety. For example, Mexico City is at risk from large earthquakes that occur on the Michoacan subduction zone off the Pacific coast of Mexico. These earthquakes, which may be very large, are often located nearly 300 km away from Mexico City. Experience, such as that of the 1985 Michoacan earthquake, has shown that the soft sediments that underlie portions of Mexico City can strongly amplify the relatively weak motions that occur in the bedrock beneath Mexico City and cause substantial damage. The Seismic Alert System (SAS) is an earthquake warning system that has been operating in Mexico since August, 1991. The SAS uses seismometers placed in the "Guerrero Gap," an area in which large earthquakes are anticipated in the future, to provide a warning of potential significant ground motion to heavily populated Mexico City. The system is capable of providing about 60 sec warning of the first S-wave arrivals to Mexico City. The SAS provides a general warning disseminated by commercial AM/FM radio stations for earthquakes of $M > 6$ and a restricted warning for $5 < M < 6$. The largest seismic event detected by the SAS to date has been the September 14, 1995 Copala earthquake (M = 7.3). In response to this event, a general warning that reached an estimated 4 million persons was issued in Mexico City 72 seconds prior to the onset of strong ground motion.

In southern California, Caltech and the United States Geological Survey (USGS) operate a network of over 250 seismographs. In recent years, a system for notification of strong earthquakes has been developed. This system, called CUBE (Caltech-USGS Broadcast of Earthquakes), has the goals of (a) providing near real-time locations, magnitudes, and ground motions for earthquakes, (b) developing a system to warn of imminent ground shaking while an earthquake is in progress, and (c) developing strategies for using ground motion information for more efficient post-earthquake response. After an event, CUBE participants (primarily utilities, emergency services

agencies, railroads, and interested earth scientists to date) receive earthquake epicentral information via pager. A direct radio link between the CUBE computers and the paging system ensures reliable communications independent of local telephone services. Messages are sent to pocket pagers for all regional earthquakes of M > 3.5 and to pagers connected to computers for earthquake of M > 1.8. The computer systems can immediately display the pager information on a map along with demographic and infrastructure information. The CUBE system currently makes use of 64 telemetered seismographs but is being upgraded to use more than 220 stations. The enhanced network will allow estimation of the geographic distribution of ground motion intensity within minutes of the earthquake.

The Pacific Northwest Seismograph Network (PNSN) has developed a pager-based earthquake information system called RACE (Rapid Alert for Cascadia Earthquakes), which broadcast preliminary location and magnitude estimates within minutes after an earthquake. An earlier version of the RACE system has been in use to provide PNSN personnel with rapid notification of earthquakes, but expansion of the PNSN network and advances in pager technology now allow broadcast of this information to multiple users via a commercial paging system. As with the CUBE system, the RACE system is designed and intended more for post-earthquake emergency response and rapid damage estimation purposes than for ground motion warning.

LOCAL WARNING SYSTEMS

Other warning systems operate on a more localized basis, typically to provide warning of motions affecting spatially distributed systems such as pipelines, railways, etc. The goals of such systems are to provide a signal to shut down the facility in case of potentially damaging motions, and to detect motions that are strong enough to require inspection but not shutdown.

In the mid-1990s, Tokyo Gas Co., Ltd. developed an earthquake monitoring and rapid damage assessment system (Yamazaki et al., 1994; 1995). The SIGNAL (Seismic Information Gathering and Network Alert) system included 331 sensors that measured peak acceleration, *PGA*, and spectrum intensity, *SI*, at district regulator stations. The measured quantities are used, along with early damage reports, to determine the extent

and location of gas system shutdowns. Tokyo Gas recently developed a new spectrum intensity sensor (Shimizu et al., 2000) which can store and process recorded accelerations in on-board memory and send the processed information (e.g. peak acceleration and spectrum intensity) to a central computer using public telecommunication systems. This SUPREME (Super-Dense Real-time Monitoring of Earthquakes) system is being installed at all 3,700 Tokyo Gas district regulator stations. The new spectrum intensity sensor is also used to detect soil liquefaction, which is judged to occur if all of the following conditions are satisfied:

1. $PGA > 100$ cm/sec^2,
2. $SI > 20$ cm/sec,
3. Estimated displacement, $D = 2SI^2/PGA$. 10 cm
4. Estimated predominant period (by zero-crossing method) > 2.0 sec

The Great Taipei Gas Co., Ltd. installed the Tokyo Gas spectrum intensity sensors at 31 regulator stations in the Taipei basin in 1999. The sensors were set to automatically shut off the gas supply if $SI > 40$ cm/sec. The 1999 Chi-Chi earthquake ($M = 7.6$) occurred shortly after installation of the sensors. Because the epicenter of the earthquake was far (approximately 160 km) from Taipei, the motions were moderate and limited damage was observed. In the Chi-Chi earthquake, 16 of the sensors recorded motions ranging from $SI = 8.3$ cm/sec ($PGA = 38.0$ cm/sec^2) to $SI = 27.4$ cm/sec ($PGA = 139.6$ cm/sec^2). Because these values were below the threshold spectral intensity of 40 cm/sec, the gas supply was not shut down in Taipei.

The 800-mile long Trans-Alaska Pipeline pumps about 1,400,000 barrels (31.5 gallons per barrel) of North Slope oil to Port Valdez every day. The pipeline traverses the flat North Slope to enter the Brooks Range, where it climbs from sea level to the crest of Atigun Pass. From there, it descends to cross the Yukon River. The final 350 miles of the pipeline crosses the Alaska Range, descending and climbing again to 2,788 feet to top Thompson Pass before plunging through Keystone Canyon to the terminal at Valdez. Along this path, the pipeline crosses three active faults. The oil, which leaves the ground at roughly 116 F, is pushed south at about 5 mph by six pump stations. The journey from

the North Slope to the 18 storage tanks at Valdez takes six days. The pipeline is instrumented with a series of strong motion instruments, which are intended to trigger closure of one or more valves in the event of strong shaking.

STRUCTURE-SPECIFIC WARNING SYSTEMS

Warning systems have also been developed for individual structures. A number of these systems are tied to instrumentation systems that are required by regulatory agencies. In 1965, for example, the City of Los Angeles began requiring three accelerographs to be installed in buildings over six stories with over 60,000 ft^2 floor area and in all buildings over 10 stories. Other cities have adopted similar instrumentation requirements. Components of buildings that can be damaged by earthquakes, such as elevators, are frequently outfitted with seismic "switches." In 1975, California began requiring elevators that travel faster than 2.5 ft/sec to install seismic switches that trigger at an acceleration of 0.15 g or a device that can detect counterweight derailment. The seismic switch, which is usually located on the top floor of the structure, causes the elevators to move to the closest floor, open their doors, and then shut down until checked by an elevator mechanic.

Many bridges in seismically active areas have been instrumented with strong motion instruments. Such instrumentation provides valuable information on seismic performance and on the level and location of potential earthquake damage within the bridge. As part of the California Strong Motion Instrumentation Program (CSMIP), the Vincent Thomas suspension bridge in Los Angeles was instrumented with 26 sensors; records have been obtained from the 1987 Whittier Narrows (M5.9) and 1994 Northridge (M6.7) earthquakes.

Due to the closure of part of Highway 271 near Leggett in Mendocino County, California, two older arch bridges over Big Dann Creek and Cedar Creek provided the only access to a few residences in the lightly populated areas. The bridges were seismically deficient, but retrofitting was estimated to cost tens of millions of dollars (Hipley, 1998). After public meetings with local residents, a system of "seismic gates" was installed at the bridges. The gates are similar to the gates commonly used at railroad crossings, but are activated by a spread spectrum radio signal generated when nearby

strong motion instruments detect exceedance of a threshold level of earthquake ground motion. Each bridge has its own sensor; to provide a measure of redundancy, both gates are closed if either sensor detects motions exceeding the threshold. Local Caltrans and Highway Patrol personnel also receive a signal if the gates are closed, and are responsible for lifting the gates after inspection. Caltrans has also used temporary seismic gates at the Somoa Channel crossing in Eureka as an interim measure prior to planned seismic retrofitting.

COMPONENTS

Earthquake warning systems can be configured in many different ways. In general, however, an earthquake warning system will require sensing elements, data acquisition/storage elements, communications elements, triggering algorithms, and a relay that can activate a physical device to warn people who might be at risk. While technical developments are occurring rapidly with respect to each of these components, the following paragraphs present brief discussions of systems that have been used by others.

A number of different sensing elements have been used in earthquake warning systems. The simplest systems are usually based on geophones (velocity transducers) oriented to measure vertical motions. These transducers are typically tuned to the anticipated frequency of p-waves, and rely on the difference between p-wave and s-wave/Rayleigh wave velocities to provide warning of impending earthquake motion. More advanced systems typically use triaxial accelerometers to sense ground motions. Some of these monitor peak values and others monitor the entire time history of motion.

Different data acquisition systems are used in earthquake warning systems, depending on the data that is to be acquired and how it is to be used. Relatively simple systems only acquire peak values of parameters such as velocity or acceleration. More advanced systems may acquire, store, and process complete time histories of acceleration for three orthogonal components of ground motion. Such systems typically have on-board CPU and RAM, which may be programmed to compute ground motion parameters from the acceleration time histories.

Typically, a warning signal is broadcast over an area-wide transmitter if the ground motion amplitude exceeds a given threshold. This warning signal may contain earthquake parameter estimates, and an estimate of the reliability of the information since many users of the warning signal would incur significant costs by taking action based on the alert message. In general, an earthquake warning system should produce more reliable estimates of earthquake location and magnitude as the earthquake evolves and as more stations in the network transmit data that can be used in determining the extent of the hazard. It is therefore important for alert information packets to be rapidly updated so that the new, more reliable estimates can be transmitted to the users.

Each user of the warning signal typically has a dedicated receiver and processor with preprogrammed responses based on earthquake parameter values. The extent and specifics of alert information analysis that a particular user may require before executing alert or shutdown functions depends on the user's application. Some applications, such as opening a fire station door, do not have a significant cost associated with a false alarm, so minimal or limited processing may be desirable to maximize lead time. However, the shutdown of a bridge using the alert signal would have a potentially high cost. Consequently, maximum alert information analysis that trades off the time left to execute a safe shutdown against the probability that a shutdown is unnecessary may be desired. Simple warning systems are usually based on the exceedance of a scalar quantity – for example, a system might be triggered by the exceedance of 0.05 g acceleration. To limit false alarms, multiple sensors distributed spatially can be used with *m*-of-*n* logic. With this logic, activation thresholds from a minimum number of sensors may be required (e.g. 3-of-5 sensors) for a warning to be issued. Advanced warning systems utilize ground motion parameters computed from recorded time histories of acceleration to trigger warnings; such parameters could include spectrum intensity, cumulative absolute velocity, etc. Triggering by exceedance of one or more ground motion parameters can be manifested in many different ways. Trigger signals can be used to operate one or more relays that might control traffic signals, barriers, or horns and sirens. Selection of the system by which the public is to be alerted to earthquake shaking should generally be done on a case-by-case method.

Of primary importance is the communication system used to transmit information to the end users. There are two possible strategies that can be adopted:

- Direct communications from a central processing center to each user.
- An area-wide alert transmission to all users.

Direct communications from the central processing center to each end user would result in high communication costs since a dedicated communication channel to each user must be available at all times. However, for some structure-specific systems, a hard-wired communications system is used, though cables can be severely damaged by excessive ground and/or structural deformations.

An area-wide alert broadcast can be accomplished via satellite, radio and television broadcasts, and FM radio and television subcarrier communications. Satellite communication is a very expensive option, requiring a large initial receiving-equipment cost for the earthquake warning system and for each user. Radio and television broadcasts would, when part of an earthquake warning system, be interrupted automatically whenever an alert signal is transmitted. FM radio and television subcarrier communications are relatively new data transmission techniques The advantages of FM radio and television subcarrier communications are: (1) low start-up costs, (2) wide area coverage, (3) low user receiver costs, (4) acceptable digital data transmission rate and, (5) high reliability. However, there are areas of concern in using broadcast stations subcarrier communications to issue the earthquake warning alert information that fall into two categories: (1) transmitter concerns, and (2) user reception concerns The alert signal broadcast stations must, besides providing adequate area-wide coverage, operate 24-hours a day. Many do not. Furthermore, many broadcast stations do not have adequate back-up power if a main power failure takes place. A power failure due to a large earthquake can be expected and, consequently, at least a few minutes of immediate back-up power using an uninterruptable power supply is necessary. Furthermore, user reception of the alert signal is solely dependent on receiver location. Locations in deep valleys and in steel or steel-reinforced concrete structures inhibit penetration of the electromagnetic signal. Finally, multipath problems could be encountered: (1) if strong-signal reflectors are present and (2) in certain locations relative to the receiver location.

SUMMARY

Earthquake warning systems can operate on different scales and with different levels of sophistication. They are based on a number of technologies, many of which are currently in states of flux. Design of an earthquake warning system for a particular structure or group of structures should be performed by specialists that are familiar with current developments with respect to each of the technologies.

Chapter 3

Seismic Vulnerability of the Alaskan Way Viaduct

The seismic vulnerability of the Alaskan Way Viaduct is influenced by many factors, including its location, age, and construction. The performance of the Alaskan Way Viaduct and of other viaducts in previous earthquakes also provides information regarding the Alaskan Way Viaduct's seismic vulnerability. Background information on these important factors is presented in the following sections.

GEOLOGIC SETTING

From the standpoint of geologic and geotechnical conditions, the Alaskan Way Viaduct site is dominated by thick deposits of loose, saturated soil. Most of the loose soils were placed as fill during reclamation of Seattle's tideflats and extension of the Seattle waterfront toward the Elliot Bay in the late 1800s and early 1900s. Some of the loose soils, particularly those south of about Yesler Way, are natural tideflat soils. Those soils are underlain by very dense, natural soils. The thicknesses of these loose soils vary along the length of the Viaduct, as illustrated in Figure 3.1.

The natural shoreline of Elliot Bay actually lies east of all but the very northern portion of the Viaduct; in other words, the current location of the Alaskan Way Viaduct was part of Elliot Bay a century ago. The filling operations that extended the waterfront to its current position were typical of those used around the world at that time. The fill soils either were mixed with water and pumped to the site or were dumped through waters of Elliot Bay. To retain the the fill in a manner that would allow large ships to berth, the City of Seattle designed and constructed a timber and concrete seawall that runs parallel to much of the current alignment of the Viaduct. The seawall, constructed in the early 1930s with four different types of walls, was designed according to the procedures that were accepted at that time.

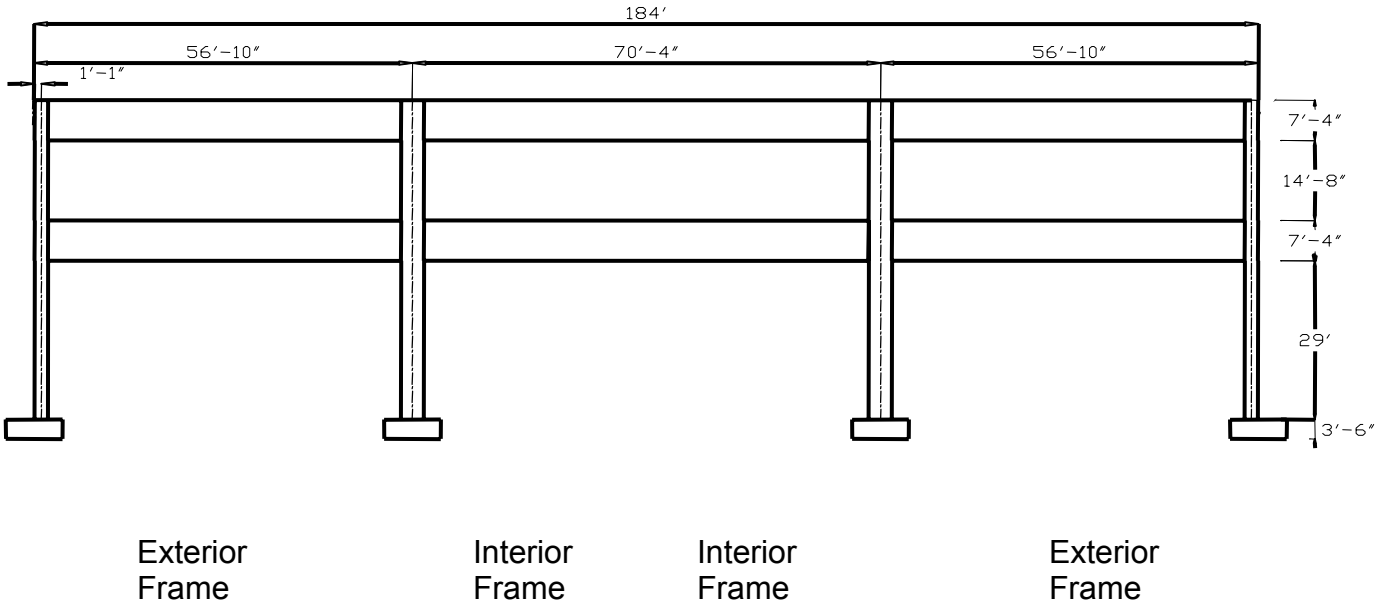

Figure 3.1. Longitudinal elevation of WSDOT typical unit

VIADUCT CONSTRUCTION

The Alaskan Way Viaduct was constructed from 1949 to 1956 in three main sections. The northern third of the Viaduct consists of two side-by-side, single-deck structures, which were designed by the City of Seattle. Near Pike Place Market, the Viaduct transitions to a double-deck configuration, which is maintained over most of the Viaduct. The middle third of the Viaduct was also designed by the City of Seattle, while the southern third was designed by the Washington State Department of Transportation. The two agencies selected different member geometries, reinforcement details, and foundation details.

Notwithstanding variations to accommodate off-ramps, superelevations and curves, the double-deck portion of the Viaduct consists mainly of three-span units that are separated from adjacent units by 1 1/2-inch and 2-inch expansion joints. The two decks are supported by beams that run in the transverse direction (perpendicular to traffic) and deep girders that run in the longitudinal direction (parallel to traffic). Unlike many other bridges, the beams and girders frame directly into the columns. The girders and columns

form two frames that provide the unit's longitudinal lateral force resistance (Figure 3.1). In the transverse direction, the beams and columns form four frames that provide the lateral force resistance of the three-span unit (Figure 3.2).

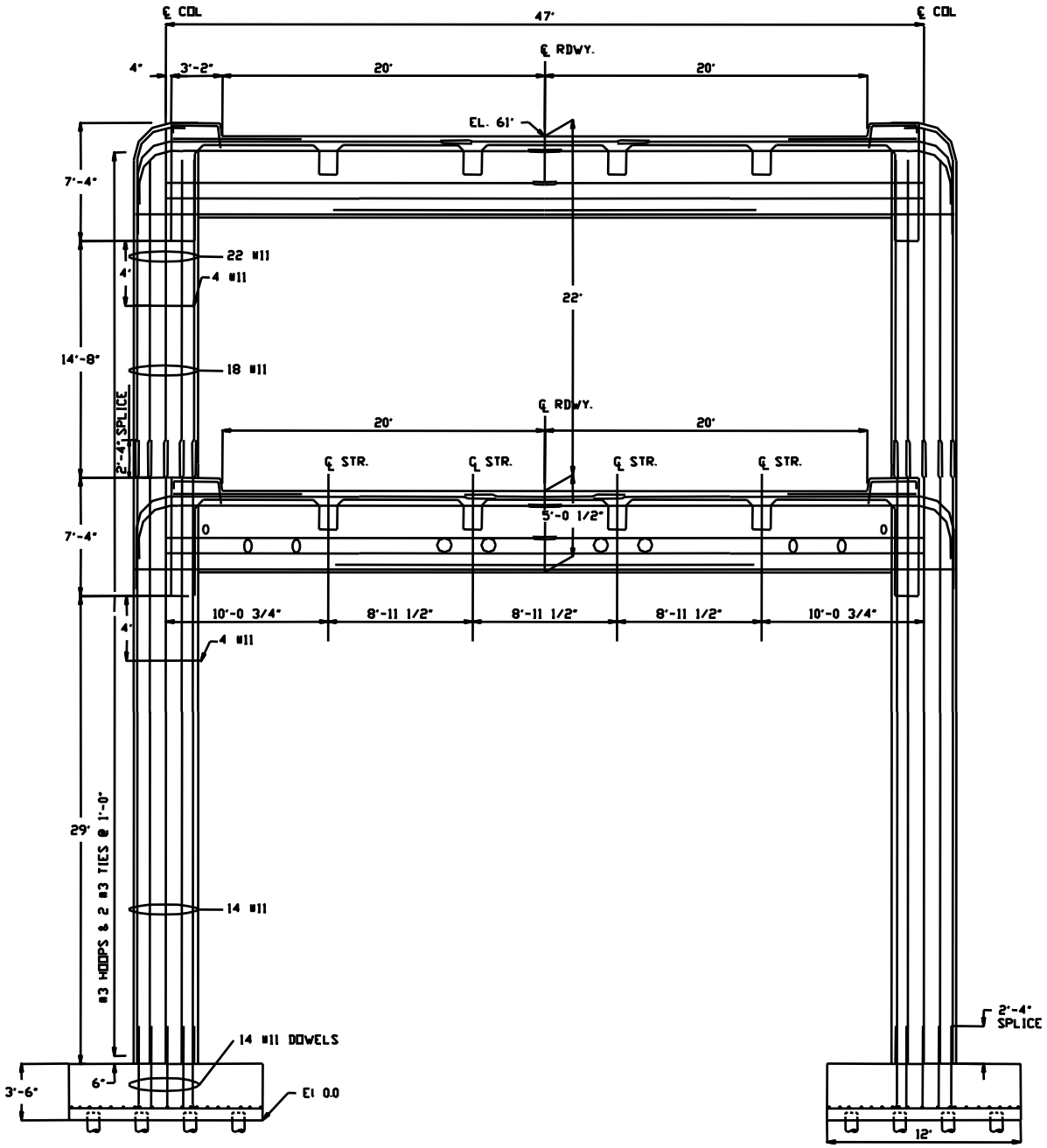

Figure 3.2. Interior transverse frame for WSDOT typical unit

The Viaduct is supported on pile foundations that extend through the waterfront fill and tideflat deposits to the underlying dense soil (except for the southernmost portion, for which pile driving records indicate that dense soils were not reached). Each column of the Viaduct is supported by a group of piles connected by a buried footing. The number and arrangement of piles in each group vary along the length of the Viaduct, and between interior and exterior columns, and the sizes of the footings vary to accommodate the various pile groups. Available pile driving records indicate that most of the piles were driven only a short distance into the dense soil; consequently, pile-bearing support is derived from the top few feet of the dense soil.

The construction details of the Viaduct are typical of reinforced concrete bridges built before the 1971 San Fernando earthquake. The Viaduct is relatively stiff and strong, but its reinforcement details fall short of those required by current national seismic codes. The most significant difference between the Alaskan Way Viaduct and modern bridges is the Viaduct's shortage of transverse reinforcement. Transverse reinforcement increases the shear strength of the columns and beams, and the confinement that the transverse reinforcement provides is essential in preserving the integrity of the concrete columns and joints during an earthquake. The need for sufficient transverse reinforcement is one of the most important lessons engineers have learned from earthquakes in the past 25 years.

Another difference between the Alaskan Way Viaduct and modern construction is the presence of longitudinal reinforcement splices at the column bases and directly above the first deck. The lap splices are much shorter than those required by current standards, are enclosed by inadequate transverse reinforcement, and are located in regions that are likely to undergo large flexural demands during an earthquake. Other significant differences between the Viaduct and new construction are that the bottom transverse beam and longitudinal girder reinforcement extends into the columns all the short distance, and the footings lack top reinforcement.

PERFORMANCE OF THE ALASKAN WAY VIADUCT

Since its completion, the Alaskan Way Viaduct has been subjected to significant earthquake shaking twice: during the 1965 Seattle earthquake and during the 2001

Nisqually earthquake. The Seattle earthquake, which had a magnitude of 6.5 with its epicenter some 25 km from the Viaduct, produced a modest level of shaking at the bridge site. Inspection of the Viaduct following the 1965 earthquake revealed no apparent signs of distress in the structure.

Some evidence of soil liquefaction was observed near the site of the Alaskan Way Viaduct following both the 1949 earthquake (before the Viaduct had been built) and the 1965 earthquake. Liquefaction is a phenomenon in which soil loses a large portion of its strength during an earthquake. Liquefaction has been responsible for tremendous damage to waterfront facilities in earthquakes around the world. The liquefaction that occurred in 1949 and 1965 was not extensive, but it did produce damage at Pier 66, Pier 36, east of the Viaduct at 177 Southwest Massachusetts, and just north of the Viaduct along Elliott Ave. Following the 1965 earthquake, breaks in underground water supply mains were observed near Piers 64 through 66. The effects of liquefaction near the Alaskan Way Viaduct site following the 1949 and 1965 earthquakes were modest, but the levels of shaking in both earthquakes were relatively low. The triggering of liquefaction by these relatively weak motions indicates that the loose, saturated soil near the Viaduct is highly susceptible to liquefaction. If either earthquake had produced stronger shaking, or if the duration of shaking of either had been longer, more liquefaction-induced damage would have occurred.

The 2001 Nisqually Earthquake had a relatively large magnitude (M_w=6.8), but was deep (52 km), and its epicenter was located far from the Viaduct (60 km). As a result, the level of shaking at the Viaduct location was much less than can be expected for this location in future earthquakes. Nearby stations, located on till, recorded peak ground accelerations in the range of 0.09g to 0.13g. Liquefaction was not observed directly below the Viaduct itself, but liquefaction was observed in the area east of the southern portion of the Viaduct.

Immediately after the Nisqually earthquake, the Viaduct was closed and inspected for damage. Structural damage appeared light at first, so the Viaduct was opened soon after the earthquake. Damage appeared to consist mainly of crack initiation and extension within joints at the lower and upper levels. Figure 3.3 shows one such crack a few days after the earthquake.

Figure 3.3. Damage to bent 100 knee joint immediately after the 2001 earthquake

With time, cracks near Bent 100 lengthened and widened, resulting in closure of the Viaduct until that region could be shored. Figure 3.4 shows the same joint as shown in Figure 3.3, but approximately one month after the earthquake. This joint may have been particularly vulnerable to failure because one longitudinal bar fractured near the end of a welded splice.

Following the earthquake, a panel was charged with assessing the structural adequacy of the Viaduct.

Figure 3.4. Damage to bent 100 knee joint of Alaskan Way Viaduct one month after the 2001 earthquake

COMPARISON WITH OAKLAND AND SAN FRANCISCO VIADUCTS

Comparison of the Alaskan Way Viaduct with the Oakland Cypress Viaduct and the viaducts that failed in the 1989 Loma Prieta earthquake is useful for understanding the vulnerability of the Alaskan Way Viaduct. All of these viaducts have two decks, have reinforcement details typical of pre-1971 construction, and provide vital transportation links in urban areas. Portions of the Cypress Structure collapsed during the 1989 Loma Prieta earthquake, and the San Francisco viaducts were so heavily damaged that they had to be either demolished or subjected to a costly rehabilitation program.

Although the viaducts are similar in many ways, extrapolation from one structure to another is difficult because each viaduct's deficiencies are different. The Cypress Viaduct had inadequately reinforced column hinges just above the first deck. At this location, the Alaskan Way Viaduct does not have structural hinges but instead has short lap splices. Unlike the Alaskan Way Viaduct, the San Francisco viaducts did not have longitudinal girders that frame directly into the columns. Most importantly, the geotechnical conditions differ for all of the viaducts.

SEISMIC VULNERABILITY EVALUATION

The initial evaluation of the seismic vulnerability of the Alaskan Way Viaduct involved determining design-level ground motions along the length of the Viaduct, evaluating the potential for liquefaction of the soil beneath the Viaduct, and estimating the structural response. Because the initial evaluation determined that the potential for collapse strongly depended on the behavior of the seawall that runs along the waterfront immediately west of the Viaduct, a subsequent investigation of potential seawall movements was conducted (Kimmerling and Kramer, 1996). The primary results of these investigations are summarized in the following sections.

Design-Level Ground Motion

The seismic vulnerability of any structure depends on the strength of ground shaking to which it is subjected. Modern earthquake engineering procedures evaluate seismic vulnerability in relation to a design-level ground motion. Current national design codes for buildings and bridges recommend the use of design-level motions with a 10

percent probability of exceedance for an exposure period of 50 years. Such motions are likely to be exceeded about once every 475 years. Of course, earthquakes do not occur at regular intervals, so the elapsed time between design-level motions will vary. This "10 percent in 50 years" hazard level was used to develop design-level motions for seismic vulnerability evaluation of the Alaskan Way Viaduct. The design-level ground motion with a 10 percent probability of exceedance in a 50-year period represents a strong level of shaking at the Alaskan Way Viaduct site. The peak ground acceleration produced by the design-level motion would be about three times higher than the peak acceleration that occurred in the vicinity of the Viaduct during the 1965 and 2001 earthquakes.

Ground Response

The level of ground shaking at a given site is strongly influenced by the soil conditions at that site. Because soil conditions vary along the length of the Alaskan Way Viaduct, various portions of the viaduct will be subjected to different levels of ground shaking. The Viaduct's acceleration levels will likely be highest at locations underlain by 10 to 20 feet of fill; most of these locations are north of about Dearborn Street. South of Dearborn Street, acceleration levels will generally be lower, but larger ground displacements are likely to occur.

Liquefaction Hazards

Historical accounts of the placement of the waterfront fills, observations of their performance in the 1949 and 1965 earthquakes, and the results of the subsurface investigations suggested that the liquefaction potential of the waterfront fills and tideflat deposits is high. Consequently, a great deal of effort was devoted to evaluating liquefaction hazards. Previously available subsurface soil data were supplemented by data from additional tests performed as part of the investigation. The liquefaction resistance of the soils beneath the Viaduct was evaluated in three different, independent ways; each was used to evaluate liquefaction potential. Additionally, the same procedures were used to evaluate the level of liquefaction that would have been expected in the 1965 earthquake.

The manner in which the waterfront fills beneath the Alaskan Way Viaduct were placed is a virtual recipe for creating a liquefiable soil deposit. Other soil deposits placed

in the same way have liquefied and caused extensive damage in earthquakes around the world. These techniques are no longer used in seismically active areas. In the present investigation, three independent analyses indicated that widespread liquefaction of the loose, saturated soils beneath the Alaskan Way Viaduct is expected to occur in a design-level ground motion. Furthermore, the investigation indicated that widespread liquefaction could also be caused by a lower (and consequently more likely) level of motion. The same liquefaction evaluation procedures were repeated for the 1965 earthquake motion. The results, which indicated that modest liquefaction should have occurred, were consistent with observations following that earthquake.

Effects of Liquefaction

The occurrence of liquefaction can have a number of damaging effects on structures. For a structure such as the Alaskan Way Viaduct, the most important of these are permanent deformations. Permanent soil deformations can be divided into vertical (settlement) and horizontal (lateral movement) components.

Settlement

The effects of liquefaction on the seismic vulnerability of the Viaduct are likely to be severe. Widespread liquefaction is expected to cause vertical settlement of the Viaduct foundations ranging from 0 to 24 inches. These settlements, which would begin during the earthquake and continue for several minutes afterward, would be highly irregular and would induce large vertical differential foundation settlements. These vertical settlements could lead to collapse of multiple sections of the Viaduct.

Lateral Movement

Widespread liquefaction is also expected to cause lateral movement of the waterfront fill toward Elliot Bay. The amount of movement would be strongly influenced by the seismic performance of the seawall. Seawalls retaining similar liquefiable soils have failed with large lateral movements in past earthquakes. These lateral soil movements would occur in an irregular pattern and could induce large differential

movements of the Viaduct's foundations. These lateral foundation movements could cause multiple sections of the Viaduct to collapse.

The need for better understanding of the ability of the seawall to resist lateral earth pressures from liquefied soil motivated a supplemental investigation of the seawall. This investigation included numerical modeling of typical seawall profiles at different locations along the length of the seawall. The purpose of these analyses was to estimate the range of seawall displacements that could be expected to occur in the event of widespread soil liquefaction, and to identify the locations where the largest soil displacements adjacent to the Viaduct would be expected to occur. This investigation indicated that soil displacements large enough to need mitigation (by appropriate soil improvement methods) could be expected roughly from the centerline of University Street to about 15 m south of the centerline of Madison Street, and from 15 m north of the centerline of Columbia Street to 15 m south of the centerline of Washington Street.

Structural Performance

All evaluations of earthquake vulnerability include uncertainty. The soil, concrete, and steel properties vary; the placement of the reinforcement can differ somewhat from that specified on the structural plans; and the evaluation procedures involve approximations. Most importantly, the level of shaking at a site varies greatly from one earthquake to the next. Despite this uncertainty, it is clear that the Alaskan Way Viaduct does not meet current design standards for earthquake resistance.

To investigate the likelihood and consequences of various failure modes, the research team implemented widely used guidelines written by consulting engineers, researchers, and state and federal highway engineers (Applied Technology Council, 1983). The Viaduct was also evaluated with assessment procedures that were developed recently by researchers at the University of California, San Diego (Priestley et al., 1992), and at the University of California, Berkeley (Moehle et al., 1994). At the time of the evaluation, these were the most up-to-date assessment procedures available to the structural engineering profession.

The general assessment that resulted from implementing the older procedure and the newly developed procedures was the same. The evaluations indicated that the Viaduct is vulnerable to a design-level earthquake because the design motion would

strongly excite the Viaduct, and the Viaduct's structural details make it brittle. The evaluations identified the following structural deficiencies.

- The lap splices at the bases of the WSDOT-section first-story columns would almost certainly lose their flexural strength during the design motion. Loss of flexural strength would lead to increased damage in other parts of the structure. The splices could fail in shear. If the splices failed in shear, the columns would not be able to support the decks.
- The beam-to-column joints at the lower-level joints would be vulnerable in a design-level motion. Although the likelihood of joint failure is less than the likelihood of failure of the lower-level splices, the consequence of joint failure could be catastrophic. Complete joint failure would lead to collapse of the Viaduct. The upper-story splices increase the risk of failure in the joint area because the transverse reinforcement is inadequate.
- The beam-to-column joints at the upper level joints could be vulnerable, too. Welded lap splices in the Seattle Engineering Department (SED) typical units make this region particularly brittle. Damage near such welds was observed during the 2001 Nisqually earthquake.
- Most of the Viaduct's columns have inadequate shear strength because their transverse reinforcement is too sparse. Shear failures must be avoided because many bridge collapses during past earthquakes (for example, the 1994 Northridge Earthquake and 1995 Kobe Earthquake) were caused by this type of failure.
- Though the footings are not as vulnerable as the splices, joints, and shear-critical columns, the pile-supported footings were also found to be vulnerable. The consequence and likelihood of footing failure are uncertain, because few such failures have been observed during past earthquakes.
- Liquefaction-induced vertical settlement and lateral spreading would damage the piles and pile-footing connections, and could cause the Viaduct to collapse.

Peer Review

The University of Washington study was reviewed by eminent structural and geotechnical engineering experts who are active in assessing the seismic vulnerability of

bridges. The UW structural evaluation of the WSDOT unit was reviewed by Professor Jack Moehle and Dr. Andrew Whittaker at the University of California, Berkeley, and by Professor Frieder Seible at the University of California, San Diego. The peer reviewers agreed that the UW study had identified the most likely weaknesses in the Viaduct. They agreed also that the Alaskan Way Viaduct structural vulnerabilities are probably less severe than those of the San Francisco viaducts, but that the Viaduct is vulnerable. All three reviewers stressed that the level of retrofit that is needed (and the associated costs) will vary greatly according to the performance criteria. The geotechnical engineering aspects of the seismic vulnerability investigation were reviewed by Professor Geoffrey R. Martin of the University of Southern California. Professor Martin agreed that liquefaction poses a severe hazard to the Viaduct and surrounding area.

CONCLUSIONS

Evaluation of the seismic vulnerability of older structures is a complicated task. Earthquake shaking levels are difficult to predict, and estimates of liquefaction and structural response include significant uncertainty. Nevertheless, the engineering profession has developed vulnerability criteria that are consistent with past experience and with the results of research. Using up-to-date hazard evaluation criteria, previous studies have shown that the Alaskan Way Viaduct is clearly vulnerable to severe damage and possible collapse in a design-level earthquake. In fact, the Viaduct is vulnerable to damage and possible collapse in ground motions significantly less intense (and hence more likely to occur) that the design-level motion.

Chapter 4

Evaluation of Liquefaction Hazards

Since the first widespread observations of liquefaction in the 1964 Niigata and 1964 Alaska earthquakes, liquefaction has been responsible for significant damage to buildings and bridges in numerous earthquakes. The phenomenon of liquefaction has been studied extensively over the past 35 years, and substantial advances in the understanding of its development and effects have been made. These advances have led to a series of practical procedures for evaluating the potential for liquefaction occurrence and for estimating the effects of liquefaction. In this chapter basic concepts related to liquefaction, susceptibility, triggering conditions, and effects are presented together with common practical procedures for evaluating liquefaction hazards.

SOIL LIQUEFACTION

Liquefaction is one of the most important, interesting, and complex topics in geotechnical earthquake engineering. Its devastating effects sprang to the attention of geotechnical engineers in a three-month period in 1964 when the Good Friday earthquake (M_w=9.2) in Alaska was followed by the Niigata earthquake (M_w=7.5) in Japan. Both earthquakes produced spectacular examples of liquefaction-induced damage, including slope failures, bridge and building foundation failures, and flotation of buried structures.

Liquefaction is a complicated phenomenon. Research on this topic has progressed to the point at which an integrated framework of understanding has been developed. Historically, the term liquefaction has been used in conjunction with a variety of phenomena that involve soil deformations caused by monotonic, transient, or repeated disturbance of saturated cohesionless soils under undrained conditions. The generation of excess pore pressure under undrained loading conditions is a hallmark of all liquefaction phenomena. The tendency for dry cohesionless soils to densify under both static and cyclic loading is well known. When cohesionless soils are saturated, however, rapid loading occurs under undrained conditions, so the tendency for densification causes excess pore pressures to

increase and effective stresses to decrease. Liquefaction phenomena that result from this process can be divided into two main groups: *flow liquefaction* and *cyclic mobility*.

Flow liquefaction is a phenomenon that is triggered in a soil whose residual strength is lower than that needed to maintain static equilibrium (i.e., static driving stresses exceed residual strength). Flow liquefaction only occurs in loose soils with low residual strengths. It can produce extremely large deformations (e.g., flow slides); the deformations, however, are actually driven by the static shear stresses.

Cyclic mobility is a phenomenon that occurs when cyclic shear stresses induce excess porewater pressure in a soil whose residual strength is greater than that required to maintain static equilibrium. The phenomenon of cyclic mobility is often manifested in the field in the form of lateral spreading. Lateral spreading is characterized by incremental displacements during earthquake shaking. Depending on the number and strength of the stress pulses that exceed the strength of the soil, lateral spreading can produce displacements that range from negligible to quite large. Lateral spreading is quite common near bridges, and the displacements it produces can damage the abutments, foundations, and superstructures of bridges. Related to the latter, the phenomenon of level-ground liquefaction does not involve large lateral displacements but is easily identified by the presence of sand boils produced by groundwater rushing to the surface. Although not particularly damaging by themselves, sand boils indicate the presence of high groundwater pressures whose eventual dissipation can produce subsidence and damaging differential settlements.

Both flow liquefaction and cyclic mobility are very important, and any evaluation of liquefaction hazards should carefully consider both. In the field, flow liquefaction occurs much less frequently than cyclic mobility, but its effects are usually far more severe. Cyclic mobility on the other hand, can occur under a much broader range of soil and site conditions than flow liquefaction; its effects can range from insignificant to highly damaging. In this chapter, the generic term liquefaction will be taken to include both flow liquefaction and cyclic mobility.

LIQUEFACTION HAZARD EVALUATION

Evaluation of liquefaction hazards involves three primary steps. First, the susceptibility of the soil to liquefaction must be evaluated. If the soil is determined to be not susceptible to liquefaction, liquefaction hazards do not exist and the liquefaction hazard

evaluation is complete. If the soil is susceptible to liquefaction, however, the liquefaction hazard evaluation moves to the second step, evaluation of the potential for initiation of liquefaction. This step involves comparison of the level of loading produced by the earthquake with the liquefaction resistance of the soil. If the resistance is greater than the loading, liquefaction will not be initiated and the liquefaction hazard evaluation can be considered complete. If the level of loading is greater than the liquefaction resistance, however, liquefaction will be initiated. If liquefaction is initiated, the liquefaction hazard evaluation must move to the third stage, which is evaluation of the effects of liquefaction. If the effects are sufficiently severe, the engineer and owner may consider improvement of the site, or alternative sites for the proposed development. In the following sections a brief description of each step is presented.

SUSCEPTIBILITY

For liquefaction to occur, the soil must be susceptible to liquefaction. Some soils are susceptible to liquefaction, and some are not. The susceptibility of individual soils to liquefaction can be judged by several criteria.

Historical observations of liquefaction in past earthquakes can provide an indication of liquefaction susceptibility in future earthquakes. At a number of sites, repeated instances of liquefaction have been observed in different earthquakes. Therefore, observed field evidence of liquefaction provides a strong indication of susceptibility to future liquefaction.

Geologic conditions can also provide a good indication of liquefaction susceptibility. Liquefaction susceptibility is strongly influenced by soil composition, specifically by factors such as grain size distribution and particle shape. Uniformly graded soils and soils with rounded particle shapes are most susceptible to liquefaction. Consequently, geologic processes that sort soils into deposits of uniform gradation with rounded particles will tend to produce soil deposits with high susceptibility to liquefaction. For many years, only sands were considered to be susceptible to liquefaction. It is now recognized, however, that liquefaction can occur over a broader range of soil types. Liquefaction of gravels and non-plastic silts has been observed in several earthquakes, though the database of these observations is small in comparison to that of clean and silty sands.

Liquefaction susceptibility is also strongly influenced by soil state. The "state" of an element of soil is defined by its density and effective stress. Castro (1969) showed that soils with low density under high effective stress consistently exhibited highly contractive behavior (with flow liquefaction) under monotonic loading (see Curves A in Figure 4.1); soils with high density under low effective stress consistently exhibited dilative behavior under monotonic loading (Curves C in Figure 4.1); and soils of intermediate density and/or intermediate effective stresses exhibited limited liquefaction (Curves B in Figure 4.1). Building upon the critical void ratio concept first identified by Casagrande (1936), Castro postulated that a given soil sheared to large strain levels would eventually reach a steady state condition, and that the steady state stress conditions would be a function of void ratio alone. By plotting the steady state effective confining pressure as a function of void ratio, Castro defined a steady state line that marked the boundary between states susceptible to flow liquefaction and states not susceptible to flow liquefaction (Figure 4.2).

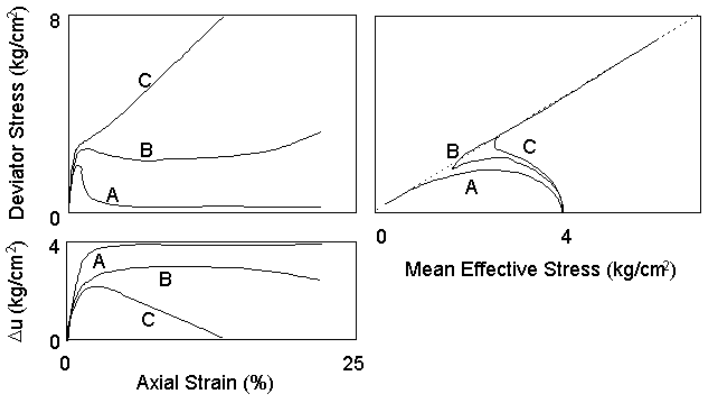

Figure 4.1. Three basic types of response observed by Castro (1969) in static triaxial tests: A – liquefaction, B – limited liquefaction, and C – dilation.

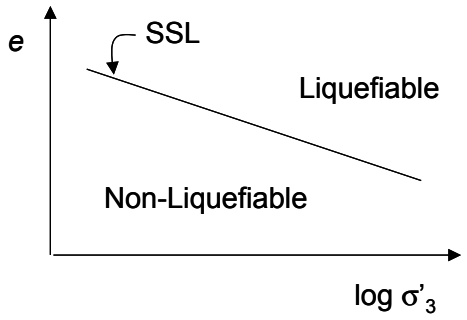

Figure 4.2. Steady state line.

For frictional materials such as most liquefiable soils, the existence of a unique relationship between density and steady state effective confining pressure implies a unique relationship between density and steady state shear strength. Castro observed such a relationship in triaxial compression tests. Subsequent triaxial testing (e.g., Vaid and Chern, 1985; Vaid et al., 1990; Verdugo and Ishihara, 1996; Reimer and Seed, 1997) suggests that the relationship between steady state strength and density may not be unique; instead, it may be a function of stress path (with extensional stress paths producing lower steady state strengths than compressional stress paths) and soil fabric. These conclusions, however, are actually based on observations of the so-called quasi-steady state strength, which is reached when the soil crosses the phase transformation line. The phase transformation line is the line at which the volume change behavior of a liquefiable soil changes from contractive to dilative. In general the quasi-steady state is mobilized at considerably lower strain levels than the steady state strength. The distinction between the quasi-steady state and the steady state is an important one, for both theoretical and practical reasons.

INITIATION OF LIQUEFACTION

Liquefaction can be initiated by non-seismic loading such as low amplitude vibrations produced by train traffic or by static loads such as those that might be caused by rapid drawdown. It is most commonly caused, however, by earthquake loading. Several approaches for evaluating the potential for earthquake-induced initiation of liquefaction have been proposed. The following sections provide a brief review of two of these approaches.

(a) Cyclic Stress Approach

The most well-documented and commonly used procedure for evaluating liquefaction potential is referred to as the cyclic stress approach. In the cyclic stress approach, both the loading imposed on the soil by the earthquake and the resistance of the soil to liquefaction are characterized in terms of cyclic shear stresses. By characterizing both loading and resistance in common terms, they can be directly compared to determine the potential for liquefaction.

Characterization of Loading

For the purposes of liquefaction evaluation, loading is typically characterized in terms of the cyclic stress ratio, *CSR*, which is defined as the ratio of the equivalent cyclic shear stress, τ_{cyc}, to the initial vertical effective stress, σ'_{vo}.

$$CSR = \frac{\tau_{cyc}}{\sigma'_{vo}} \tag{4.1}$$

The equivalent cyclic shear stress is generally assumed to be equal to 65 percent of the peak cyclic shear stress, a value arrived at by comparing rates of porewater pressure generation caused by transient earthquake shear stress histories with rates caused by uniform harmonic shear stress histories. The factor was intended to allow comparison of a transient shear stress history from an earthquake of magnitude, *M*, with that of *N* cycles of harmonic motion of amplitude $0.65\tau_{max}$, where *N* is an equivalent number of cycles of harmonic motion. If *N* is obtained from Figure 4.3, the porewater pressures generated by the transient and harmonic shear stress histories should be generally equivalent. In a procedure commonly referred to as the "simplified method," the peak cyclic shear stress is estimated from the peak ground surface acceleration and a depth reduction factor, r_d, which represents the average rate at which peak shear stress attenuates with depth. In the simplified method, therefore, the cyclic stress ratio is defined as

$$CSR = 0.65 \frac{a_{\max}}{g} \frac{\sigma_v}{\sigma'_{vo}} r_d \tag{4.2}$$

The simplified method is very commonly used in geotechnical engineering practice.

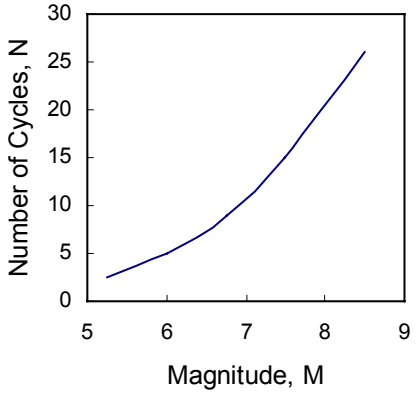

Figure 4.3. Number of equivalent cycles of loading to evaluate liquefaction potential.

Characterization of Resistance

Liquefaction resistance is also typically expressed in terms of a cyclic stress ratio, although that ratio is now commonly referred to as the cyclic resistance ratio, *CRR*. The cyclic resistance ratio is defined as the cyclic stress ratio that just causes initial liquefaction. The cyclic resistance ratio is typically determined as a function of two parameters: penetration resistance and earthquake magnitude.

Early procedures for evaluating liquefaction potential determined liquefaction resistance from the results of laboratory tests. Subsequent investigations showed that laboratory test results were significantly influenced by a number of factors, such as soil fabric, that could not be reliably replicated in laboratory test specimens. As a result, it is now most common to relate cyclic resistance ratio to corrected Standard Penetration Test resistance, i.e., $(N_1)_{60}$. Youd and Idriss (1997) recently proposed a graphical relationship between CRR and $(N_1)_{60}$ (Figure 4.4). This graphical relationship is appropriate for M7.5 earthquakes; correction factors for other earthquake magnitudes have been proposed by various researchers (Figure 4.5). Youd and Idriss (1997) recommended the use of magnitude scaling factors in the range between the curves of Idriss and Andrus and Stokoe (Figure 4.5).

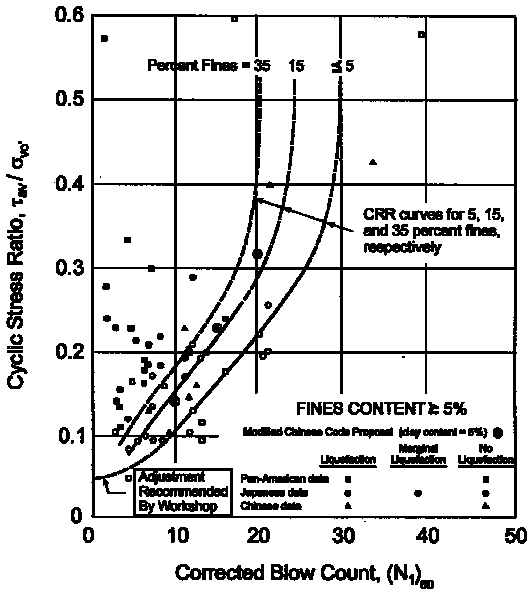

Figure 4.4. Relationship between cyclic stress ratio and $(N_1)_{60}$ for M_w = 7.5 earthquakes.

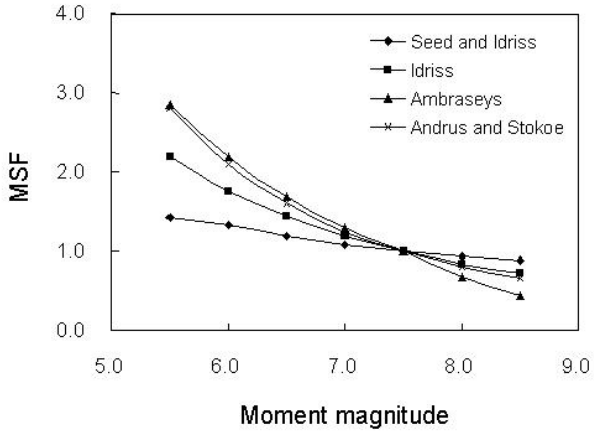

Figure 4.5. Magnitude scaling factors.

Evaluation of Liquefaction Potential

The potential for initiation of liquefaction in a particular earthquake is usually expressed in terms of a factor of safety against liquefaction. The factor of safety is defined in the usual way, as a ratio of capacity to demand. In the case of liquefaction, the factor of safety can be expressed as

$$FS = \frac{CRR}{CSR} xMSF \tag{4.3}$$

Factor of safety values less than 1.0 indicate that initial liquefaction is likely. Note that this factor of safety does not distinguish between flow liquefaction and cyclic mobility, and it provides no information on post-liquefaction behavior. Because it is based on case history data from locations where liquefaction is evidenced by ground surface disruptions such as sand boils, cracks, ground oscillation, etc., it provides an indication of the likelihood of such effects at the site of interest.

(b) Energy Approach

Although the method based on cyclic stresses has seen widespread use in geotechnical engineering practice, it has significant limitations. In particular, because liquefaction is caused by the generation of excess porewater pressure, and excess porewater pressure generation is caused by the tendency of individual soil particles to move into a denser configuration, liquefaction should be strongly influenced by the level of strain induced in the soil. In fact, detailed laboratory investigations (e.g., Dobry and Ladd, 1980) have shown that the rate at which pore pressure is generated in saturated sand is largely controlled by cyclic shear strain amplitude.

One measure that reflects both cyclic stress and strain amplitudes is dissipated energy. Nemat-Nasser and Shokooh (1979) developed a relatively simple theory that related soil densification (drained conditions) and pore pressure generation (undrained conditions) to dissipated energy. Others have since attempted to characterize the relationship between excess pore pressure and dissipated energy experimentally.

Kayen and Mitchell (1997) noted that Arias intensity is equal to the total energy absorbed by a population of simple oscillators spaced evenly in frequency, and proposed that

liquefaction potential could be evaluated by using Arias intensity. Arias intensity (two-component) can be computed from two orthogonal accelerograms as

$$I_h = \frac{\pi}{2g}\left[\int_0^{t_O} a_x^2(t)dt + \int_0^{t_O} a_y^2(t)dt\right] \tag{4.4}$$

or estimated at the surface as a function of source parameters from an attenuation relationship (Figure 4.6).

$$FS = \frac{I_{hb,l}}{I_{hb,eq}} \tag{4.6}$$

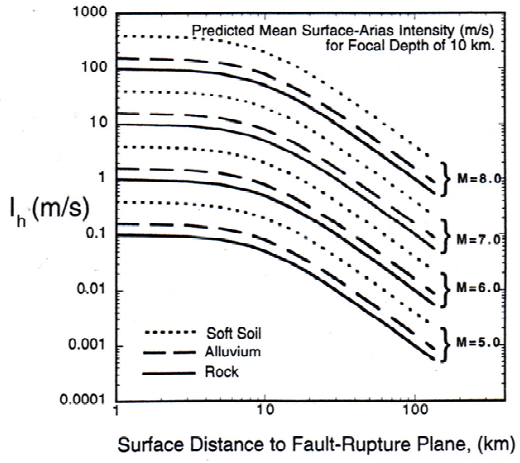

Figure 4.6. I_h for 50th percentile earthquake response plotted as a function of surface distance to fault rupture, r; moment magnitude, M; and site material properties of rock, alluvium, and soft soil, based on 10 km earthquake focal depth (after Kayen and Mitchell, 1997).

To account for the effect of depth on Arias intensity, a depth-reduction parameter, r_b, was suggested to correct the estimated Arias intensity at the surface:

$$I_{hb} = r_b * I_h \tag{4.5}$$

The parameter r_b represents the average rate at which Arias intensity attenuates with depth. Liquefaction resistance was correlated to *in situ* test parameters such as $(N_1)_{60}$ and q_{c1} by careful evaluation of liquefaction case histories (Figure 4.7.a and 4.8). Kayen and Mitchell (1997) showed that the use of Arias intensity provided a better discrimination between cases of liquefaction and non-liquefaction than can be obtained for the cyclic stress approach (Figure 4.7.b). In this approach, the factor of safety against liquefaction is defined

as the ratio of the Arias intensity required to cause liquefaction, $I_{hb,l}$, to the Arias intensity produced by the ground motion, $I_{hb,eq}$.

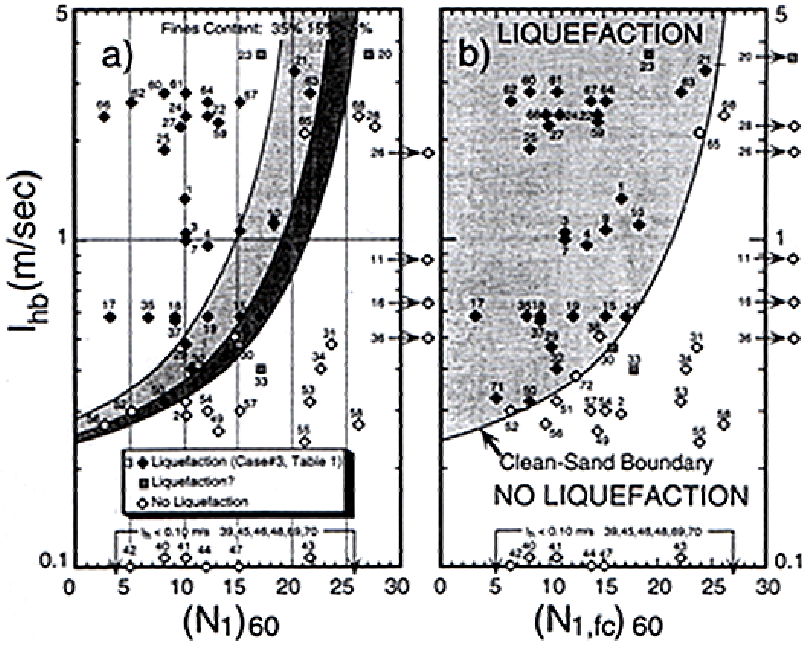

Figure 4.7. Relationship between SPT resistance and Arias intensity required to trigger liquefaction a)Plot without fines content correction; b)Plot with fines content correction to equivalent "clean sand"(after Kayen and Mitchell, 1997).

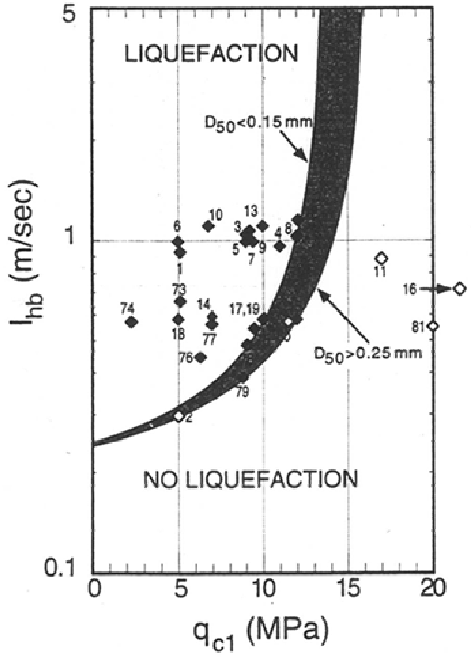

Figure 4.8. I_{hb} versus q_c. Boundary curves for $D_{50} > 0.25$ mm and $D_{50} < 0.15$ mm are based on field data and q_c-N relations (after Kayen and Mitchell, 1997).

Advantages of Arias Intensity Method Over Simplified Approach

The Arias intensity approach has several advantages over the cyclic-stress method that uses peak ground acceleration (PGA) as a basis for characterizing loading and resistance, including the following:

1- Arias intensity integrates in one value the effect of both stress and strain.
2- Arias intensity is derived from the entire acceleration records of both horizontal components of motion, whereas PGA uses a single, arbitrarily selected value.
3- Arias intensity incorporates the intensity of motions over the full range of recorded frequency, whereas PGA is often associated with high-frequency motion.
4- Because Arias intensity incorporates both amplitude and duration of earthquake motion, it leads to one magnitude-independent boundary curve for the assessment of initial-liquefaction potential. Therefore, the Arias intensity approach does not require arbitrary magnitude correction factors.
5- The breakdown of soil structure that results in liquefaction is fundamentally more dependent on input energy than on a single level of acceleration
6- Arias intensity is appropriately compatible with energy-based penetration tests, such as SPT, and appears to be compatible with other destructive penetration tests, such as the CPT, that impart work to the soil.

EFFECTS OF LIQUEFACTION

Liquefaction can affect buildings and bridges in a number of different ways. Liquefaction phenomena can alter ground motions in terms of amplitude, frequency content, and duration. Liquefaction can also lead to ground failure, either through flow liquefaction or lateral spreading.

(a) Effects on Site Response

The characteristics of ground surface motions are well known to be influenced by local site conditions. The thickness, stiffness, and damping characteristics of the various soil layers that underlie a particular site control the relative amplification, or de-amplification, of various components of a bedrock motion. Stiff soil deposits tend to amplify the higher frequency components of a bedrock motion, while soft soil deposits amplify low frequency motions. Site response of liquefiable sites is somewhat unusual in that the stiffness of a

specific soil deposit can change rapidly and drastically between the beginning and end of the earthquake.

In general, the development of excess porewater pressure and consequent reduction in effective stress will lead to the softening of a liquefiable soil deposit. Therefore, a soil layer that may amplify relatively high frequency components of the early portion of a bedrock motion will tend to amplify successively lower frequency components as the motion proceeds.

Ground motions recorded at the surface of liquefiable soil deposits showed a pronounced reduction in high-frequency amplitude and increase in low frequency amplitude following initial liquefaction (Figure 4.9). This change in frequency content corresponds to the dramatic reduction in stiffness and strength that accompanies initial liquefaction. However, these ground motions often also display several isolated spikes of high accelerations (e.g., Figure 4.9). Viewed in accelerograms, these spikes have a distinctive concave-upward shape. Through the pioneering analyses of Elgamal and Zeghal (1992), the spikes are now known to be produced by episodes of dilation within the liquefied soil. As the soil dilates above the phase transformation line, it stiffens thereby leading to an increasing ability to transmit higher frequency motions with time.

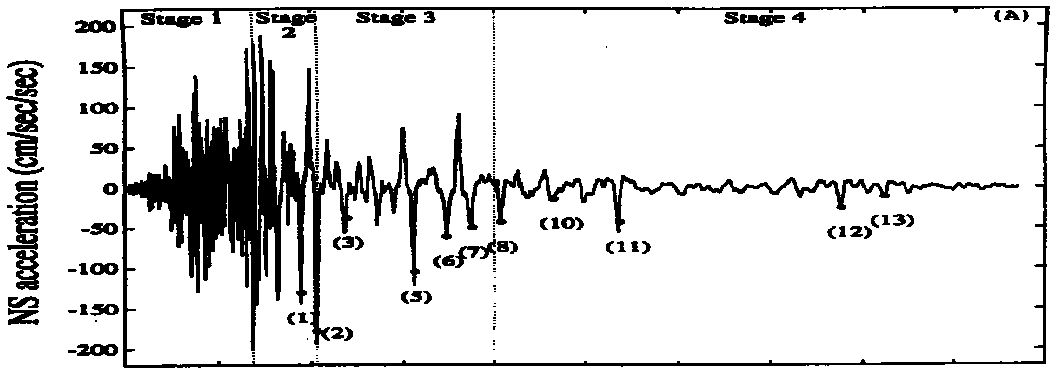

Figure 4.9. Time history of ground surface acceleration from Niigata, Japan. Note dramatic change in frequency content after initiation of liquefaction at 6 – 7 sec.

Evaluation of the effects of liquefaction on structures, particularly those located on level ground where permanent horizontal displacements do not occur, requires the ability to predict the generation of excess pore water pressure with time. When liquefaction occurs early in an earthquake, strong portions of the input motion may induce strong dilation pulses

in the liquefied soil; these pulses may produce high accelerations with high velocities and displacements. If liquefaction occurs later in the earthquake, the stronger portion of the input motion may occur before initial liquefaction has occurred. The resulting ground motions for these two cases can be significantly different.

(b) Settlement

The tendency for contraction, i.e., for densification due to applied shear stresses, produces liquefaction in saturated soils. The generation of excess porewater pressure, however, is a transient event. Following strong earthquake shaking, the presence of excess porewater pressure implies the presence of hydraulic gradients that will cause the porewater to flow until hydrostatic porewater pressure conditions are once again reached. This dissipation of excess porewater pressure occurs through the process of consolidation and is accompanied by a reduction in the volume of the soil, which is typically manifested in the form of settlement of the ground surface.

Ground surface settlement following liquefaction has been observed in numerous earthquakes. Large areas of settlement can produce regional subsidence, which can lead to submergence of low-lying coastal areas (Figure 4.10). While regional subsidence can produce relatively uniform settlements of the area occupied by an individual structure, more localized settlement can produce significant differential settlement. Differential settlement can impose high demands on structures and lead to significant damage of structures supported on shallow foundations (Figure 4.11). Structural damage due to settlement can often be avoided by the use of deep foundations; piles that extend through liquefiable soils to derive their support from underlying dense/stiff soils will tend to hold the structure at its original elevation, even when settlement occurs. Though such foundations can prevent structural damage due to settlement, damage to non-structural elements such as utility connections can occur.

Figure 4.10. Coastal flooding due to liquefaction-induced subsidence in Golcuk (from Izmit Collection, Earthquake Engineering Research Center, University of California, Berkeley)

Figure 4.11. Structural failure due to liquefaction-induced settlement of isolated footing at Port of Taichung (from Izmit Collection, Earthquake Engineering Research Center, University of California, Berkeley)

(c) Flow Slides

The development of flow liquefaction can obviously lead to devastating damage. Structures founded in areas involved in deep flow slides can be carried long distances by those slides. Estimation of the forces exerted on pile foundations by flowing soil, for example, is an important contemporary challenge in geotechnical earthquake engineering.

Flow slides can be triggered during or after strong ground shaking. If the ground motion produces high porewater pressure in an area of a slope that is critical to the maintenance of stability, flow liquefaction may be triggered during the earthquake. In some cases, however, the highest porewater pressures are generated in zones that are not critical for stability – for example, under the central portion of an earth dam. Following earthquake shaking, redistribution of excess porewater pressure will cause porewater pressure to decrease in some areas but to temporarily increase in others. If excess porewater pressures migrate into areas that are critical for stability, a flow slide may be triggered at some period of time after earthquake shaking has ended. The occurrence of delayed flow slides depends on hydraulic as well as dynamic soil properties, and is likely to be strongly influenced by the presence and distribution of layers and seams of fine-grained soils.

Reliable evaluation of the effects of flow liquefaction on structures requires reliable estimation of the residual strength of liquefied soil. Accurate estimation of residual strength

has proven to be very challenging. Part of this challenge results from different interpretations of the term residual strength. Yoshimine and Ishihara (1998) provide a useful framework for understanding the mechanics of liquefiable soil behavior, and the different terms used to describe it, when liquefaction is produced by monotonic (static) loading.

(d) Lateral Spreading

Lateral spreading occurs when earthquake-induced shear stresses temporarily exceed the yield strength of a liquefiable soil that is not susceptible to flow liquefaction. Lateral spreading is characterized by lateral deformations that occur during earthquake shaking (and end when earthquake shaking has ended). The displacements may be small or large, depending on the slope of the ground, the density of the soil, and the characteristics of the ground motion.

Lateral spreading can occur in gently sloping areas or in flat areas adjacent to free surfaces. In both cases, static shear stresses that tend to drive displacements in a downslope direction exist. As earthquake-induced stresses produce softening and yielding of the soil, the static shear stresses cause permanent strain to accumulate preferentially in one direction. Because the residual strength exceeds the static shear stress, large flow deformations that could continue after the end of earthquake shaking do not develop.

Lateral spreading can have a severe impact on structures. Because it occurs so frequently in waterfront areas, it has historically had a profound effect on structures such as bridges and wharves (Figure 4.12) and, consequently, a strong economic impact on transportation systems and ports.

Several approaches are available for estimating permanent deformations associated with lateral spreading. The lateral spreading phenomenon is a complex one, and it has proven to be extremely difficult to make accurate *a priori* predictions of permanent deformations using analytical/numerical procedures alone. As a result, currently available procedures are empirically based.

Figure 4.12. Examples of the effects of lateral spreading on bridges and wharf structures: (a) Nishinomiya Bridge, (b) Port of Kobe wharf.

Bartlett and Youd (1992) used a large database of lateral spreading case histories with multiple linear regression analysis to develop empirical equations for ground surface displacement caused by lateral spreading. The database included a series of borehole logs and a series of measured displacement vectors; Bartlett and Youd (1992) used an interpolation procedure to estimate the average soil properties at the location of each displacement vector. By evaluating the statistical significance of a large number of possible source and site parameters, Bartlett and Youd (1992) were able to identify a set of parameters that produced reasonable predictions of ground surface displacement for two types of conditions: sites with gentle, constant slope (ground slope model) and sites with slopes of limited extent or steep banks (free-face model).

Rauch (1997) developed a procedure referred to as EPOLLS (Empirical Prediction Of Liquefaction-induced Lateral Spreading), which included three complementary components that could be used with different levels of site information. Rauch used essentially the same data as Bartlett and Youd but grouped nearby displacement vectors into individual slides and computed an average displacement and average soil properties for each slide. The number of boreholes per slide ranged from 0 to 10 with a median and mode of 2.

The regression analyses used to develop these predictive equations unexpectedly produced a negative coefficient for the peak acceleration term in the regional model; the implication of this is that the permanent displacements would decrease with increasing peak ground acceleration. Therefore, the EPOLLS model should be used very carefully for

conditions other than those corresponding to the database from which it was developed, particularly for very strong ground motions.

(e) Foundation Failure

Liquefaction can cause the failure of foundation systems by a variety of mechanisms. Both shallow and deep foundations can be damaged by soil liquefaction.

Perhaps the most visible of these shallow foundation failure mechanisms is through the loss of bearing capacity associated with loose, saturated soils with low residual strength. By this mechanism, the earthquake shaking can trigger flow liquefaction and dramatic bearing failures of the type shown in Figure 4.13.

Figure 4.13. Liquefaction-induced bearing capacity failure in Adapazari, Turkey (from Izmit Collection, Earthquake Engineering Research Center, University of California, Berkeley).

Local failure of shallow foundations can occur through the mechanism of cyclic mobility. In a manner analogous to the accumulation of lateral spreading displacements in sloping ground, the static stresses imposed in the soil beneath a shallow foundation can cause the accumulation of permanent strain in a particular direction. Permanent strains that develop in this manner lead to settlement of the shallow foundation. Such settlement in combination with lateral spreading can be extremely damaging to structures supported on shallow foundations (Figure 4.14).

Liquefaction can also have a significant impact on pile foundations. Liquefaction and lateral spreading in Niigata caused failure of pile foundations beneath the NHK Building (Figure 4.15) and the Showa Bridge (Figure 4.16). Liquefaction-induced failure of deep foundations has been observed in many other earthquakes (e.g., Figure 4.17).

Figure 4.14. Damage to Monterey Bay Aquarium Research Institute following 1989 Loma Prieta earthquake.

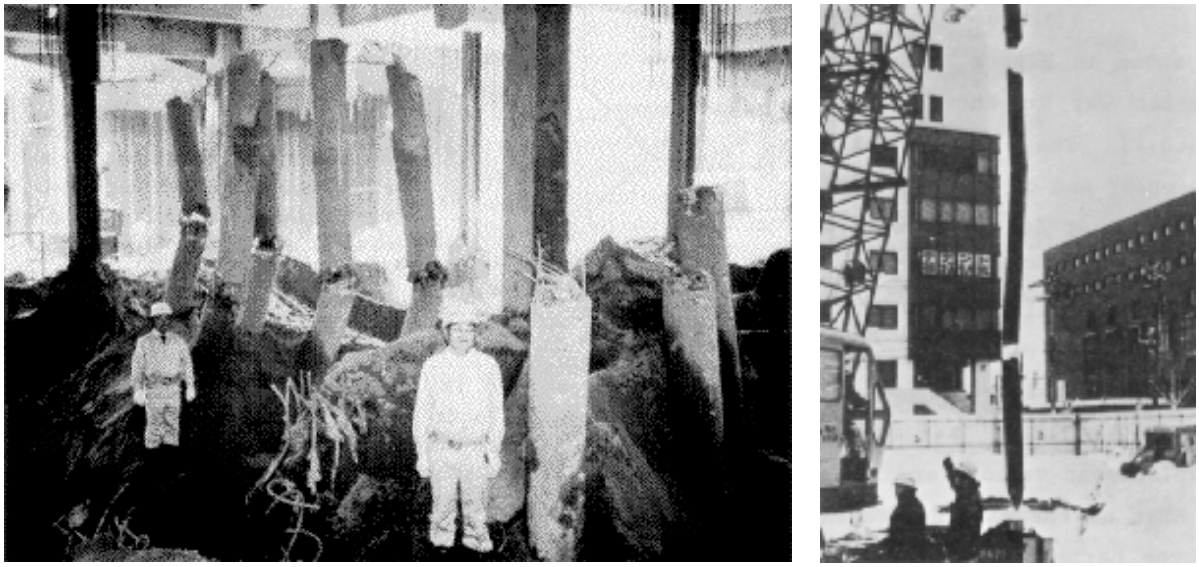

Figure 4.15. Pile damage due to lateral spreading beneath the NHK Building in Niigata, Japan.

Figure 4.16. Failure of Showa River bridge in Niigata, Japan, due to lateral spreading.

Figure 4.17. Pile damage due to lateral spreading in Kobe, Japan (from Izmit Collection, Earthquake Engineering Research Center, University of California, Berkeley).

SUMMARY

Liquefaction is a complex phenomenon that can strongly influence the response of structures during earthquakes. A number of practical procedures have been developed for evaluating liquefaction potential. Most of these procedures are deterministic.

While procedures for evaluating liquefaction susceptibility and liquefaction potential are well established and verified, procedures for evaluating the effects of liquefaction are less well established. The primary effects that lead to structural damage are permanent

deformation (lateral and vertical). These deformations can be produced by lateral spreading or flow sliding.

Practical, empirical procedures are available for estimating the ground surface displacements caused by lateral spreading. These procedures have been developed by regressing a large number of potential parameters against a database of observed lateral spreading case histories and retaining the parameters that showed high statistical significance. The resulting relationships are easily used, but they imply behavior that is inconsistent with some of the known characteristics of liquefiable soil.

The potential for flow sliding depends on the residual strength of a liquefied soil. Accurate estimation of residual strength has proven to be a difficult challenge, as apparent residual strengths can be produced by different physical mechanisms and apply to different strain ranges.

Chapter 5

A Warning Algorithm for Liquefaction-Induced Failure

This chapter describes the development of a warning algorithm for liquefaction-induced failure of the Alaskan Way Viaduct (AWV). The objectives of this study were to investigate the feasibility of a system that would reliably warn drivers of likely collapse early enough to react.

Variabilities in subsurface soil conditions and ground motions, combined with uncertainties in the modeling of seawall displacements, pile movements, and collapse make determination of a single, "right" answer virtually impossible. The most reasonable approach to dealing with these uncertainties is to quantify and account for them in a probabilistic framework. This approach provides a measure of the probability of collapse for a given measured ground-motion level.

A probabilistic framework can allow WSDOT to select levels of warning based on estimated probabilities of collapse of the AWV. This will allow for early or late warning, depending on the threshold, or probability, levels that WSDOT wishes to use. Balancing the cost of errors resulting from false alarms (early warning with a higher probability of occurring) and missed events (later warning with a lower probability of occurring) will likely dictate the threshold levels used for the algorithm.

SEQUENCE OF LIQUEFACTION-INDUCED FAILURE

Liquefaction-induced failure of the AWV is expected to result from a series of related events, as shown in Figure 5.1. This sequence would begin with sufficient strong ground motion from an earthquake to cause significant liquefaction of the underlying loose saturated sands. The onset of liquefaction would then soften the soils beneath the Viaduct and behind the seawall, resulting in significantly lower soil strength. The seawall immediately west of the Viaduct was not designed to resist the lateral pressures that would be imparted on it by low strength soils and would begin to move outward toward Elliott Bay. Movement of the seawall would cause significant lateral soil

movement at the location of the AWV; because of the variability of the soil, this movement would not occur uniformly. These variable soil movements would cause differential movement between the pile groups that support the AWV. This differential movement could lead to joint and column shear that exceeds capacity and causes the eventual collapse of the structure.

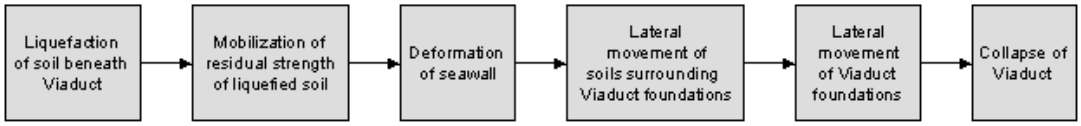

Figure 5.1. Sequence of events leading to potential liquefaction-induced collapse of Alaskan Way Viaduct.

Several sources of uncertainty exist within the sequence of events leading to the potential collapse of the AWV. An important part of this study was the identification and quantification of sources of uncertainty for input into a collapse analysis. This approach required the development of a probabilistic framework that would relate the potential for collapse to the level of ground motion measured at the Viaduct. The primary sources of uncertainty include the following:

1) *Subsurface soil conditions in the general vicinity of critical areas of the AWV.* Because site soils were historically placed as hydraulic fills, soil properties will vary along the AWV alignment. Furthermore, because soil explorations were accomplished at discrete locations, variation in the subsurface conditions will be present between borings.
2) *Ground motions that could cause liquefaction and subsequent damage to the AWV.* Seismic hazards in the vicinity of the AWV can come from intraplate, interplate, and subduction zone sources. This study considers ground motions with a range of different amplitudes, frequency contents, and durations that could occur within the design life of the AWV.
3) *Residual strength of liquefied soil.* As stated in Chapter 4, accurate estimation of residual strength has proven to be very difficult and is dependent on the

mechanism and strain range. The probabilistic approach used in the algorithm quantifies the uncertainties in the residual strength.

4) *Seawall displacements.* The seawall, which includes a pile-supported relieving platform, is a complicated structure and its interaction with liquefying soil is also complex. Kimmerling and Kramer (1996) performed a series of analyses to estimate the range of lateral displacements of the seawall displacements and the free-field at the location of the AWV, which could occur for various residual strengths. These analyses used a number of simplifying approximations, so their results include significant modeling uncertainty.

5) *Lateral pile displacement caused by free-field soil displacement.* The soil surrounding the AWV foundations will cause lateral movement of those foundations. Soil-pile interaction analyses can provide an approximate, but not exact, estimate of the lateral displacements of the AWV foundations.

6) *Differential movement of AWV columns.* The pile foundations support the AWV columns. Therefore, differential displacements between adjacent columns will induce potentially damaging shear and bending demands in the columns. Estimation of these demands requires characterization of uncertainty in differential foundation movement.

7) *Collapse displacement.* At some level of differential column displacement, brittle failure of one or more elements of the AWV superstructure could lead to collapse. Uncertainties in the design, construction, material properties, and behavior of the structure lead to uncertainties in estimates of the differential displacement required to cause collapse.

FRAMEWORK FOR WARNING CRITERION

A system intended to warn of the potential collapse of a structure must have some criterion by which it is activated. The criterion must be expressed in terms of some quantitative parameter(s), e.g., in terms of one or more measured ground-motion parameters. The system could be designed to provide a warning when a threshold value of the ground-motion parameter is reached. However, selection of the ground-motion threshold must balance conflicting requirements. It must ideally (a) be low enough that

all motions capable of causing collapse activate the warning system, (b) be high enough that the warning system is not activated by motions not capable of causing collapse, and (c) be of a form that can be determined as early as possible to maximize the amount of time available for people to react to the warning.

The uncertainties described in the previous section are large enough to require consideration in development of a criterion for collapse potential. Therefore, the warning criterion was expressed probabilistically, i.e., in terms of the probability of collapse given the warning criterion. The basic philosophy was to determine threshold ground-motion levels that give sufficient warning time and acceptable reliability of collapse prediction. Using the sequence of events leading to collapse, the following equation describes the basic framework:

$$P[C \mid \boldsymbol{Y}] = \sum P[C \mid d_{rel}]\, P[d_{rel} \mid d_{pile}]\, P[d_{pile} \mid d_{soil}]\, P[d_{soil} \mid S_r]\, P[S_r \mid L]\, P[L \mid \boldsymbol{Y}] \qquad (5.1)$$

where

$P[\ ]$ = probability,

C = collapse state,

$\boldsymbol{Y}$ = vector of ground-motion parameters,

d_{rel} = relative pile displacement,

d_{pile} = displacement of pile head,

d_{soil} = free-field ground surface displacement at location of AWV,

S_r = residual strength of soil after liquefaction, and

L = initiation of liquefaction.

The equation is based on the total probability theorem, which states that the probability of an event can be determined by summing the product of a series of conditional probabilities across all ranges of values. To evaluate the desired probabilities of collapse, conditional probability distributions for the parameters shown above are required.

As discussed in Chapter 4, an integral parameter (i.e., one that reflects the cumulative "strength" of shaking as it builds up with time) can be used to define the trigger for the initiation of liquefaction. An integral parameter is selected as a triggering criterion because it allows time rates of ground-motion intensity to be easily computed

from acceleration time histories. This parameter represents an important element of the vector of ground-motion parameters used in the above equation. The vector allows specification of a triggering criterion in terms of exceeding a specified threshold value ***Y**** at a specified time, *t**. Figure 5.2 shows a particular triggering criterion (i.e., a particular *t** - ***Y**** pair), along with plots of ***Y*** (in this case, Arias intensity is used as the integral ground-motion parameter) for two ground motions. For a given time, *t**, some events will generate sufficient energy to trigger liquefaction and are above the specified level of ***Y****. However some events will not generate the necessary intensity as they are below the trigger level of ***Y****.

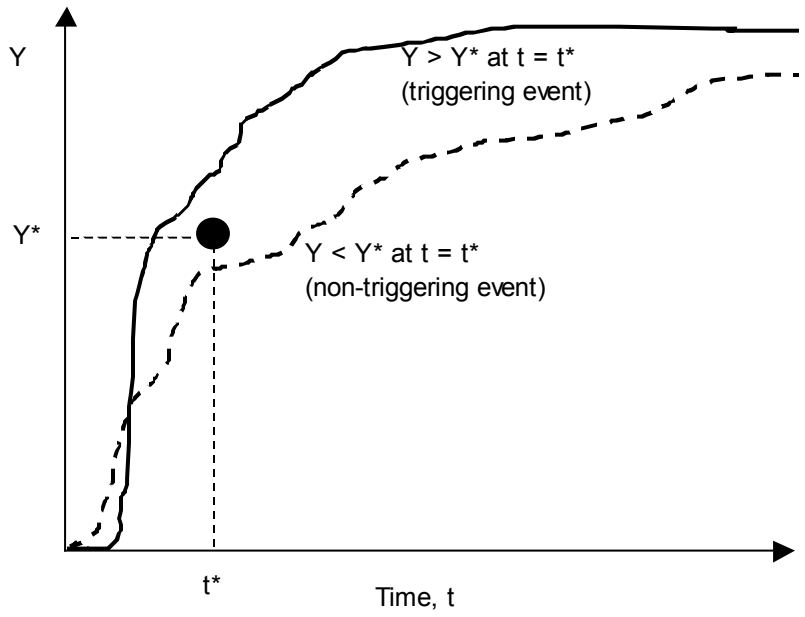

Figure 5.2 Variation of ground motion intensity with time relative to a particular trigger criterion.

UNCERTAINTIES IN EVALUATING LIQUEFACTION-INDUCED FAILURE POTENTIAL

The conditional probabilities listed in Equation 5.1 each represent the uncertainty in a parameter given the value of some other parameter. Each can be represented by a conditional probability density function, the nature of which will directly influence the reliability with which the eventual probability of collapse, P[C|**Y**], can be determined.

This section presents a detailed discussion of the sources of uncertainty considered in Equation 5.1. The approach was to identify and quantify the uncertainty in each parameter used in the analysis.

Subsurface Soil Conditions

Uncertainty in subsurface soil conditions was quantified by analyzing the results of SPT tests performed for the design of the AWV and for the seismic vulnerability evaluation reported by Kramer et al. (1995). These investigations indicated that the waterfront fill and tide flat deposit had a mean $(N_1)_{60}$ value of approximately 10, a standard deviation of approximately 4, and a scale of fluctuation of about 5 feet. This variability was used to simulate $(N_1)_{60}$ values for five soil profiles that were generated as one-dimensional Gaussian random fields in the liquefiable portions of the soil profile. This approach accounted for the variability in soil conditions with depth. The soil profiles used for this study represented those at the critical sections of the AWV as identified by Kimmerling and Kramer (1996). These profiles consisted of 10 feet of unsaturated sand underlain by 14 feet of saturated, liquefiable sand (below the ground water table) and 200 feet of very dense glacial till (silty, gravelly sand). The simulated SPT profiles are shown in Figure 5.2. Deterministic values of $(N_1)_{60}$ in the unsaturated sand and till were assumed to be 10 and 100, respectively. With the exception of soil density, soil properties (shear wave velocity, soil friction angle, dilation angle, etc.) were directly computed from published SPT blow count correlations. Soil density values used for this study are shown in Table 5.1.

Table 5.1. Soil density values.

Soil Material	Average Soil Density lb/ft^3 (Mg/m^3)
Unsaturated Sand	100 (1.60)
Liquefiable Sand	109 (1.75)
Glacial Till	140 (2.24)

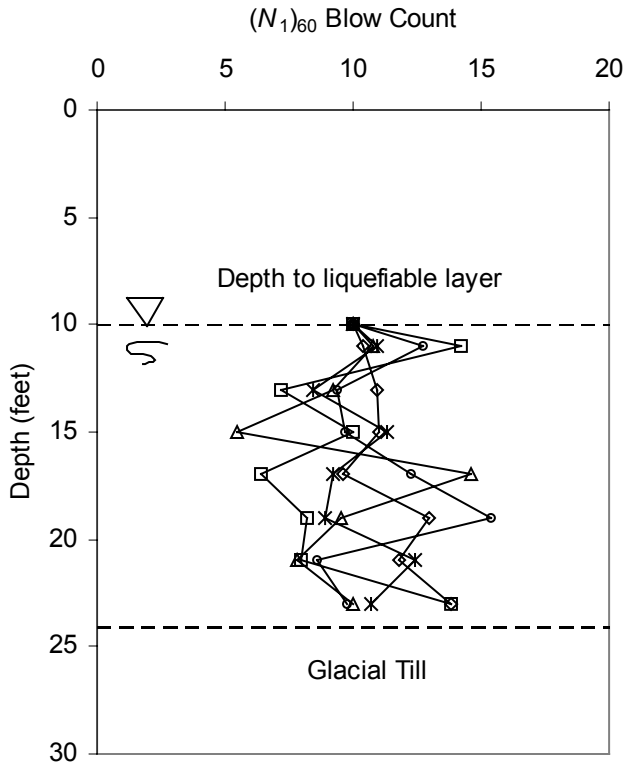

Figure 5.3. SPT profiles used for analysis.

Ground Motions

The uncertainty in ground motions was accounted for by using a large suite of representative strong ground motions. A total of 161 input base ground motions that were consistent (in terms of their distributions of magnitude and peak acceleration) with the results of a probabilistic seismic hazard assessment (PSHA) performed for another structure near the AWV were used. The spectra acceleration for the 161 base motions are shown in Figure 5.4. Arias intensity for the first 40 seconds of the base motions are shown in Figure 5.5. Time histories of normalized acceleration are shown in Appendix A. These motions were then applied to the program WAVE to obtain acceleration time history, resulting Arias intensity, and pore water pressure distribution with depth for a given value of a_{max}. WAVE is a one-dimensional, nonlinear, effective stress-based site response analysis program. Originally developed by Horne (1996), it has been extended with a new constitutive model, *UWsand*, which captures important elements of

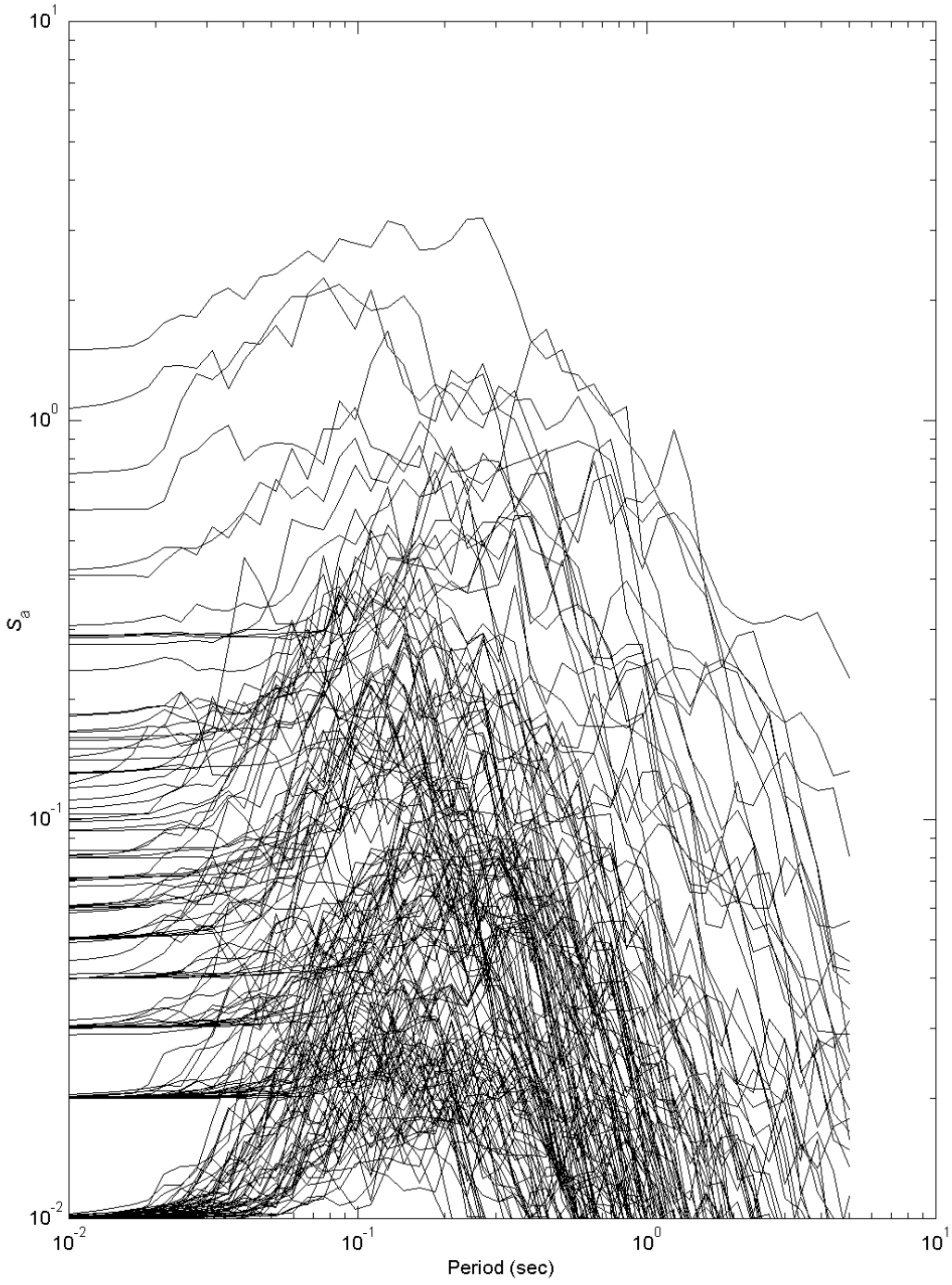

Figure 5.4. Response spectra for all input motions. Note that weaker motions (a_{max} < 0.08 g) were scaled to specific a_{max} values to obtain distribution of a_{max} that was consistent with the results of a probabilistic seismic hazard analysis.

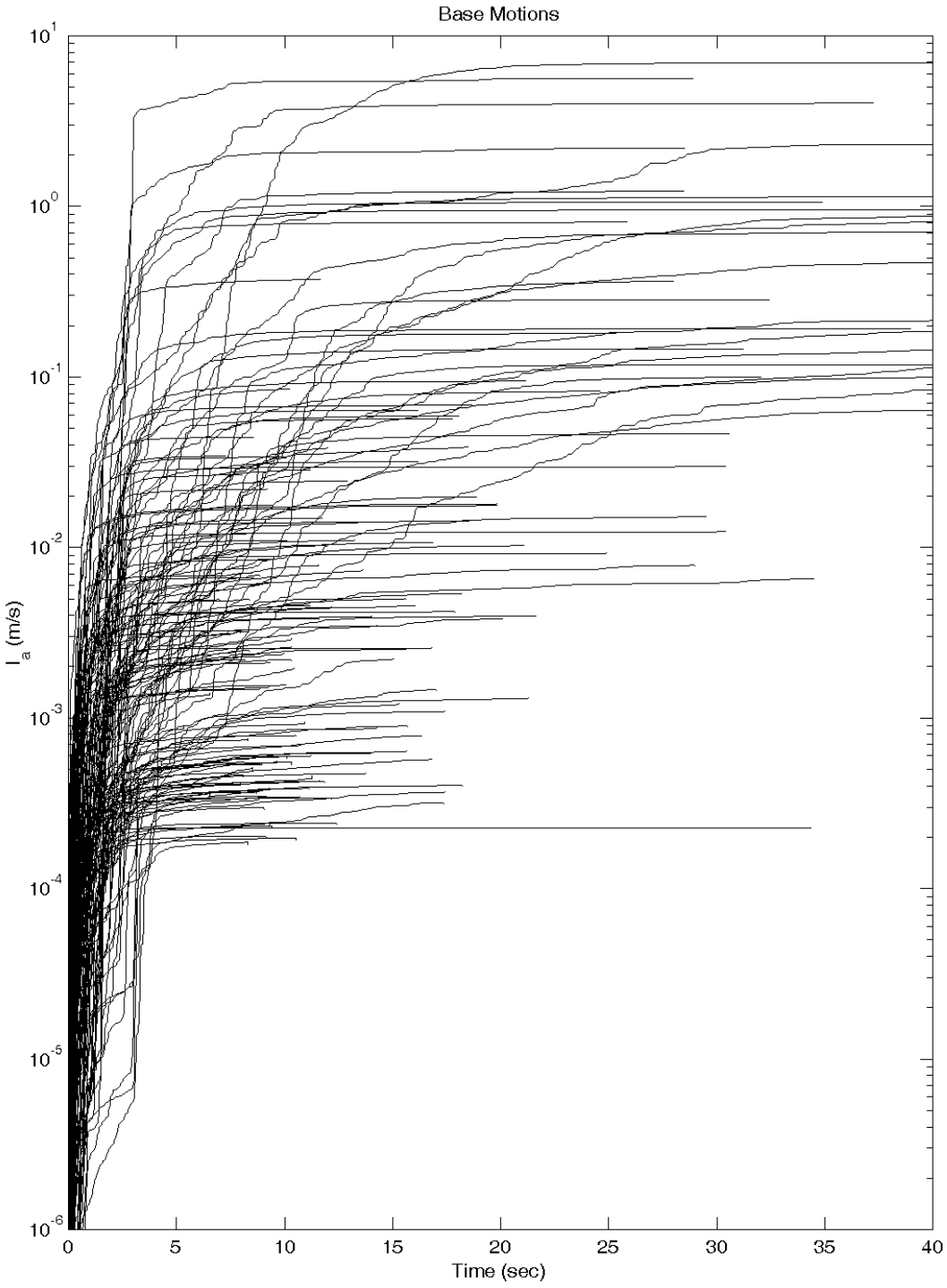

Figure 5.5. Arias intensity for the first 40 seconds of the base motions.

liquefiable sand behavior in a manner that can easily be calibrated. A more complete description of the *UWsand* model can be found in Appendix B.

Following the work of Kayen and Mitchell (1997), Arias intensity was selected as the ground-motion parameter to be used for setting the threshold. Arias intensity, defined for a single ground-motion component

$$I_a = \frac{\pi}{2g}\int_0^{\infty}[a(t)]^2 \tag{5.2}$$

is related to the cumulative energy dissipated by a population of single-degree-of-freedom systems subjected to that motion. It is an integral parameter, which means that its value can be determined at any point in an acceleration time history.

Pore pressures from the WAVE analyses were averaged in the lower part of the liquefiable layer (depths of 18, 20, and 22 feet), which is where liquefaction would be expected to occur first. Figure 5.6 shows the variation of average pore pressure ratio, r_u, with time for one particular ground motion scaled to peak accelerations of 0.05, 0.15, and 0.25g. Using a threshold of $r_u = 0.98$ for initiation of liquefaction, Figure 5.6 shows that liquefaction is not initiated in this motion for a peak acceleration of less than about 0.2 g. Now, consider a trigger time, t^*, at which a decision on whether to activate the warning system must be made. Figure 5.7 shows the same data with a potential triggering point at $\{t^* = 15$ sec, $I^*_a = 1$ m/sec$\}$. In this figure, the motion scaled to a peak acceleration of 0.05g has an Arias intensity well below $I_a^* = 1$ m/sec at $t^* = 15$ sec. Figure 5.6 also shows that this motion does not produce liquefaction (the maximum value of the average pore pressure ratio is approximately 0.88). The motion scaled to 0.15g does exceed $I_a^* = 1$ m/sec at $t^* = 15$ sec (Figure 5.7) and just reaches liquefaction (Figure 5.6). However, not all motions that exceed the trigger criterion eventually reach liquefaction. For this motion, 25 percent of the motions that exceeded the triggering point eventually produced liquefaction. Therefore, a motion with these characteristics has a 25 percent probability of producing liquefaction given that the Arias intensity exceeds 1.0 m/sec at a time of 15 sec after the beginning of shaking. Mathematically, this can be expressed as a conditional probability, i.e.,

$$P[L \mid I_a > 1 \text{ m/sec}, t < 15 \text{ sec}] = 0.25$$

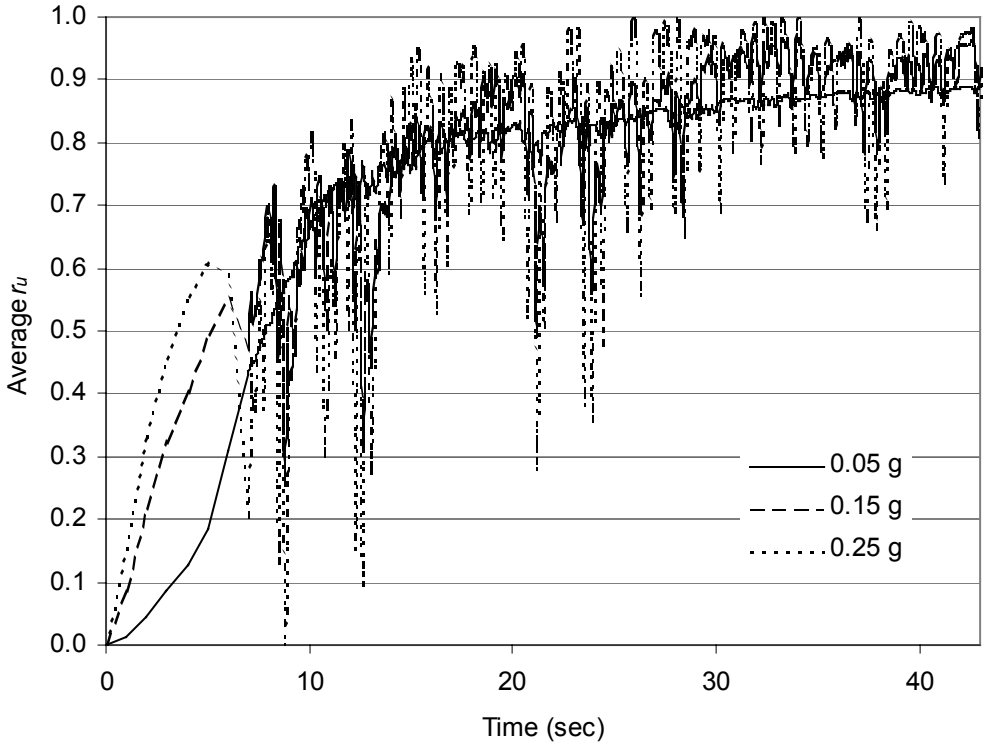

Figure 5.6. Variation of average pore pressure with time.

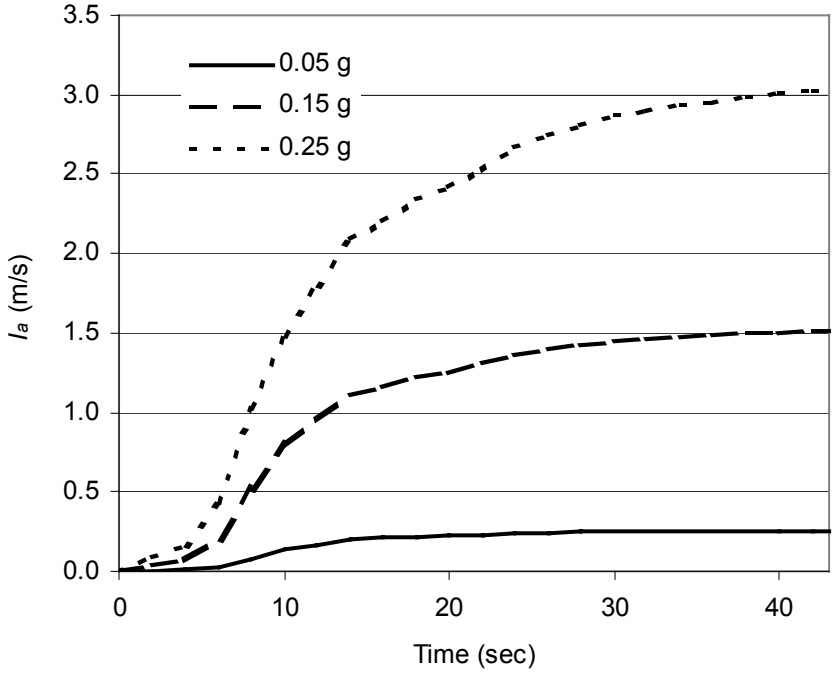

Figure 5.7. Variation of I_a with time.

This process was repeated for all of the ground motions and for a wide variety of Arias intensity (I^*_a = 0.0 – 0.6 m/sec) and trigger time values (t^* = 1, 5, 10, and 20 sec), resulting in a probability distribution consistent with the PSHA conditional on I^* and t^*.

The results can be expressed in the three-dimensional plot shown in Figure 5.8; this figure shows that the probability of liquefaction for a given trigger time increases as the Arias intensity level increases, and that the probability of liquefaction for a given Arias intensity level decreases as the trigger time increases. For a specified time threshold, t^*, events that exceeded a given Arias intensity, I^*, were included in determining whether the corresponding pore pressure ratio value, r_u, exceeded the value of 0.98 that was considered to represent the occurrence of liquefaction. Time zero was defined as the first time at which the absolute value of acceleration exceeded 0.005g. From this, the conditional probabilities of liquefaction occurring, given a time threshold, and exceeding a value of Arias intensity, could be computed. The resulting probability distribution as a function of Arias intensity and time to initiation of liquefaction is presented in Figure 5.8. Note that the probability of liquefaction increases with increasing Arias intensity for a given trigger time, and decreases with increasing trigger time for a given value of Arias intensity.

Residual Strength of Liquefied Soil

Uncertainty in the residual strength of the soil was characterized by using empirical relations developed by Seed and Harder (1990) in which the apparent residual shear strength was back analyzed from liquefaction-induced flow slides. Seed and Harder characterized the site conditions for each case history in terms of a singl, equivalent, clean sand blow count. For the case of the AWV, where average SPT blow counts are 10 bpf, the Seed and Harder chart predicts residual strength values of 100 – 400 psf. Because little is known of the distribution of residual strength, a uniform distribution across the range of residual shear strength recommended by Seed and Harder was assumed. The resulting probability density function for residual shear strength is shown in Figure 5.9.

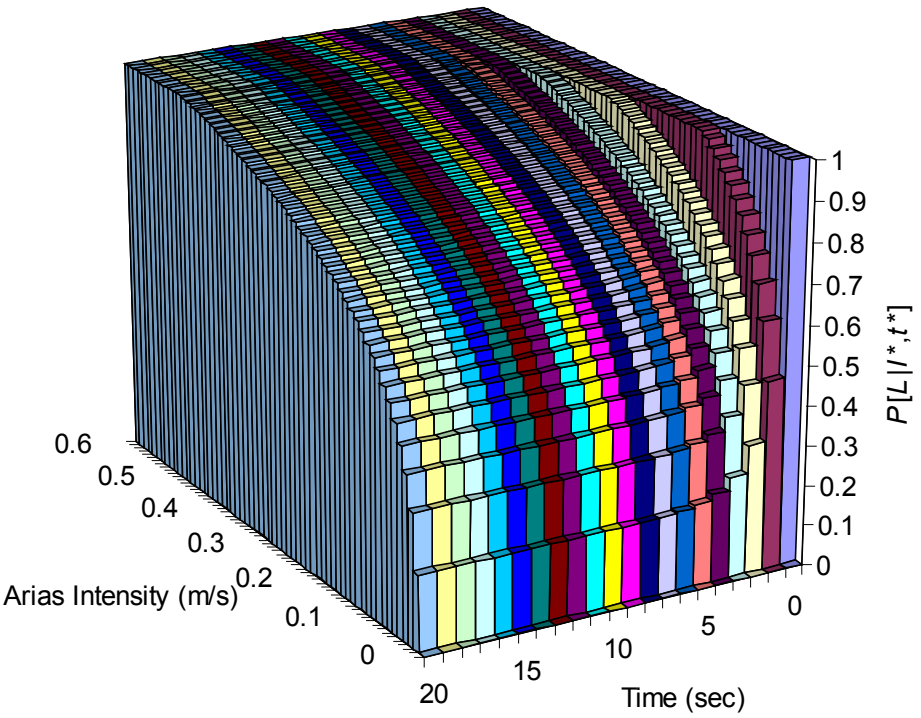

Figure 5.8. Liquefaction probability distribution

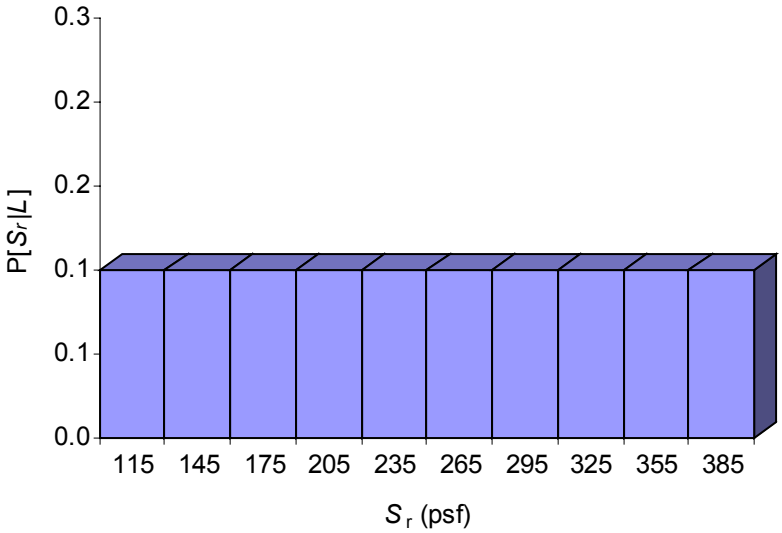

Figure 5.9. Residual strength probability density function

Uncertainty in Lateral Soil Displacement

As described earlier, studies of the seawall by Kimmerling and Kramer (1996) established an approximate relationship between the residual strength of the soil and soil displacement at the location of the AWV. The analyses showed that little soil displacement would be expected if the residual strength were greater than 1000 psf. For lower residual strengths, higher soil displacements can be expected. At residual strengths of about 200 psf or less, the analyses of Kimmerling and Kramer (1996) suggested catastrophic failure of the seawall with very large deformations. Although no probabilistic simulations of seawall deformations were performed by Kimmerling and Kramer, the approximate nature of the analyses indicated that considerable uncertainty should be assumed for the resulting displacement values; this uncertainty is expected to be higher for cases of lower residual strength (and higher displacement). On the basis of this interpretation, the total soil displacements were assumed to be lognormally distributed, with a median value given by the results of Kimmerling and Kramer and a coefficient of variation (on the natural logarithm of displacement) that ranged from 100 percent at a residual strength of about 100 psf to 65 percent at a residual strength of about 800 psf (Figure 5.10). Given the preceding, the resulting probability density function for total soil displacement, conditional on residual strength, can be computed as shown in Figure 5.11. The probabilities of all total displacements greater than 500 inches were lumped into the 500-inch bin, thereby producing higher probabilities associated with that displacement level. These probabilities and very low probability have been omitted from the figure for clarity; therefore the sum of the probabilities shown in Figure 5.11 is less than 1.0.

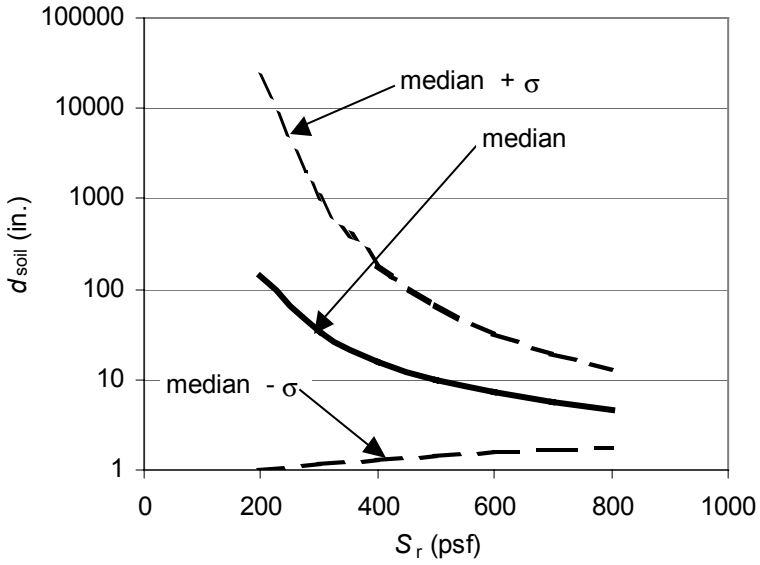

Figure 5.10. Free field soil displacement related to soil strength

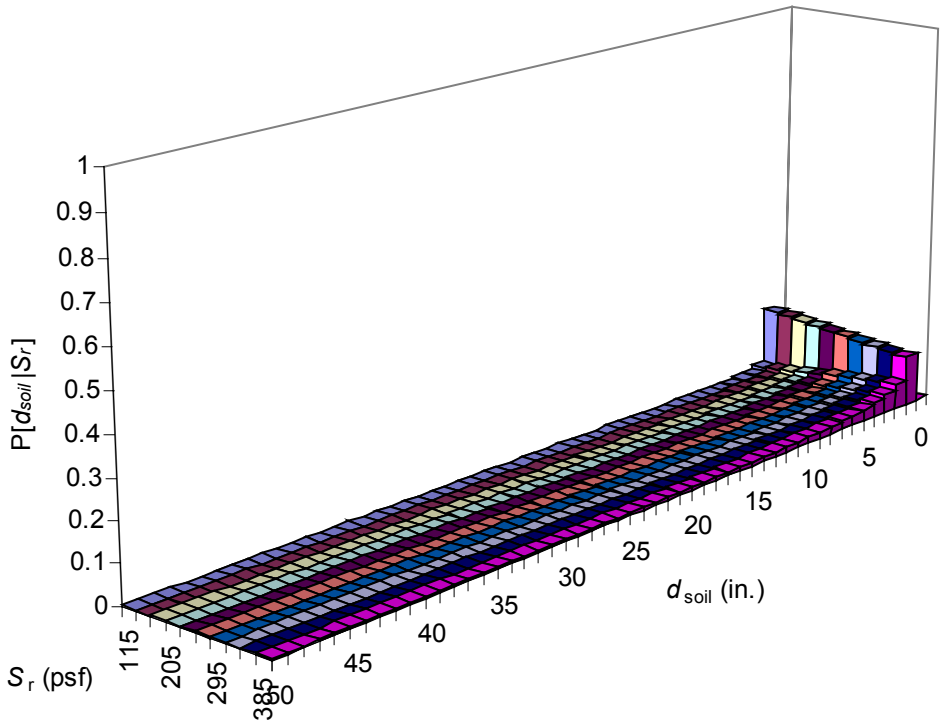

Figure 5.11. Probability density function of seawall displacement

Uncertainty in Total Pile Displacement

Uncertainty in total pile displacement was quantified by using the effect of total soil displacements imposed on the pile foundations. This was accomplished by using the effect of soil profile variability and ground-motion variability as input to a non-linear pile response analysis. The analysis was completed with a program called DYNOPILE (Horne 1996; Arduino and Kramer, 2001). DYNOPILE is a 1-dimensional soil-pile interaction model recently developed for the dynamic analysis of pile foundations. In DYNOPILE, the pile is modeled using a Beam-on-Nonlinear Winkler Foundation (BNWF) model. The BNWF model is coupled to the free-field by using a nonlinear rheologic model composed of separate near-field and far-field elements replicating hysteretic and radiation damping. Nonlinear, inelastic, *p-y* curves are used to characterize the stiffness of the near-field model, while the model proposed by Nogami and Konagai (1992) is adopted for the far-field. Excitation is provided by the free-field displacement and velocities generated by WAVE. Degradation of *p-y* curves with increasing excess pore pressure is also considered. The analysis proceeded as follows:

1) Ten random soil profiles were generated with procedures similar to those outlined in the Subsurface Soil Conditions section of this report. The profiles were assumed to have a slope of 3 percent.
2) Five ground motions were created by scaling a representative strong ground motion to a_{max} values of 0.1, 0.2, 0.3, 0.4 and 0.5 g.
3) Each profile was subjected to a one-dimensional site response analysis using WAVE to obtain the vertical distribution of final pore water pressure and the final free-field soil displacement profile for the 50 combinations of subsurface conditions and ground motions. The soil free-field displacement at the ground surface was designated d_{soil}.
4) For each of the ten random profiles generated in step 1), ten nonlinear *p-y* curves were generated at each depth increment. The *p-y* curves were generated as functions of $(N_1)_{60}$ using procedures outlined in O'Neill and Murchison (1983). For each depth in each profile, *p-y* curves were generated by assuming that $(N_1)_{60}$ values were normally distributed with *C.O.V.* = 40

percent about the value obtained from the random field simulation. For each profile, the final displaced shape of the pile was computed with DYNOPILE. For this analysis, an average pile diameter of 14 inches was used to represent typical AWV pile diameters of 12, 14, and 16 inches. The final pile displacement at the ground surface was designated d_{pile}. The ratio of the displacement of the pile to ground surface soil displacement was computed for each of the 500 simulations. Uncertainty in the ratio $d_{\text{pile}}/d_{\text{soil}}$ was estimated by considering the computed variabilities in the DYNOPILE analyses, estimated uncertainty in the non-liquefiable sands near the ground surface, and the variable pile diameters. The computed mean value and estimated uncertainty in $d_{\text{pile}}/d_{\text{soil}}$ are shown in Figure 5.12.

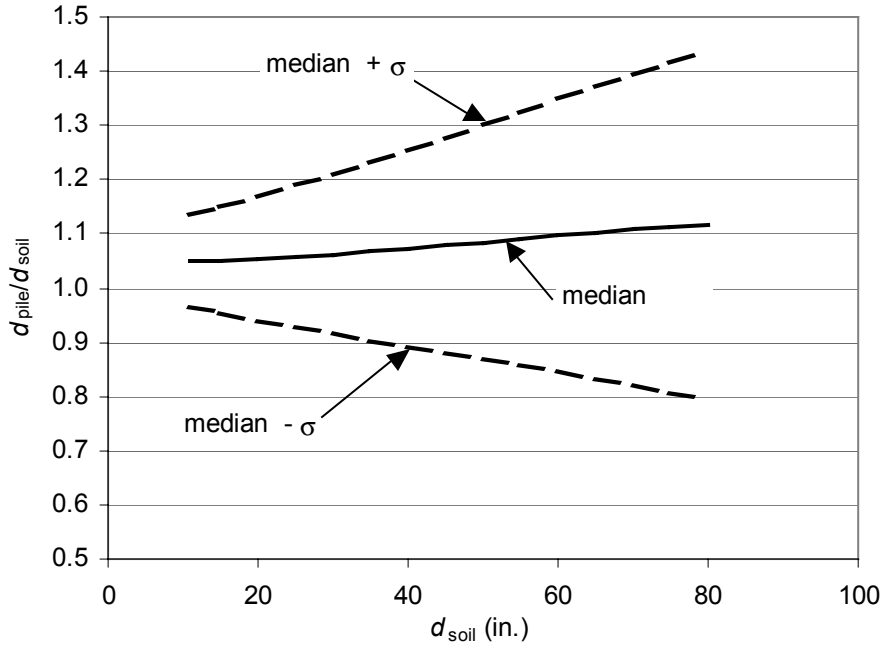

Figure 5.12. Relation between pile and soil displacements.

Given this relationship (and assuming that displacements are normally distributed), the resulting probability density functions for pile displacement given a certain soil displacement could then be generated (Figure 5.13).

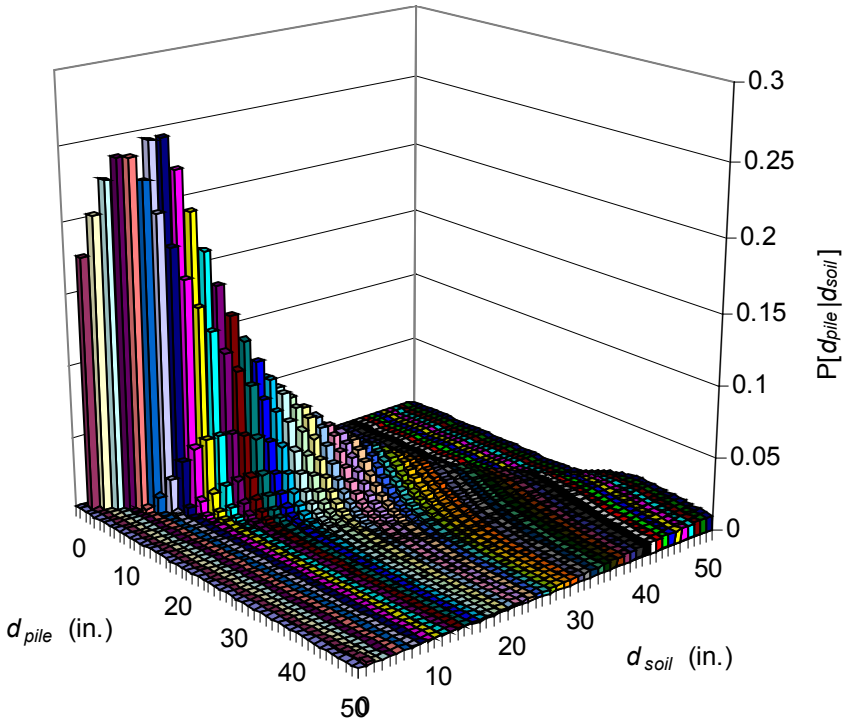

Figure 5.13. Probability density function for soil and pile displacements.

Uncertainty in Relative Pile Displacement

Most structures, including the AWV, are sensitive to relative displacements of their foundations. The results of the DYNOPILE analyses were also used to estimate uncertainty in the relative displacement between pile caps, i.e., the differential pile displacements. The final pile displacements at the ground surface for each DYNOPILE simulation were compared to each other to characterize relative displacements, which are expressed in the form of a ratio between the differential displacements to the average total pile displacement for each pair of pile analyses. For example, the relative displacements for analyses *i* and *j* would be expressed as

$$d_{rel} / d_{pile} = \frac{d_j - d_i}{\left[\frac{d_j + d_i}{2}\right]} \tag{5.3}$$

where d_i and d_j are the computed pile head displacements from analyses *i* and *j*, respectively. The ratio was doubled, purely on the basis of judgment, to reflect the fact that the pile-soil interaction analyses did not capture all sources of differential foundation movement.

A histogram was generated by sorting differential displacement versus the displacement ratio computed from Equation 5.3 (Figure 5.14). This information was used to construct the conditional probability distribution function shown in Figure 5.15. Relative pile displacements were expected to occur from 0 to 25 inches. Once again, the probabilities for soil displacements greater than 50 inches are not shown for figure clarity.

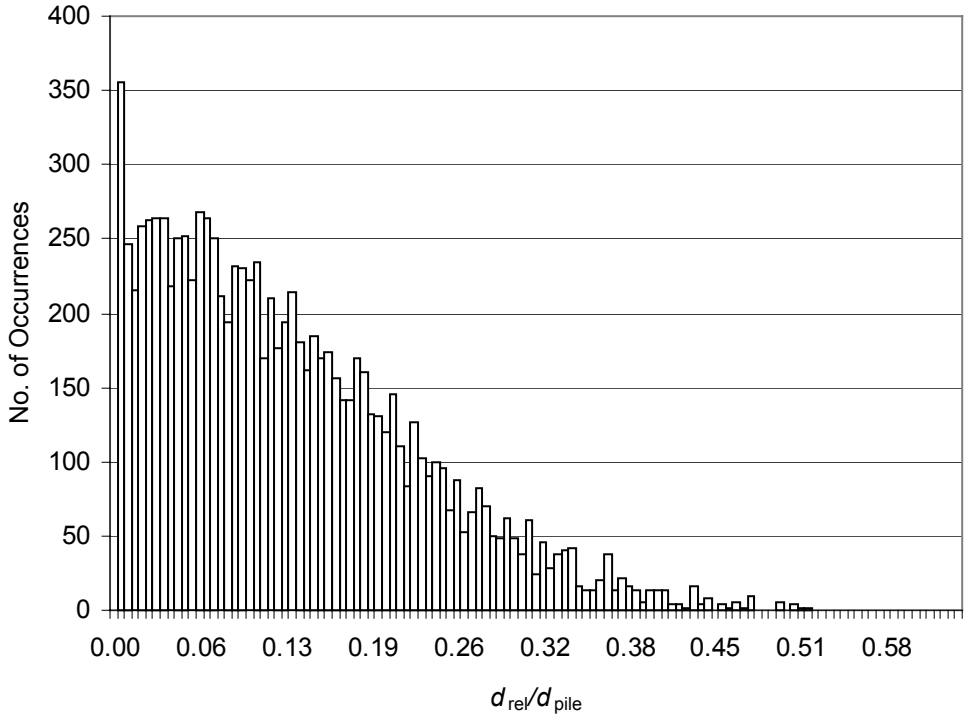

Figure 5.14. Probability distribution function for ratio of soil displacement to pile displacement (N = 10,000).

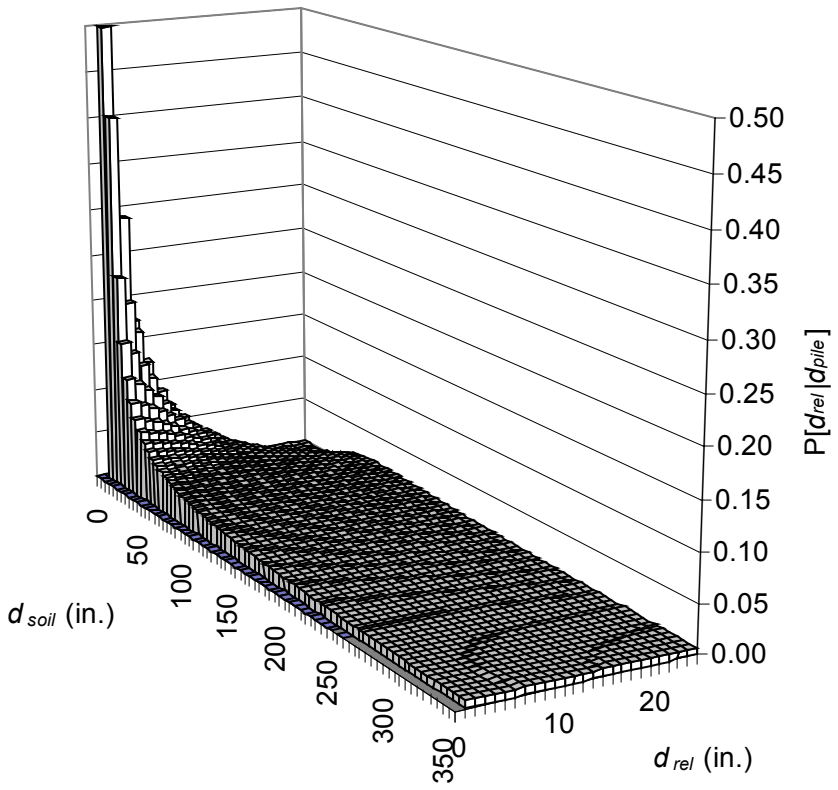

Figure 5.15. Probability density functions for relative pile displacement given displacement of the soil.

Uncertainty in Structural Failure

The vulnerability of the Alaskan Way Viaduct structure to differential pile-cap displacements is difficult to estimate because numerous sources of uncertainty affect such estimates. The strengths of the structural materials, and the extent to which they vary along the length of the Viaduct, are not known accurately. The Viaduct has a wide variety of geometric configurations and structural details (Chapter 3), and to limit the scope of this study, many of these configurations and details were not considered. Variations between the structural design and the in-place constructed structure further clouded estimates of the current state of the 50-year-old Viaduct. The timing of the pile-cap displacements also complicated the evaluation. These displacements would occur after a strong earthquake, so the relevant "initial" state at the beginning of the pile-cap displacement analysis would be the state of the structure at the *end* of the strong shaking.

The vulnerability analysis was hindered also by the paucity of quantitative information on the accuracy of assessment methods for poorly detailed reinforced

concrete structures. The few methods available have not been calibrated against a large number of tests, the methods were not developed for previously damaged structures, and the methods were not developed to predict structural collapse. In general, these methods were developed to predict less catastrophic levels of structural damage.

To keep the scope of the analysis manageable, structural calculations were performed only for the interior and exterior frames of the Seattle Engineering Department (SED) typical unit. This unit, rather than the WSDOT unit, was selected for analysis because previous analyses (Knaebel et al. 1995) had found that its columns were susceptible to shear failure. Only two failure modes were considered: shear failure of the first-story columns and shear failure of the first-level beams.

The implementation of the assessment strategy is illustrated in Figure 5.16. The strategy combined deterministic choices (e.g., selection of critical frames and failure modes), estimates of uncertainties (e.g., material strengths), and estimates of model inaccuracy (e.g., displacement ductility at the onset of shear-strength degradation).

- For a particular pile-cap displacement, the vulnerability assessment was repeated 1000 times, each time with a new set of material properties, characteristics for the member demand analyses, and the properties of the member fragility models. Table 5.2 lists the parameters that were varied and the assumed values for their mean and coefficients of variation.
- COLUMN DISPLACMENT DUCTILITY DEMAND. For a given pile-cap displacement and a particular set of analysis parameters, the displacement-ductility demands (μ) for the interior and exterior columns were estimated on the basis of their effective column strengths and column stiffnesses. Column flexural strengths were determined from the results of Knaebel et al. (1995), whereas effective column stiffnesses were determined from nonlinear, plane-frame analyses conducted with Dr. Frame (www.drsoftware.com). The coefficients of variation for column stiffness and strength were determined from comparisons on measured and calculated force-displacement responses of columns tested in the laboratory.
- COLUMN-SHEAR FAILURE. For each displacement-ductility demand, the prediction of column-shear failure was based on the degrading-shear-strength

procedures proposed by Priestley et al. (1992), which are illustrated schematically in Figure 5.17. Assumed coefficients of variation for the fragility parameters, reported in Table 5.2 were based solely on judgment.

- BEAM-COLUMN CRACK OPENING. Shear failure of the first-level beams was evaluated on the assumption that the beams would fail if a crack opened up sufficiently at the bottom of the beam at the beam-column interface. The relationship between pile-cap displacement and crack width was determined on the basis of frame analysis (assuming stick members located at member centerlines) for three scenarios: (1) rigid beam-column joint (40 percent likelihood), (2) flexible beam-column joint (50 percent likelihood), and (3) flexible beam with hinges forming in the beam end and at the second-story splice (10 percent likelihood).
- BEAM-SHEAR FRAGILITY. For each beam-column crack width, shear failure was expected when the beam-column crack width exceeded, on average, 0.75 in.
- COMBINATION. Failure by either mode in either frame was assumed to cause failure of the SED unit. Note that these analyses did not account for the large number of nominally identical frames in the Viaduct. In effect, the analysis assumed that only one exterior and one interior frame would be subjected to large pile-cap displacements.

The resulting fragility curves are shown in Figure 5.18. According to these curves, the fragility of the unit is dominated by the column-shear failure mode. The possibility of column-shear failure becomes significant at a displacement of approximately 10 inches. At a displacement of approximately 14 inches, the curves indicate that the likelihood of collapse is 50 percent.

Table 5.2**.** Parameter variation for calculating structural fragility curves.

	Parameter	**Assumed Mean Value**	**Assumed Variability**
Material Properties	Concrete Nominal Compressive Strength, f'c	6300 psi	COV = 15%
	Steel Yield Stress, fsy	36.3 ksi	COV = 10%
Column-Shear Demand Analysis	Column Effective Stiffness	88 k/in. (INT) 36 k/in. (EXT)	COV = 20%
	Column Flexural Strength	3200 k-ft (INT) 3000 k-ft (EXT)	COV = 10%
Priestley et al. (1992) Column-Shear Fragility Model	Vci	3.5 $\sqrt{f'c}$ 0.8 Ag	COV = 10%
	Vcf	1.2 $\sqrt{f'c}$ 0.8 Ag	COV = 15%
	μ_i	2	COV = 10%
	μ_f	4	COV = 15%
	Vs * (s * tan 30)/ (Av * fsy * D')	1 for $\mu \leq \mu_i$ varies for $\mu i < \mu \leq \mu f$ 0 for $\mu > \mu_f$	COV = 0%
	Vp	P tanα	COV = 15%
Crack Opening Analysis	Crack Opening / Pile-Cap Displacement	0.01 0.03 0.06	40% 50% 10%
Beam-Shear Fragility Model	Critical Crack Opening	0.75 in.	COV = 25%

Additional details and discussion about the likely structural performance of the Viaduct can be found in Chapter 6, as well as in previous reports on the WSDOT (Eberhard et al. 1995) and SED (Knaebel et al. 1995) typical, three-span units.

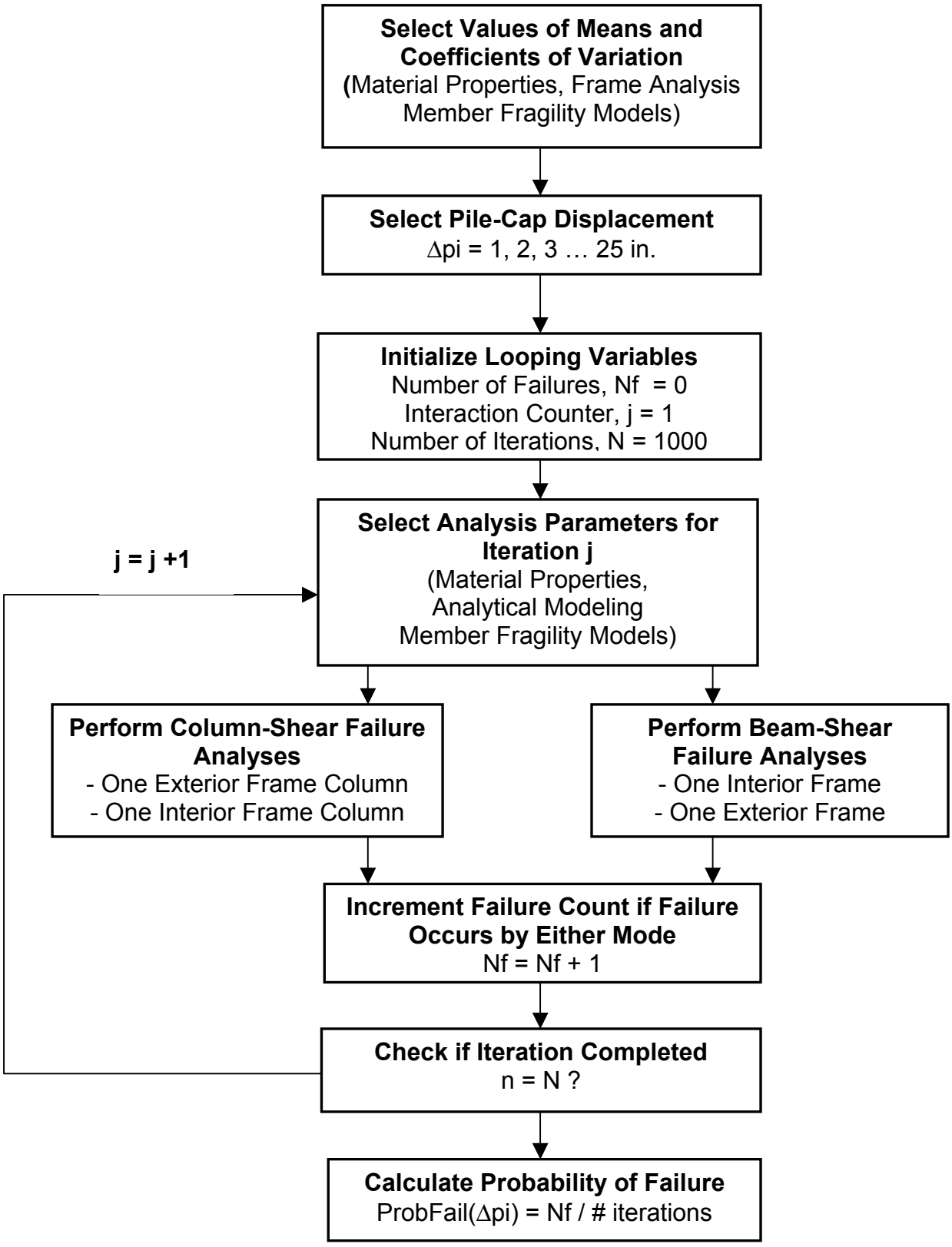

Figure 5.16. Flowchart for calculating structural vulnerability to pile-cap displacements.

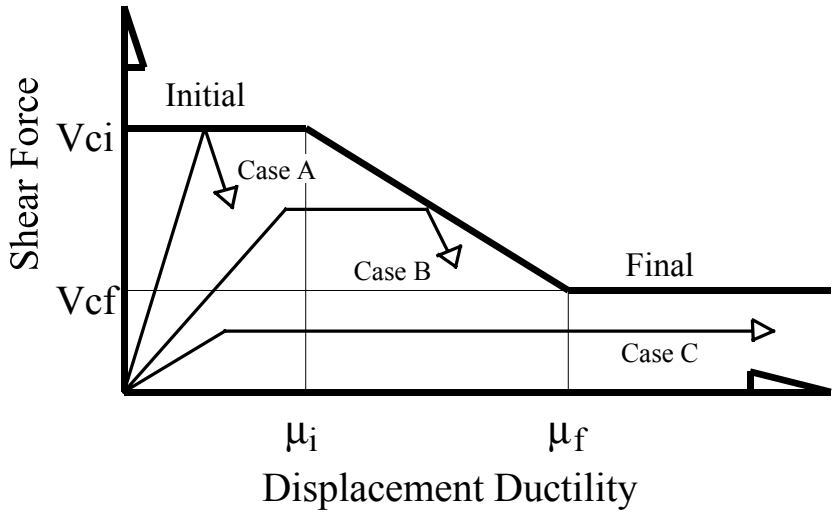

Figure 5.17. Variation of column shear resistance with displacement ductility.

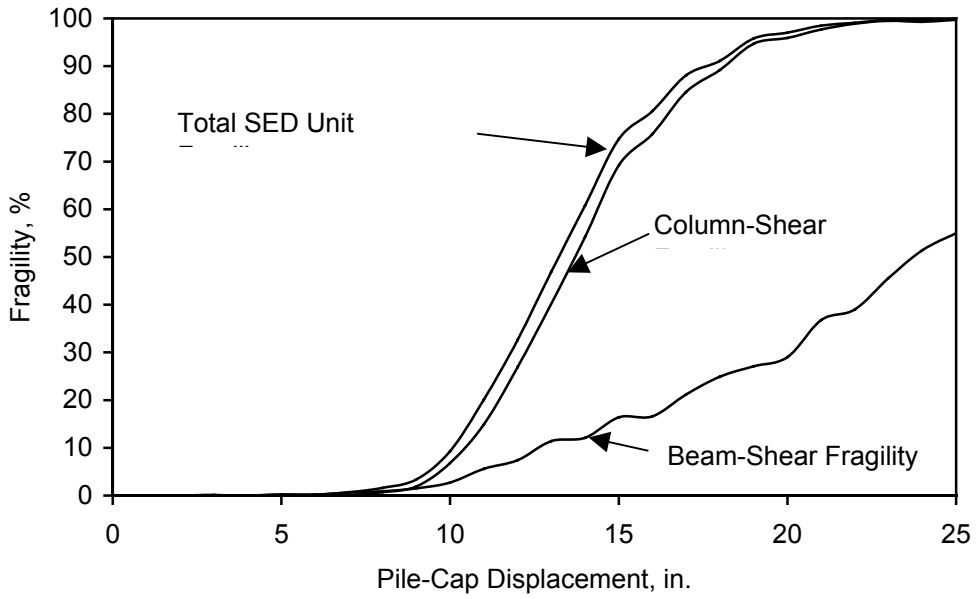

Figure 5.18. Structural fragility curves for SED typical unit.

RESULTS OF PROBABILISTIC ANALYSIS

The probability density functions in the previous section were used with Equation 5.1 to evaluate the probabilities of collapse for various triggering events as a function of *I** and *t**. When an earthquake occurs, the resulting ground motions may or may not

trigger a warning system, and liquefaction may or may not occur. Therefore, there are four possible outcomes with respect to the operation of the warning system:

1. True Positive. The warning system trigger criterion is met (positive trigger) and collapse does occur (true prediction). This represents an outcome in which the warning system operates as desired and provides a successful warning of collapse. This would be a low cost – high benefit outcome.
2. True Negative. The trigger criterion is not met (negative trigger) and collapse does not occur (true prediction). This is another outcome in which the warning system operates as desired – the motion is not strong enough to trigger the warning system and collapse does not occur. This would be a zero cost – low benefit outcome.
3. False Positive. The trigger criterion is met (positive trigger) but collapse does not occur (false prediction). This results in a false alarm – the warning system is triggered but collapse does not occur – and is an undesirable, though relatively benign, outcome. This would be a low cost – zero benefit outcome.
4. False Negative. The trigger criterion is not met (negative trigger) but collapse does occur (false prediction). This is far and away the most undesirable outcome – a missed event. This would be a high cost – zero benefit outcome.

The most important of these outcomes are the first, which has a high benefit, and the last, which has a high cost. Consequently, analyses were performed to estimate the probabilities of each with respect to various triggering criteria.

True-Positive Outcomes

The results of the analyses for true-positive outcomes are presented in figures 5.19 and 5.20 for a true positive event. Figure 5.19 shows the probability of collapse for different combinations of I^* and t^*, and Figure 5.20 shows contours of collapse probability for different I^*-t^* pairs. As an example, consider a threshold Arias intensity of $I^* = 0.10$ m/sec. If that level of shaking were reached in the first second of shaking ($t^* = 1$ sec), the probability of liquefaction-induced collapse would be 33 percent. If that level of shaking were not reached until $t^* = 5$ sec, however, the probability of

liquefaction-induced collapse would drop to 24 percent. The probability of collapse will decrease as the time required to reach a given value of *I** increases. The probabilities are presented in tabular form in Table 5.3.

Note that even when the probability of liquefaction is 1.0, the probability of liquefaction-induced collapse is only 35 percent. This condition represents an upper limit to the probability of liquefaction-induced collapse; it occurs because there are non-zero probabilities of small seawall movement, small relative soil displacement, and small pile movement that can combine to produce conditions in which the occurrence of liquefaction would not result in collapse.

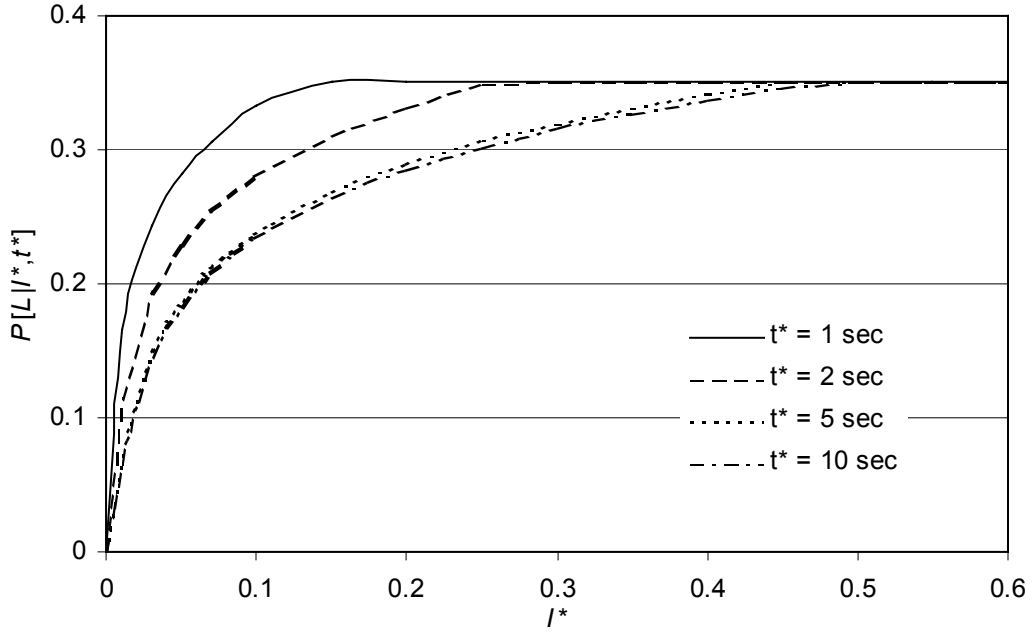

Figure 5.19. Probability of collapse (true positive) considering sources of uncertainty.

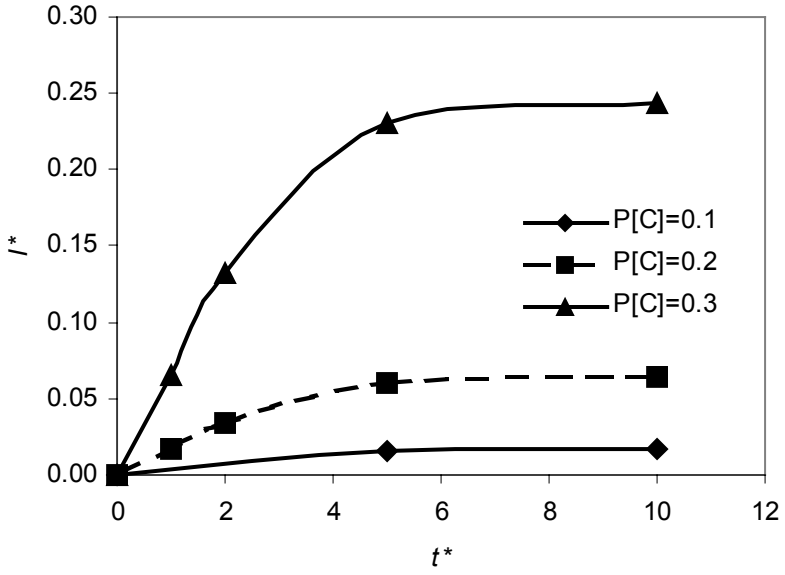

Figure 5.20. Uniform probability curves for collapse (true positive).

Table 5.3. Tabulated collapse probabilities for true positive events.

*I**	*t**					
	1	2	5	10	15	20
0.01	0.166	0.113	0.071	0.067	0.067	0.067
0.05	0.282	0.229	0.187	0.182	0.182	0.182
0.10	0.333	0.280	0.238	0.234	0.233	0.233
0.15	0.351	0.310	0.268	0.264	0.263	0.263
0.20	0.351	0.332	0.290	0.285	0.285	0.285
0.25	0.351	0.349	0.307	0.302	0.302	0.302
0.30	0.351	0.351	0.320	0.316	0.316	0.316
0.35	0.351	0.351	0.332	0.327	0.327	0.327
0.40	0.351	0.351	0.342	0.338	0.337	0.337
0.45	0.351	0.351	0.351	0.346	0.346	0.346
0.50	0.351	0.351	0.351	0.351	0.351	0.351
0.55	0.351	0.351	0.351	0.351	0.351	0.351
0.60	0.351	0.351	0.351	0.351	0.351	0.351

False-Negative Outcomes

The results of the probabilistic analyses for false-negative outcomes are presented graphically in Figure 5.21 and in tabular form in Table 5.4. The probabilities of a false-

negative outcome also vary for different combinations of I^* and t^*. As in the case of the true-positive outcomes, consider the case of a threshold Arias intensity of $I^* = 0.10$ m/sec. If that level of shaking were reached in the first second of shaking ($t^* = 1$ sec), the probability of a false-negative outcome would be 6.3 percent, i.e. a missed event. If that level of shaking were not reached until $t^* = 5$ sec, the probability of a missed event would drop to 3.5 percent. The probability of a missed event is smaller at longer triggering times.

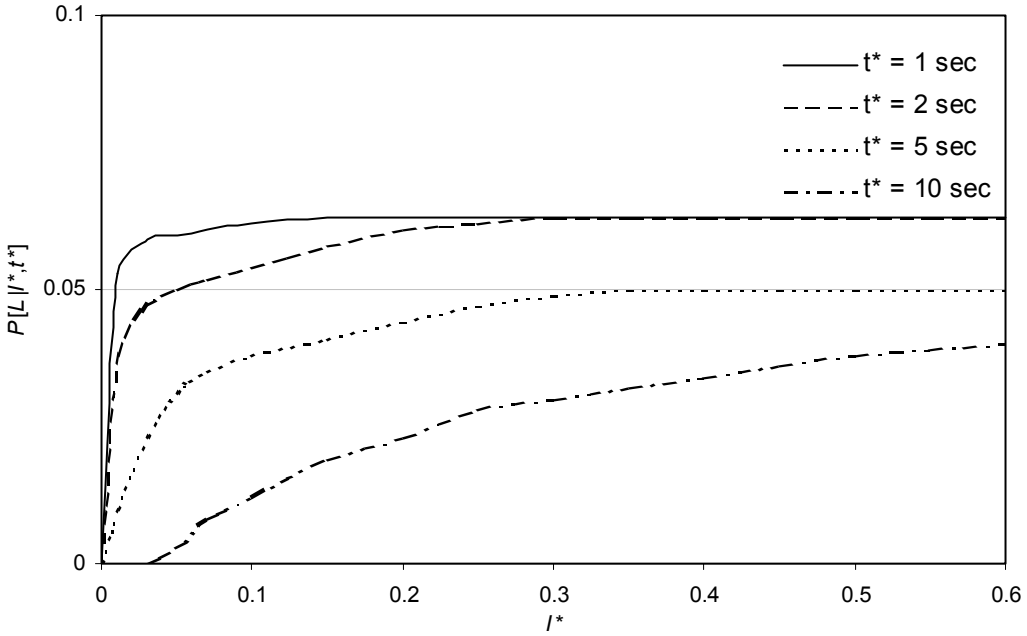

Figure 5.21. Probability of unpredicted collapse (false negative).

Table 5.4. Tabulated collapse probabilities for false negatives.

*I**	*t**					
	1	2	5	10	15	20
0.01	0.053	0.042	0.010	0.000	0.000	0.000
0.05	0.060	0.049	0.031	0.003	0.000	0.000
0.1	0.063	0.054	0.035	0.012	0.000	0.000
0.15	0.063	0.058	0.041	0.019	0.003	0.000
0.2	0.063	0.061	0.041	0.023	0.006	0.003
0.25	0.063	0.061	0.044	0.028	0.011	0.005
0.3	0.063	0.063	0.049	0.029	0.013	0.008
0.35	0.063	0.063	0.048	0.032	0.015	0.010
0.4	0.063	0.063	0.050	0.034	0.020	0.015
0.45	0.063	0.063	0.050	0.034	0.025	0.018
0.5	0.063	0.063	0.050	0.036	0.025	0.020
0.55	0.063	0.063	0.050	0.040	0.027	0.022
0.6	0.063	0.063	0.050	0.040	0.029	0.027

Discussion

Different combinations of I^* and t^* can produce the same probability of collapse. For a probability of collapse of 20 percent, for example, the triggering criteria could be set at {t^* = 1 sec, I^* = 0.017 m/sec} or {t^* = 10 sec, I^* = 0.064 m/sec} or many other combinations of I^* and t^*. Although both triggering criteria lead to the same (true positive) probability of collapse, the use of the former would allow a warning to be issued 10 seconds earlier than the use of the latter. Such a time difference could be critical in reducing risks to the traveling public. However, the probability of a false-negative outcome with the earlier warning would be substantially higher. This indicates that as the trigger, t^*, increases, more accurate predictions of potential collapse can be made, reducing the potential for a false trigger (false-positive or false-negative outcome). The results can also be presented in the form of uniform probability curves, as shown in Figure 5.20 and tabulated in Table 5.3. Several points along a given uniform probability curve could be selected as warning system trigger points.

In the context of the development of an instrumentation-based warning system, the values of triggering parameters, I^* and t^*, would require selection. The benefit of an early trigger (low value of t^*) is that it would provide more warning for drivers. However, a low value of t^* would result in a higher probability of a false trigger or a missed event. Several triggers can also be selected for incorporation into the warning

system. Therefore, missing an event with an early trigger would only delay action until the next trigger was checked.

The specified acceptable level of risk and corresponding trigger values could be based on a benefit-cost analysis of the action levels for closing the AWV. This analysis would consider the costs associated with the effects of false alarms and missed events. The recommended triggering parameters would correspond to minimum total cost. For example, the expected costs of a false alarm would be the product of the probability of no collapse given a triggering event and the cost of a shutdown where no collapse occurs. The expected costs associated with collapse could be modeled as the product of the probability of collapse given a shutdown and the cost associated with collapse (including direct costs, costs associated with injuries, fatalities, etc., and economic losses). Total costs would be the sum of costs associated with false alarms and the costs of collapse. This concept is shown qualitatively in Figure 5.22.

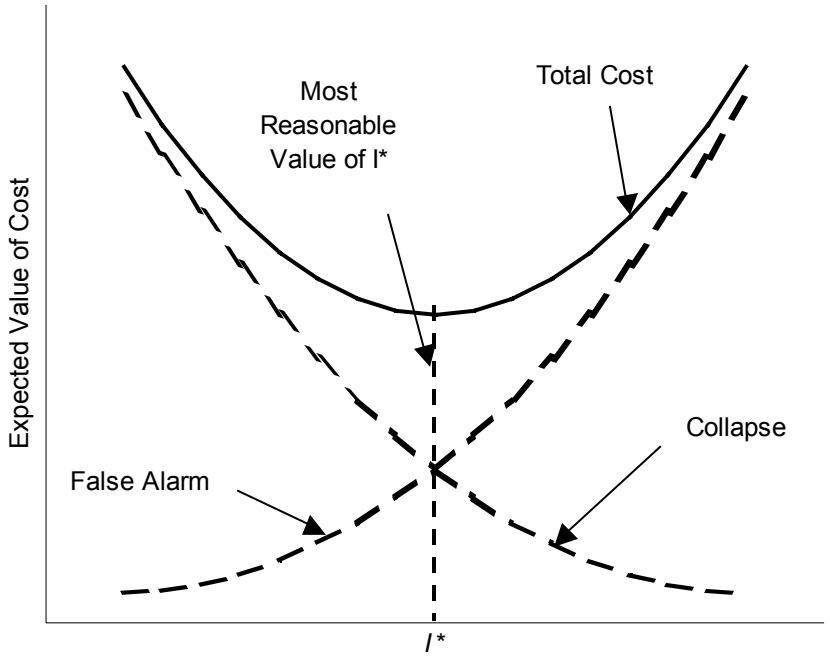

Figure 5.22. Conceptual benefit-cost analysis for a given value of t^*.

LIQUEFACTION WARNING SYSTEM INSTRUMENTATION PLAN

Implementation of the system to warn against liquefaction-induced collapse will require instrumentation to be installed at the AWV site. This instrumentation would consist of downhole accelerometers, piezometers, and slope inclinometer casings. The instrumentation could be installed at any number of sites along the length of the Viaduct; it is anticipated that at least two sites would be instrumented. One of these sites would be located in the University – Madison area and the other in the Columbia – Washington area.

For each instrumentation site, triaxial accelerometers should be installed at convenient locations beneath the Viaduct but at a distance of at least 30 ft from any Viaduct foundation (a) at a depth of 2 ft below the ground surface, and (b) at a depth of 2 ft below the upper surface of the dense glacial till that underlies the loose waterfront fill. To allow calibration/refinement of the warning system trigger criterion based on measurements from smaller earthquakes, it would be desirable to install additional triaxial accelerometers at the mid-depth of the loose waterfront fill and at a depth 2 ft above the upper surface of the dense glacial till that underlies the loose waterfront fill.

Electronically readable piezometers should be installed close to but no less than 10 ft (horizontally) from the accelerometer array at (a) the mid-depth of the loose waterfront fill, and (b) a depth of 2 ft above the upper surface of the dense glacial till that underlies the loose waterfront fill.

Slope inclinometer casings should be installed close to but no less than 10 ft (horizontally) from the accelerometer and piezometer arrays. These inclinometers would allow post-earthquake measurement of lateral soil movement. These measurements from smaller earthquakes would be used to help calibrate the warning system trigger criterion and such measurements would also aid in post-earthquake safety evaluations.

TRIGGER CRITERIA

As stated previously, the trigger criterion should be determined with due consideration of the costs and benefits of successful warnings, false alarms, and missed events. Decisions on acceptable costs and benefits must be made by WSDOT, but the algorithm used to trigger the warning system will be likely to have certain basic elements, regardless of the numerical values at which the triggers are set.

Figure 5.23 shows a simple flowchart for a potential warning algorithm. The instrumentation system would normally be in a standby mode in which it would continuously monitor all instruments (accelerometers, piezometers). If the measured acceleration level exceeded 0.005g, the system would be put in alert mode. At this time, the time scale would be initialized, and pore pressures would be checked. It would be desirable to have one trigger criterion based on measured pore pressure alone, i.e., a pore pressure level that would trigger the warning system regardless of ground motion level. That level would likely be set at a value of above 0.5 (a value of 0.8 is shown in the flow chart). After the time scale had been initialized, Arias intensity would be continuously computed and compared with the threshold value(s) for different trigger times. If any of the threshold Arias intensity values were exceeded, the warning system would be triggered. If not, the system would continue in alert mode for some period of time (a 10-minute period is shown in the flow chart).

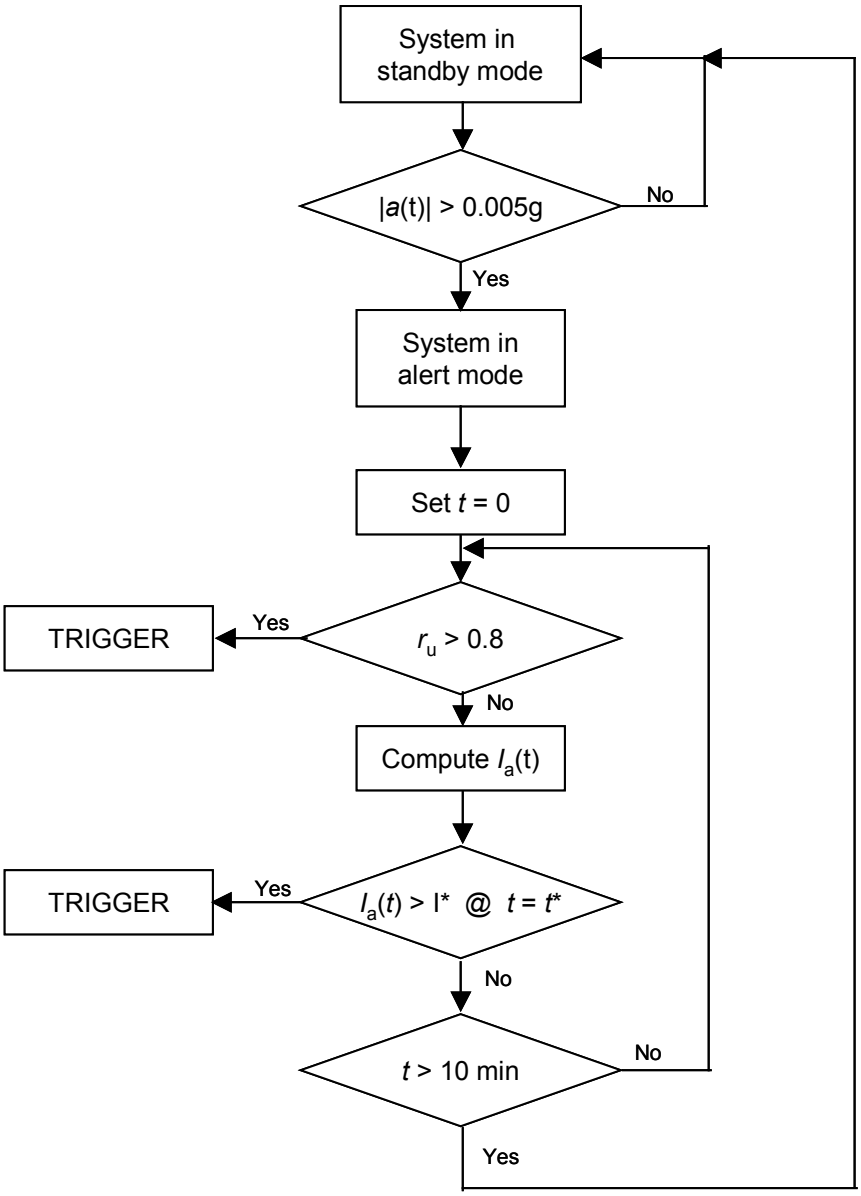

Figure 5.23. Proposed flow chart for a potential warning algorithm.

Chapter 6

Structural Instrumentation

An important benefit of installing a warning system on the Alaskan Way Viaduct is to provide the information necessary to divert traffic from the Viaduct before it collapses. For such a system to be effective in decreasing risk to life, there must be a significant length of time between the onset of strong ground shaking and collapse of the structure. Consider the following simple calculation. With a nominal driving speed of 80 km/hr, drivers take approximately 2 1/2 minutes to travel the length of the 3.5-km-long Viaduct. Therefore, if a 2- to 3-minute delay were available to divert oncoming traffic, nearly all of the Viaduct's traffic would have the time to clear the viaduct before it collapsed. If the viaduct collapses because of liquefaction-induced pile-cap displacements, delays of a minute or more are possible, so a warning system could be effective.

Delays between the onset of strong shaking and structural collapse are likely to be short if the Viaduct collapses as the result of ground shaking. If the warning time were only 15 seconds, for example, approximately 90 percent of the traffic would still be on the Viaduct at the time it collapsed. In this case, the benefits of emergency traffic diversion might be small.

Therefore, the main benefits of installing structural instrumentation are to help WSDOT decide when to inspect the Alaskan Way Viaduct and to help with post-earthquake evaluation. Inspections should be triggered when there is significant risk of structural damage. That damage could be caused either by ground shaking or by support displacements.

STRUCTURAL BEHAVIOR FOR TRANSVERSE LOADS AND FOR SUPPORT DISPLACEMENTS

The vulnerability of the Alaskan Way Viaduct has already been studied extensively by Eberhard et al. (1995), for the WSDOT typical three-span unit, and by

Knaebel et al. (1995), for the SED typical three-span unit. The results of these studies are summarized in Chapter 3.

However, the previous studies did not consider support displacements, so they are considered here and compared with the results of push-over analyses. Typical interior and exterior transverse frames of Seattle Engineering Department (SED) typical unit were analyzed with two-dimensional, nonlinear frame analysis typical (Dr.Frame, www.drstructures-home.com). Member moments of inertia were estimated as one half the gross cross-section values, and member strengths were assumed to be those reported by Knaebel et al. (1995).

The results of a typical lateral-force analysis are summarized in Figure 6.1 for a top-story displacement of 6 inches. On the left, the figure shows the applied forces, displaced shape and plastic-hinge rotations. On the right, the figure shows the corresponding moment diagrams. According to these results, plastic rotations would be largest at the base of the first-story columns and at the ends of the first-level beams. These results are similar to those reported by Knaebel.

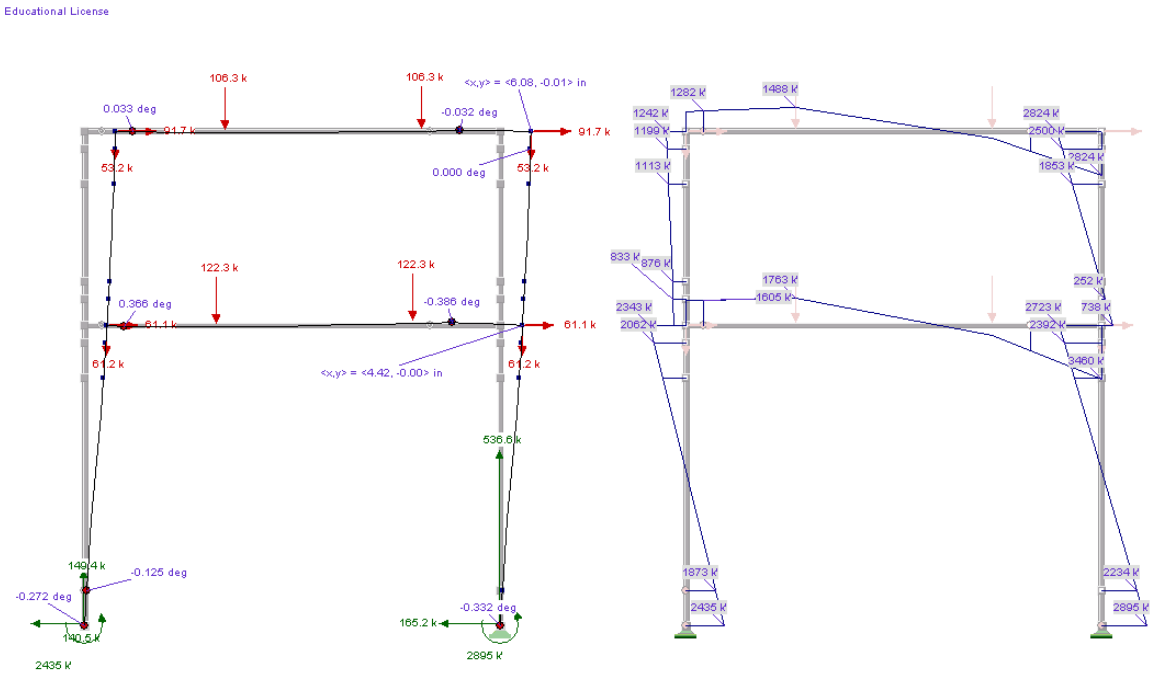

Figure 6.1. Results of pushover analysis for SED exterior frame (6 in.).

For comparison, Figure 6.2 summarizes the corresponding results for a support displacement of 6 inches. The results of these analyses are similar to those presented in Figure 6.1 in that large plastic rotations are predicted to occur at the base of the first-story columns, but there are significant differences. According to the support-displacement analyses, joint stresses would be relatively low because the first-story and second-story column moments nearly cancel each other. For this reason, joint failure was not considered in the fragility analyses discussed in Chapter 5. A second major difference between the two analyses is the prediction of yielding in the second story near the splice location. Such yielding was not predicted by the push-over analyses.

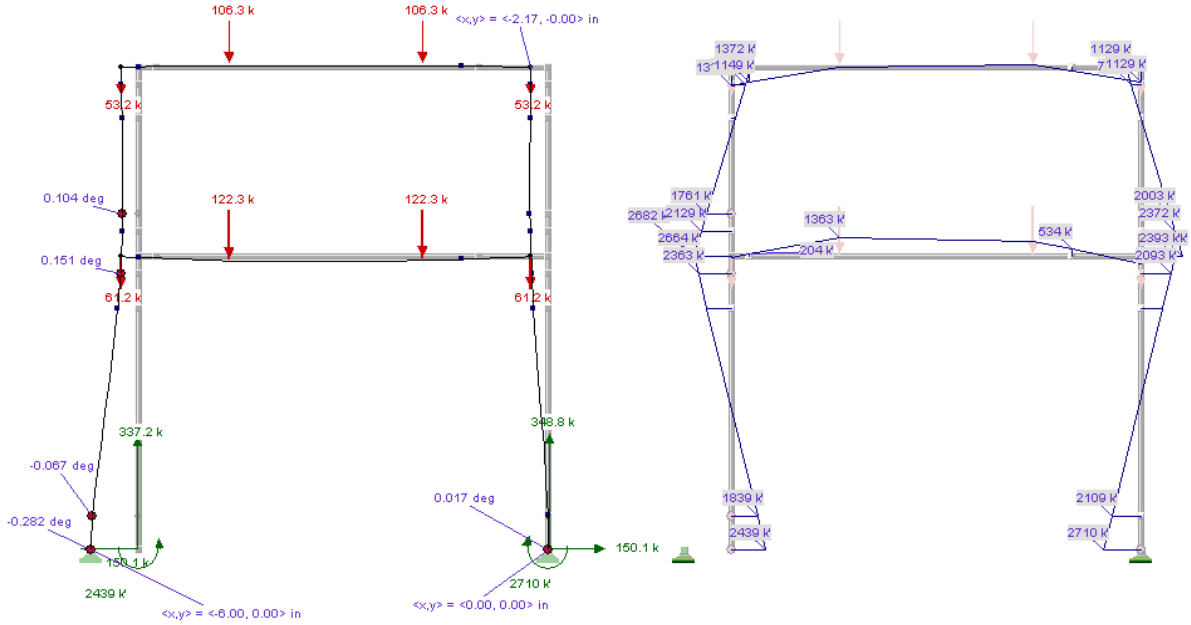

Figure 6.2. Results of support-displacement analysis for SED exterior frame (6 in.).

The ductility demands predicted for the first-story beams in response to lateral-loads (Figure 6.1) were taken into account in the fragility analyses discussed in Chapter 5. Three scenarios were considered for the first-story beam-column connection. In the first scenario (judged to be 40 percent likely), there would be little damage to the positive-moment beam reinforcement anchorage. If the beams and columns are modeled at their centerlines and rigid within the joint, the predicted beam crack width is only 1

percent of the pile-cap displacement. It is also possible that the beam bars would lose their anchorage, which would allow the column to more easily pull away from the beam (50 percent likelihood). If the column is modeled as flexible within the joint, the predicted crack width at the bottom of the beam increases to approximately 3 percent of the pile-cap displacement. A third scenario was considered (10 percent) to take into account possible yielding at the second-story column splice. The second-story column was assumed to develop a hinge at its splice location, which when combined with beam anchorage failure, would allow the column and beam interfaces to separate more easily. The beam crack width predicted for this case corresponded to 6 percent of the pile-cap displacement. These assumptions are summarized in Table 5.2.

STRUCTURAL DISPLACEMENTS AT THE ONSET OF STRUCTURAL DAMAGE

An important finding of the previous studies is that structural damage could occur in the Viaduct for relatively low levels of ductility demands. One can afford to be conservative (i.e., to adopt large factors of safety) in setting triggers for inspection because the cost of triggering unnecessary inspections is much smaller than the cost of unnecessarily diverting traffic. Given these considerations, the level of short-term structural displacement necessary to trigger inspection will be assumed as *one half the displacement at the onset of significant nonlinear behavior*.

The results of push-over analyses and support-displacement analyses for the SED typical three-span unit were used to develop criteria for triggering structural inspections

Figure 6.3 shows typical top-story displacement, base-shear relationships for push-over analyses. The results are presented up to a displacement of 8.0 in. only, because beyond that value, the analytical model predicts excessive strain hardening. According to this analysis, the base-shear strength of the SED Unit (two exterior and two interior frames) is approximately 2000 kips, which corresponds to 40 percent of the unit's weight of 5000 kips. Nonlinear behavior begins at a top-story displacement of approximately 2.0 inches and becomes significant at 3.0 inches. These results are similar to those reported by Knaebel.

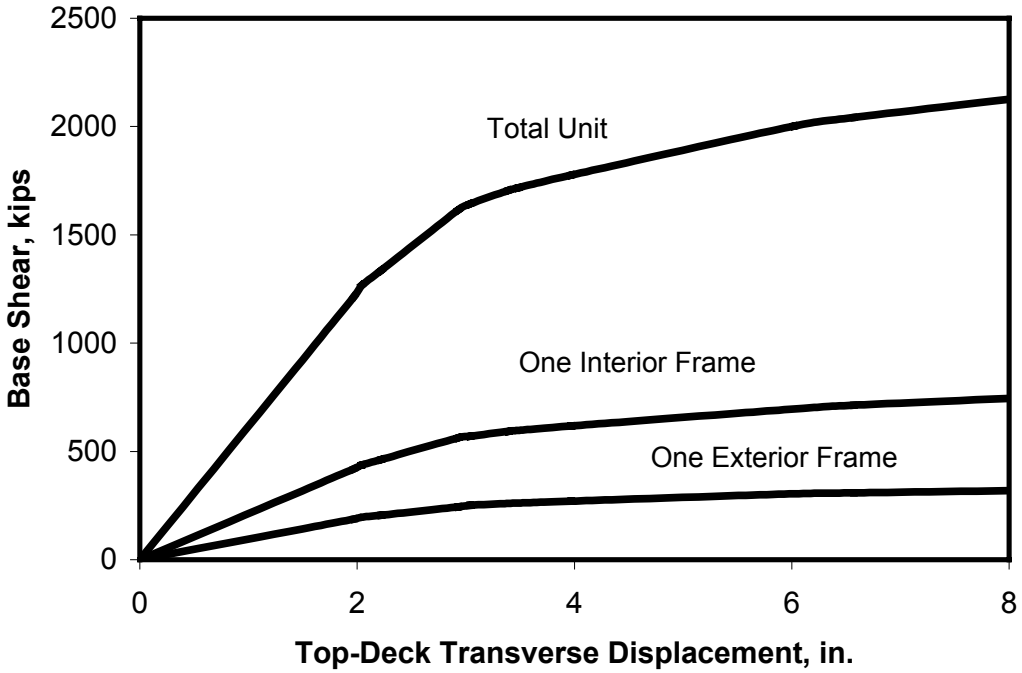

Figure 6.3. Base shear-top displacement relationships for SED transverse frames.

For comparison, Figure 6.4 shows the column-displacement, column-shear relationship that was calculated (with the same model) for support displacements away from the structure. To a first approximation, the maximum column shear for the interior and exterior columns is approximately equal to half the base-shear strength for the corresponding transverse frame (Figure 6.1). According to this analysis, nonlinear response begins at a transverse-support displacement of approximately 3.0 inches.

Based on these considerations, it seems reasonable to trigger inspection when the displacement at one joint (top, first-level or pile cap) exceeds 1.5 inches. If the viaduct displacement exceeds 2.5 inches, the viaduct should be closed, for the sake of safety, until the inspections have been completed. If one assumes that these deformations are concentrated in the first story (33-35 ft high), these two levels of displacement correspond to drift ratios of 0.4 and 0.6, respectively.

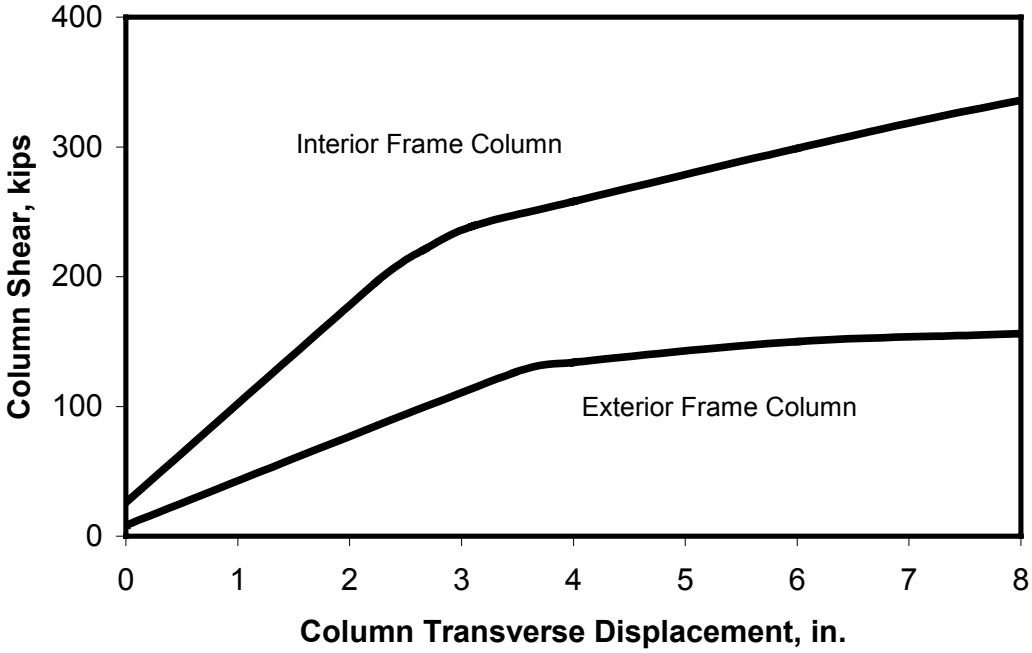

Figure 6.4. Column shear-support displacement relationships for SED transverse frames.

STRUCTURAL DAMAGE WARNING-SYSTEM INSTRUMENTATION PLAN

Because the Alaskan Way Viaduct is long and complex, it would be impossible to install seismic instrumentation to monitor every location. Therefore, it is important to install instrumentation in locations that are representative of the rest of the viaduct, and to reflect the variety of ground motions that might affect it. The instruments need to have a broad range of dynamic response, making it possible for them to measure strong accelerations and displacements. They will also need to measure response in three directions (transverse, longitudinal and vertical).

For each instrumented frame, it is important that displacements be measured at the level of the pile-cap (to monitor liquefaction-induced displacements), at the ends of the first-level beams (because deformations are likely to be concentrated in the first story), and at the top level (because top-story displacements are likely to be the largest there). A typical frame would then be instrumented in six locations, as shown in Figure 6.5. A typical unit, in which both interior and exterior frames were instrumented, would then be instrumented at twelve locations.

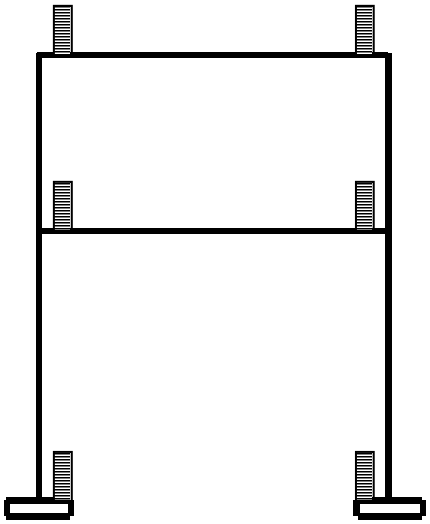

Figure 6.5. Proposed locations for structural seismic instrumentation.

WSDOT-designed units and SED-designed units, as well as locations corresponding to shallow, medium, and deep soft-soil profiles, need to be monitored. Table 6.1 summarizes a proposal for characteristics of units to be monitored.

Table 6.1. Characteristics of units to be monitored.

Site Designation	Unit Type	Depth of Soft Soils
1	SED	Shallow
2	SED	Medium
4	WSDOT	Medium
5	WSDOT	Deep

TRIGGER CRITERIA

To use the triggering information wisely, it is necessary to consider the level of event that would likely trigger the system. The triggering events can be roughly estimated by combining the results of static, nonlinear analyses, with the results of linear, dynamic analysis, in which the Viaduct is treated as a single-degree-of-freedom system. Such calculations are summarized in Table 6.2.

According to Knaebel et al. (1995) and Eberhard et al. (1995), the effective fundamental periods of the SED and WSDOT units are in the range of 1.0 to 2.0 seconds. For a three-span unit weight of 5000 kips, these effective periods correspond to effective stiffnesses of 510 k/in. and 130 k/in., respectively. For a period of 1.0 seconds, the 1.5-in. top-story displacement corresponds to a spectral acceleration of 0.13g. The 2.5-in. spectral displacement corresponds to a spectral acceleration of 0.22 g. In comparison, the Pacific Northwest Seismic Network Shake-Maps suggest that the downtown Seattle region was subjected to ground motions with spectral accelerations (at a period of 1.0 seconds) in the range of 0.2g.

If the proposed trigger levels turn out to be inadequate, WSDOT can readjust triggering levels in response to experience.

Table 6.2. Spectral acceleration for triggering events

	Property	Short-Period Assumption	Long-Period Assumption
SDOF Properties	Effective Period	1.0 sec.	2.0 sec.
	Weight of Unit	5000 kips	5000 kips
	Effective Stiffness	510 k/in.	130 k/in.
Conditions for Triggering Inspection	Top-Displacement	1.5 in.	1.5 in.
	Displacement at Force Centroid	1.28 in.	1.28 in.
	Base Shear Force	650 kips	163 kips
	Spectral Acceleration	0.13 g	0.033 g
Conditions for Triggering Inspection and Closure	Top-Displacement	2.5 in.	2.5 in.
	Displacement at Force Centroid	2.12 in.	2.12 in.
	Base Shear Force	1084 kips	272 kips
	Spectral Acceleration	0.22 g	0.054 g

DISTRIBUTED BRIDGE INSTRUMENTATION NETWORK

In previous portions of this report, a triggering algorithm was developed for a seismic warning system for a specific structure. A larger, geographically distributed network could be installed to help WSDOT (1) prioritize post-earthquake inspections and (2) calibrate procedures for seismic assessment.

Exploratory Study

To evaluate the potential benefits of installing a distributed network, an exploratory study was conducted using ground-motion and damage data from the 2001 Nisqually Earthquake (EERI, 2001, Ranf et al., 2002). Reports of bridge damage were collected from WSDOT, the City of Seattle and other public agencies. This information was combined with the Washington State Bridge Inventory (WSBI) to extract key properties of all the damaged bridges and of bridges in western Washington State that were not damaged.

The values for the peak ground acceleration and the spectral acceleration at each bridge site were estimated from ShakeMaps developed by the Pacific Northwest Seismograph Network (PNSN), an example of which is shown in Figure 5.6 (PNSN 2001). The maps provided approximate values for the peak ground acceleration and the spectral acceleration at the location of each damaged and undamaged bridge. In the figure, damaged bridges are identified by triangles.

The PNSN, centered at the University of Washington, operates a network of seismograph stations throughout the Northwest. It is operated through a joint effort by the University of Washington, University of Oregon and Oregon State University, and is funded by the United States Geological Survey (USGS), the United States Department of Energy (USDOE) and the State of Washington. PNSN developed maps of earthquake intensity (ShakeMaps) by interpolating between numerous stations within the network, taking into account geologic conditions.

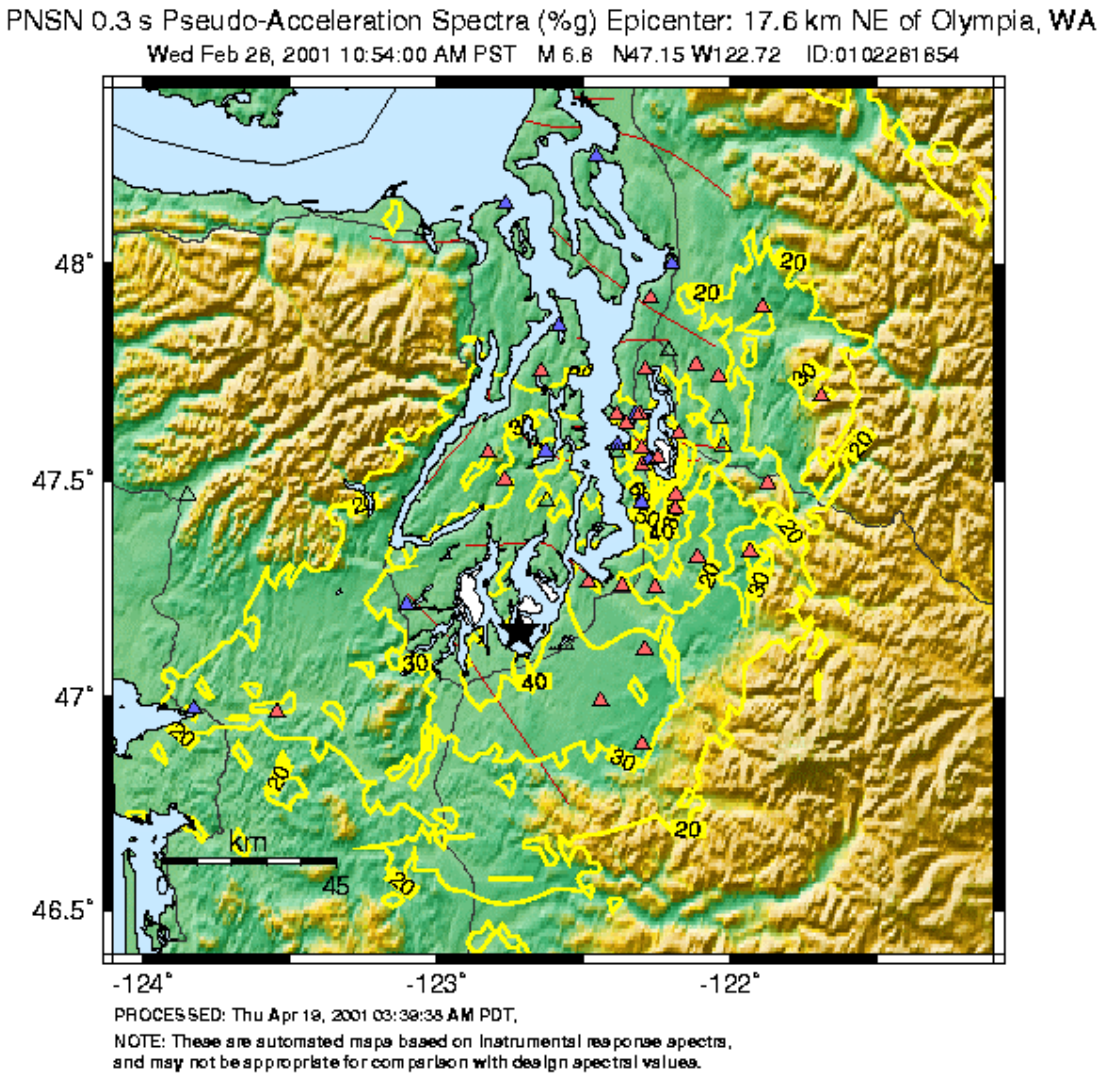

Figure 6.6. ShakeMap for spectral acceleration at period of 0.3s (PNSN, 2001)

Typical results of the vulnerability analyses are shown in Figure 6.7. The top graph of this figure shows the number of bridges that were subjected to each range of spectral acceleration. The middle graph shows the number of damaged bridges in each range, and the bottom graph shows the percentage of damaged bridges for each category. In other words, the ordinates of the bottom graph are equal to those of the top graph divided by those of the middle one.

As shown in the figure, the percentage of the bridges that were damaged correlated well with the magnitude of the spectral acceleration at 0.3 sec and with the

year of construction. Older bridges were more likely to be damaged than newer ones, and within each age category, the likelihood of damage increased consistently with increasing spectral acceleration. These correlations, when combined with estimates of ground-motion parameters at each bridge site, can be used to estimate likelihood of damage of bridges in the future, immediately following an earthquake.

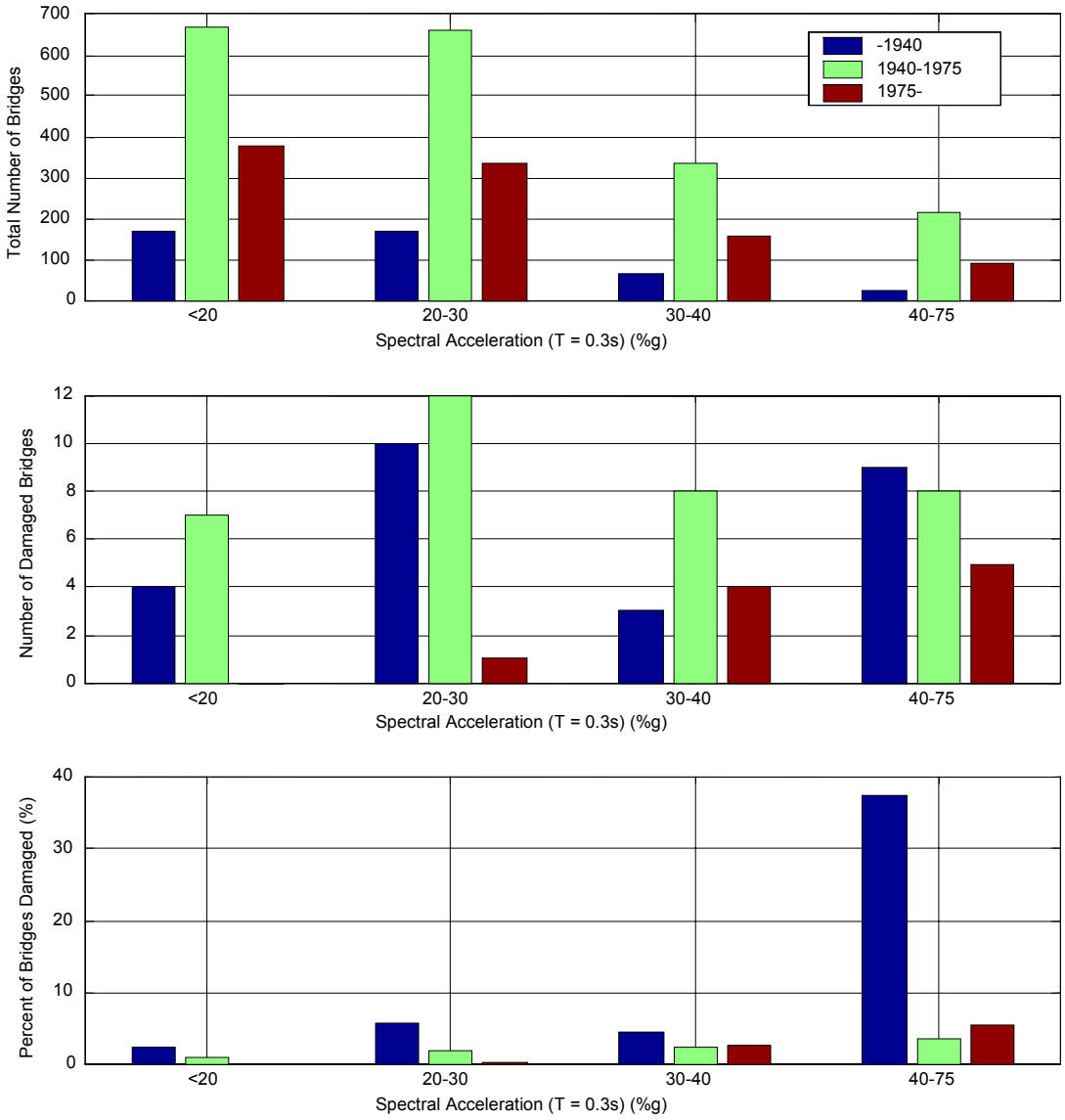

Figure 6.7. Correlation between damage likelihood and spectral acceleration at 0.3 sec.

Implementation Considerations

It would be uneconomical for WSDOT to install and monitor its own network of seismic instruments. WSDOT should take full advantage of the existing PNSN instrumentation, and of the large number of instruments that will be installed as part of the Advanced National Seismic System (ANSS). ANSS is congressionally mandated to instrument structures, and with WSDOT support, the structural instrumentation might be focused on bridges. The estimates of ground-motion parameters will be most accurate if instruments are located near key bridges.

To make a network useful to WSDOT, software will need to be developed to mesh the Washington State Bridge Inventory with the PNSN ShakeMaps. Within minutes of an earthquake, WSDOT will want to have access to:

- Detailed ShakeMaps with Estimates of Ground Shaking. At the option of the user, these maps could be superimposed over a map of the highway system.
- Preliminary Estimates of Number of Damaged Bridges. Using fragility curves developed from the Nisqually earthquake (Ranf et al., 2001), one could estimate the likelihood of damage. Of course, these estimates would be coarse, but at the moment, WSDOT have no tools with which to make quantitative estimates
- Detailed List of Critical Bridges. For example, by combining spectral acceleration with age of construction, it would be possible to identify the bridges that are most likely to be damaged. By taking into account the average daily travel on each bridge, it would be possible to even further prioritize the list.

Such tools would make it much easier for WSDOT to determine whether and where to dispatch inspection teams. Also, in the long term, this information would also make it possible for WSDOT to calibrate its procedures for seismic assessment.

No one knows whether the next earthquake will occur soon. Therefore, it is important that any instrumentation installed be monitored and maintained in the future. These activities would require small, but long-term, financial support from WSDOT.

Chapter 7

Summary and Conclusions

This report presents the results of an investigation into the feasibility and preliminary design of a system intended to provide warning of potential collapse of the Alaskan Way Viaduct following earthquake shaking. Such a system would also help WSDOT decide when to inspect the Viaduct and aid in post-earthquake evaluation.

In evaluating the recommendations presented in this report, it is important to recognize that the seismic performance of the Viaduct is extremely complex and will be influenced by many known and unknown factors that relate to the above- and below-ground portions of the Viaduct, the soils that support the Viaduct, and the performance of nearby structures such as the Seattle seawall. The investigators have attempted to consider all reasonable, known conditions, and have used that information to identify the most critical conditions relative to potential collapse of the structure (Kramer et al., 1995). It should be recognized, however, that unknown and/or differing conditions might exist and lead to unanticipated mechanisms of failure or collapse.

Most of the Alaskan Way Viaduct is located in an area that was originally within the waters of Elliott Bay. As a result, these portions of the Viaduct are located on filled ground. The filling operations that produced the current topography of the Seattle waterfront area were accomplished with techniques that were common at that time. These techniques are now known, however, to produce liquefiable soil deposits. As part of the process of developing the Seattle waterfront, a seawall was constructed in the 1930s; this seawall retains the liquefiable soils that surround the Viaduct's foundations, though it was not designed to retain liquefied soils.

Previous studies of the seismic vulnerability of the Alaskan Way Viaduct have identified liquefaction and the resulting lateral movement of the liquefied soil as an important threat to the integrity of the structure. Liquefaction could lead to collapse of portions of the Viaduct through a series of related events: liquefaction of soil beneath the Viaduct and behind the Seattle seawall, lateral movement of the seawall with consequent movement of the soil behind it, lateral

movement of the Viaduct's pile foundations, and excessive differential movements of the columns of the Viaduct. The most critical portions of the Viaduct, with respect to this potential collapse mechanism, are expected to be between University and Madison Streets and between Washington and Columbia Streets. The studies described in this report have focused on the conditions that exist in those areas, although they should not be considered the only areas with potential for severe damage and/or collapse.

The Viaduct itself is now approximately 50 years old. It is a complicated structure with a wide variety of geometric configurations and structural details. Variations between the structural design and actual construction conditions undoubtedly exist, and the current conditions are undoubtedly influenced by its sustained and heavy use. The Viaduct has been subjected to moderate shaking in 1965 and 2001; the effects of that shaking on the current condition of the Viaduct are not known entirely. The studies described in this report considered typical sections of the Viaduct at locations thought to be critical and used available information to estimate the current condition of those sections. Other sections may have different vulnerabilities to structural damage.

WARNING CRITERIA FOR LIQUEFACTION-INDUCED COLLAPSE

The cyclic stresses induced by earthquake shaking cause the incremental buildup of porewater pressure in liquefiable soils. This process takes some time to occur, and many case histories of liquefaction-induced failures have shown that some degree of pore pressure redistribution accompanies the development of large soil deformations. Therefore, liquefaction-induced failures often occur some time after earthquake shaking has ended. Although the amount of the time delay cannot be predicted reliably by available procedures, its historical occurrence offers some hope that early warning of liquefaction will provide a period of time in which defensive measures can be taken before failure.

In recognition of the numerous and significant uncertainties in most of the series of events that are expected to lead to liquefaction-induced collapse, the warning system triggering criterion was developed probabilistically. This approach required identification of a suitable ground motion parameter for prediction of liquefaction, evaluation of the probability of liquefaction for given values of that parameter, evaluation of the probability of various levels of liquefied soil displacement, evaluation of the probability of various levels of foundation

movement, and evaluation of the probability of collapse for different levels of foundation movement. Arias intensity, an integral ground motion parameter that has been used to predict liquefaction potential, was used to formulate the warning criterion. The various probability distributions required to formulate the probabilistic analyses were determined from data when available or estimated when data were not available.

A collapse warning system should desirably provide a warning early enough to allow defensive measures to be taken, but not so early that the warning is unreliable. To allow WSDOT to weigh the various trade-offs between early and later warning, triggering criteria were evaluated for a range of different triggering levels. Estimated probabilities of collapse for different combinations of trigger level-trigger time are presented. Through cost-benefit analysis techniques, these probabilities can be used, along with estimates of the costs and benefits of successful and unsuccessful warning, to select desired triggering criteria.

CRITERIA FOR STRUCTURAL INSPECTION AND CLOSURE

Previous studies have shown that structural damage could occur in the Viaduct at relatively low levels of ductility demands. To confirm that the Viaduct has not been damaged by earthquake shaking, structural inspections are conducted following most earthquakes that are felt in the Seattle area. To provide a rational basis for determining whether such inspections are advisable, the results of push-over analyses and support-displacement analyses for the SED typical three-span unit were used to develop a criterion for initiating post-earthquake structural inspections. This criterion is based on a condition in which structural displacements exceed one-half the displacement at the expected onset of significant nonlinear behavior. For a structural period of 1.0 sec, this displacement corresponds to a spectral acceleration of 0.13g for the SED.

Stronger earthquake motions may cause sufficient damage to warrant closure of the Viaduct until its safety can be established. A criterion for closure of the Viaduct is based on the condition in which structural displacements reach the level at which significant nonlinear behavior is expected to occur. For a structural period of 1.0 sec, this displacement corresponds to a spectral acceleration of 0.22g for the SED.

INSTRUMENTATION

Implementation of the warning systems described in this report will require the design, installation, and operation of an instrumentation/warning system. The instrumentation system will include transducers, cables, and a data acquisition system. The warning system will include a computer connected to the data acquisition system, cables, relays, and warning devices (e.g. red lights, electronic signs, gates, horns, etc.). To enable WSDOT to verify that the system is functioning properly and to help with post-earthquake recovery, the instrumentation will need to be monitored continuously. One option for ensuring such monitoring would be to connect the AWV instruments to the Advanced National Seismic System.

The liquefaction-induced collapse warning system will require accelerometers at and below the ground surface, electronic piezometers installed at various depths in the liquefiable soil, and the installation of slope inclinometer casings. The structural inspection and closure system will require a highly linear accelerometer system mounted on the structure.

References

Applied Technology Council. (1983). "Seismic Retrofitting Guidelines for Highway Bridges (ATC-6-2)." Redwood City, California.

Bartlett, S.F. and Youd, T.L. (1992). "Empirical analysis of horizontal ground displacements generated by liquefaction-induced lateral spread", *Technical Report NCEER-92-0021*, National Center for Earthquake Engineering Research, Buffalo, New York.

Brown, C. B., Eberhard, M. O., Kramer, S. L., Roeder, C. W., and Stanton, J. F. (1992). "Preliminary Investigation of the Seismic Vulnerability of the Alaskan Way Viaduct." WA-RD 265.1. Washington State Department of Transportation

Casagrande, A. (1936). "Characteristics of cohesionless soils affecting the stability of earth fills," *J. of the Boston Society of Civil Engineers*, January, 13-33.

Castro, G. (1969). "Liquefaction of sands," *Harvard Soil Mechanics Series 87*, Harvard University, Cambridge, MA.

Dobry, R. and Ladd, R. S. (1980). Discussion to: "Soil liquefaction and cyclic mobility evaluation for level ground during earthquakes," by H.B. Seed and "Liquefaction potential: science versus practice," by R.B. Peck, *Journal of the Geotechnical Engineering Division*, ASCE, Vol. 106, No.GT6, pp. 720-724.

Dodson, J., Rochelle, S. G., and Stoddard, R. B. (1990). "Earthquake Analyses of the Alaskan Way Viaduct." Executive Summary. Washington State Department of Transportation.

Earthquake Engineering Research Institute (2001), "The Nisqually Earthquake of 28 February 2001: Preliminary Reconnaissance Report," Oakland, California, March.

Eberhard, M. O., De la Colina, J., and Ryter, S. (1995). "Seismic Vulnerability of the Alaskan Way Viaduct: WSDOT Typical Unit." WA-RD 363.1. Washington State Department of Transportation.

Elgamal, A. -W. and Zeghal, M. (1992). "Analysis of Wildlife Site Liquefaction During the 1987 Superstition Hills Earthquake," *4th Japan - U.S. Workshop on Earthquake Resistant Design of Lifeline Facilities and Countermeasures Against Soil Liquefaction*, Tokai Univ. Pacific Center, Hawaii, NCEER, SUNY-Buffalo Report No. NCEER-92-0019, Hamada M. And O'Rourke, T.D., (eds.), May, 87-96.

Hipley, P. (1998). "California Department of Transportation Seismic Gates," <www.dot.ca.gov/hq/esc/earthquake_engineering/Research/seisgate.pdf>, available from <http://www.dot.ca.gov/hq/esc/earthquake_engineering/Research/techreps.html>, December 26, 2001.)

Horne, J.C., (1996), "Effects of liquefaction-induced lateral spreading on pile foundations," Ph.D. Dissertation, University of Washington.

Kayen, R.E., and Mitchell, J. (1997). "Assessment of liquefaction potential during earthquakes by Arias intensity", *Journal of Geotechnical and Geoenvironmental Engineering*, ASCE, Vol.123, No.12, pp. 1162-1174.

Kimmerling, R.E. and Kramer, S. (1996). "Alaskan Way Viaduct: Phase III Seismic Vulnerability Study," Geotechnical Report, Washington State Department of Transportation, 8 pp.

Knaebel, P., Eberhard, M. O., and De la Colina, J. (1995). "Seismic Vulnerability of the Alaskan Way Viaduct: SED Typical Unit." WA-RD 363.3. Washington State Department of Transportation.

Kramer, S. L., Sivaneswaran, N., and Tucker, K. (1995). "Seismic Vulnerability of the Alaskan Way Viaduct: Geotechnical Engineering Aspects." WA-RD 363.2. Washington State Department of Transportation.

Moehle, J. P., Thewalt, C. R., Mahin, S. A., and Lowes, L. N. (1994). "Evaluation and Upgrading of Multi-Column Bridges." Proceedings, 2nd U.S.-Japan Workshop on Seismic Retrofit of Bridges, Berkeley, California.

Nogami, T., Otani, J., Konagai, K., and Chen, H.L. (1992). "Nonlinear soil-pile interaction model for dynamic lateral motion," *Journal of Geotechnical Engineering*, ASCE, Vol. 118, No.1, pp 89-116.

Nemat-Nasser, S., and Shokooh, A. (1979). "A Unified Approach to densification and liquefaction of cohesionless sand in cyclic shearing", *Canadian Geotechnical Journal*, Vol.16, No.4, pp. 649-678.

O'Neill, M., and Murchison, J.M. (1983), "An evaluation of p-y relationships in sands," Research Report No. GT-DF02-83, University of Houston-University Park.

Pacific Northwest Seismograph Network (2001), University of Washington, <http://www.geophys.washington.edu/shake/0102281854/intensity.html>.

Priestley, M. J. N., Seible, F., and Chai, Y. H. (1992). "Design Guidelines for Assessment Retrofit and Repair of Bridges for Seismic Performance." Report No. SSRP-92/01. Department of Applied Mechanics and Engineering Sciences. University of California, San Diego.

Ranf, R.T., Eberhard, M.O., and Berry, M.B. (2002), "Damage to bridges during the 2001 Nisqually earthquake," Pacific Earthquake Engineering Research Center report, in press.

Rauch, A.F. (1997). "EPOLLS: An empirical method for predicting surface displacement due to liquefaction-induced lateral spreading in earthquakes," Ph.D. dissertation, Virginia Polytechnic Institute and State University, Blacksburg, Virginia.

Reimer, M.F. and Seed, R.B. (1997). "Factors affecting apparent position of steady-state line," *Journal of Geotechnical and Geoenvironmental Engineering*, 123(3), 281-288.

Seed, R.B. and Harder, L.F. (1990). "SPT-based analysis of cyclic pore pressure generation and undrained residual strength," in J.M. Duncan ed., *Proceedings, H. Bolton Seed Memorial Symposium*, University of California, Berkeley, Vol. 2, pp. 351-376.

Vaid, Y. P., and Chern, J. C., (1985). “Cyclic and monotonic undrained response of saturated sands”, in V. Khosla ed., *Advances in the Art of Testing Soils under Cyclic Conditions*, ASCE, New York, pp. 120-147.

Vaid, Y.P., Chung, E.K.F., and Kuerbis, R. (1990). “Stress path and steady state,” *Canadian Geotechnical Journal*, 27(1), 1-7.

Verdugo, R. and Ishihara, K. (1996). “The steady state of sandy soils,” *Soils and Foundations*, 36(2), 81-92.

Yoshimine, M. and Ishihara, K. (1998). “Flow potential of sand during liquefaction,” *Soils and Foundations*, 38(2), 189-198.

Youd, L. T. and Idriss, I. M. (1997). "Proceedings of the NCEER Workshop on Evaluation of Liquefaction Resistance of Soils," *Report NCEER 97-0022*, National Center for Earthquake Engineering Research, Buffalo, NY.

Appendix A

Input Motions

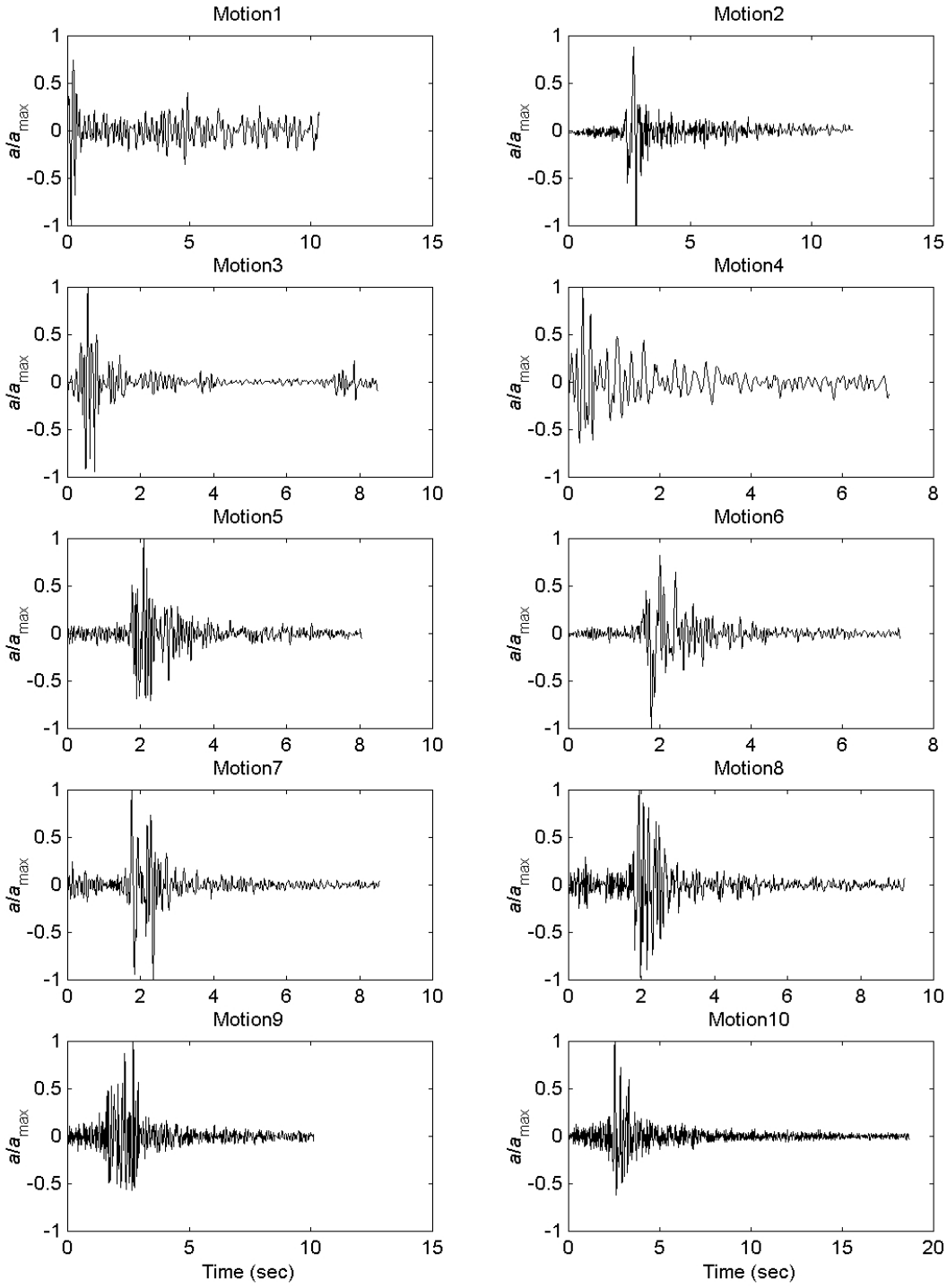

Figure A.1 Motions 1 through 10.

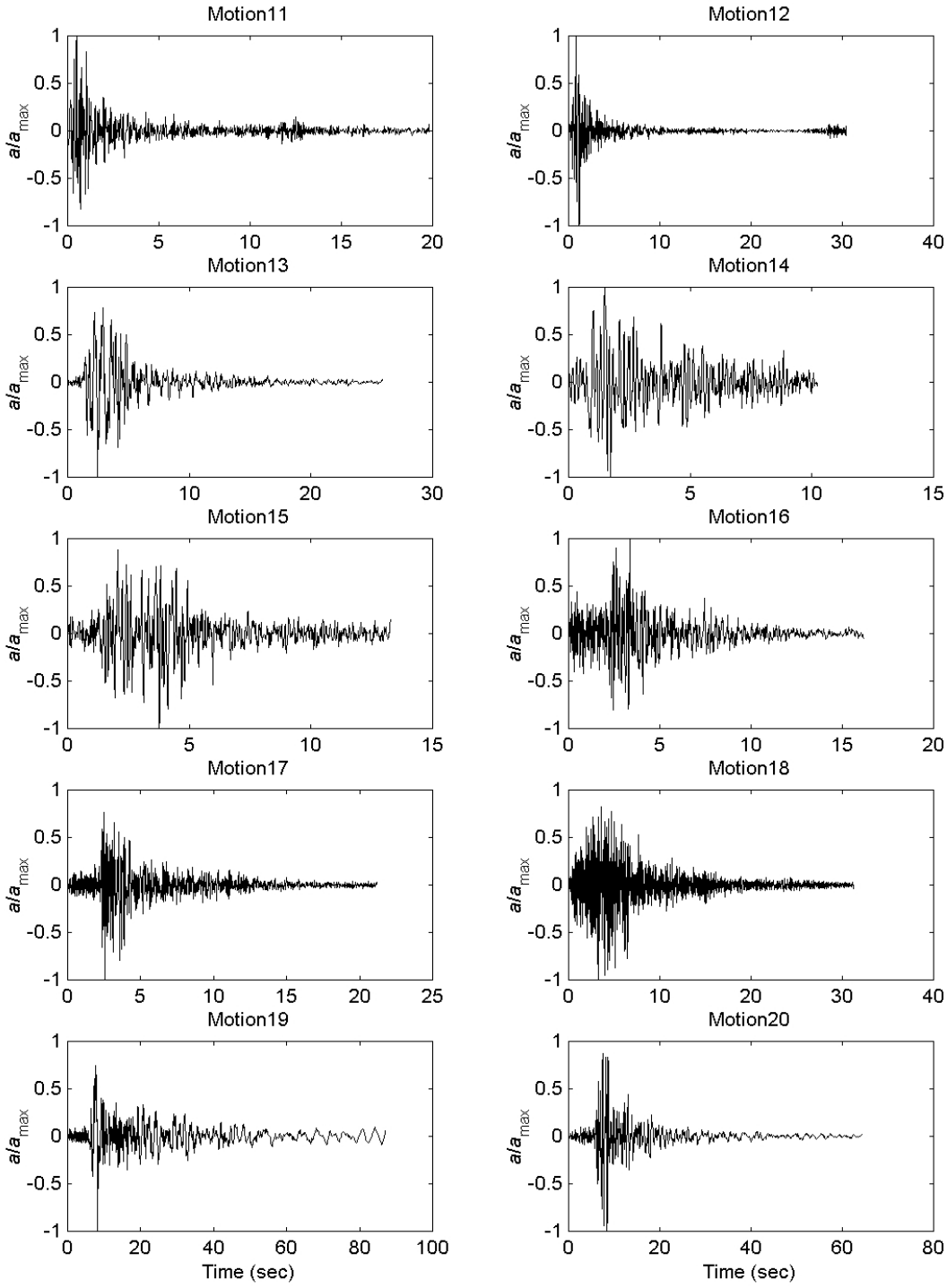

Figure A.2 Motions 11 through 20.

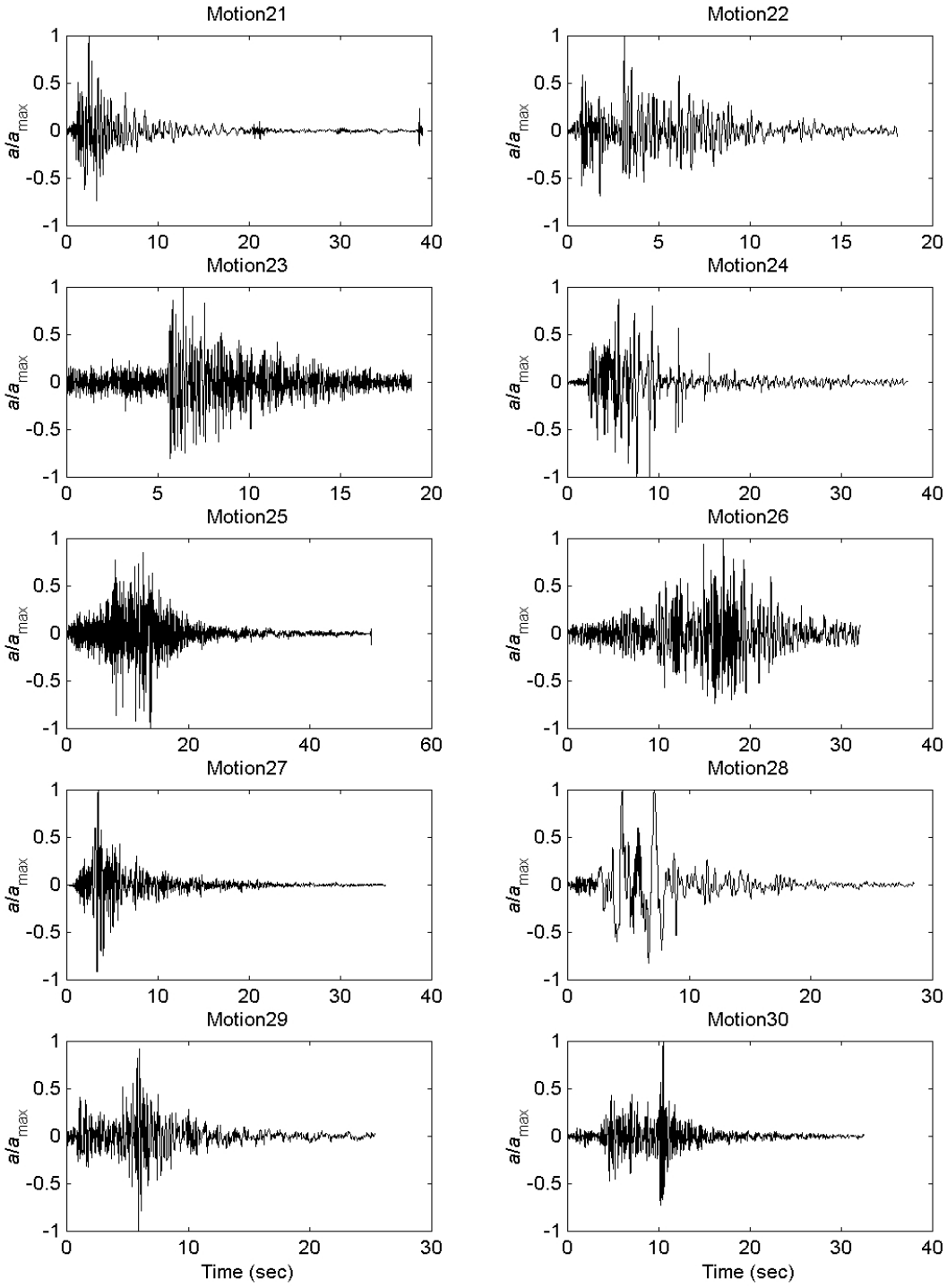

Figure A.3 Motions 21 through 30.

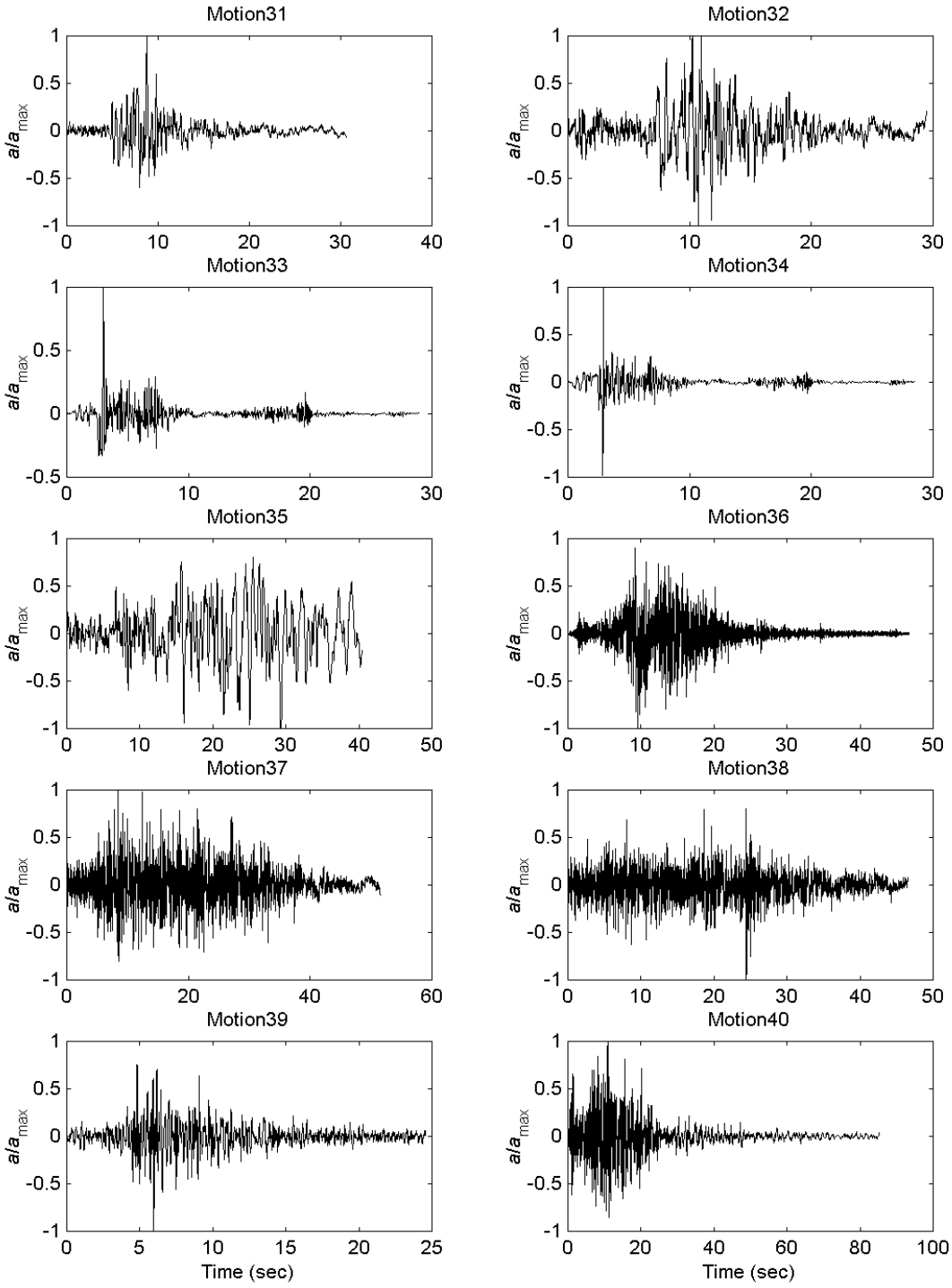

Figure A.4 Motions 31 through 40.

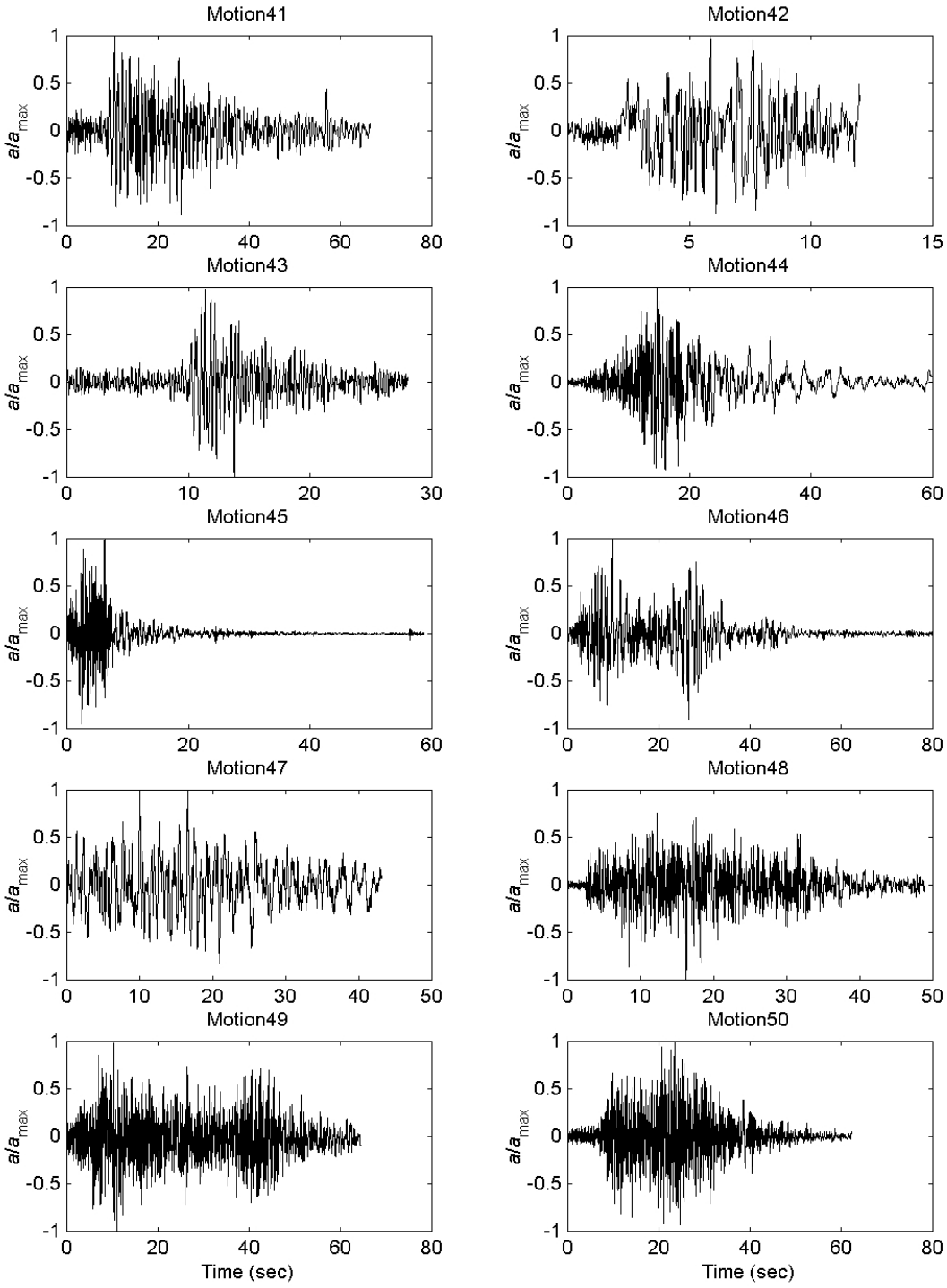

Figure A.5 Motions 41 through 50.

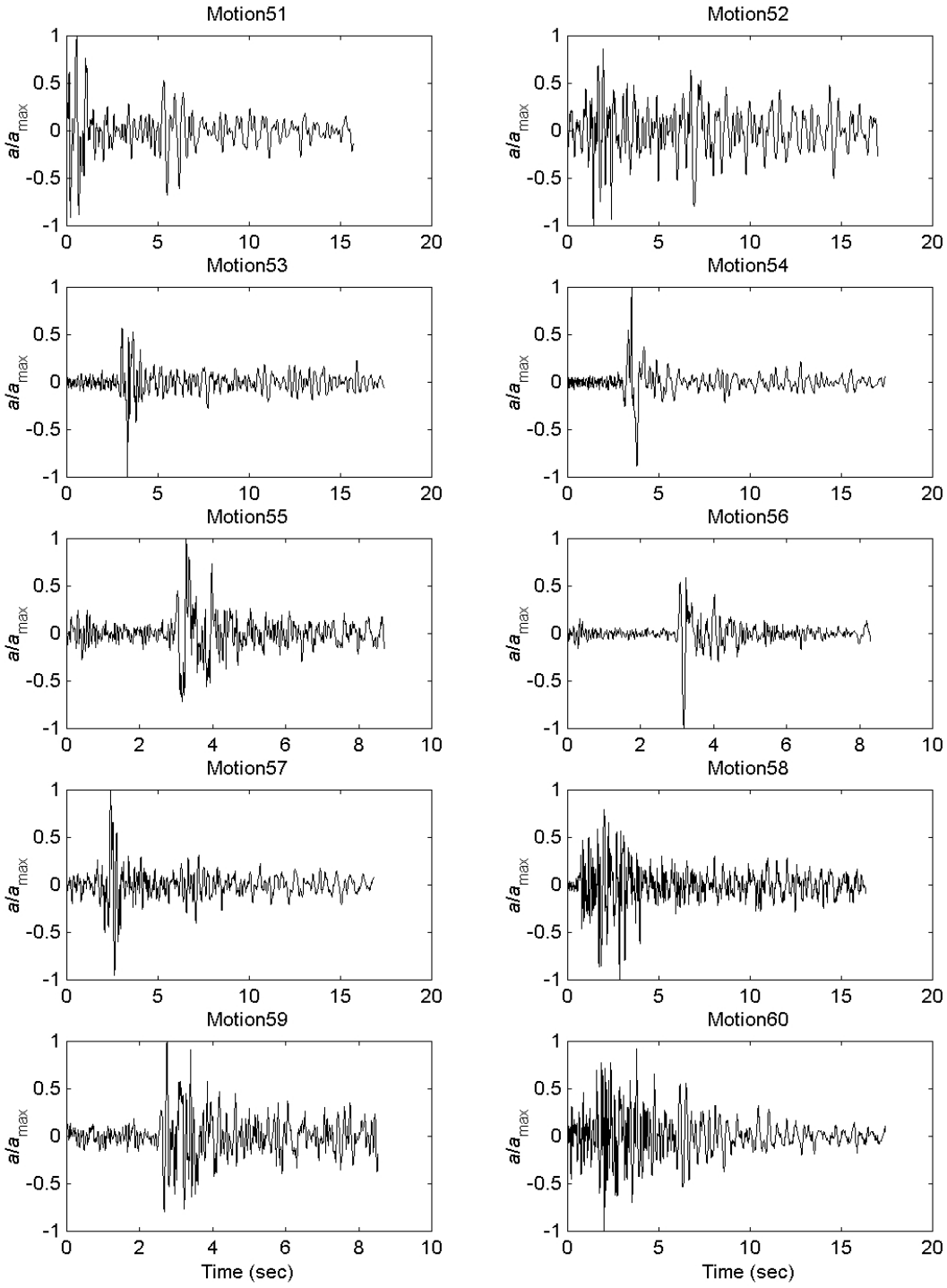

Figure A.6 Motions 51 through 60.

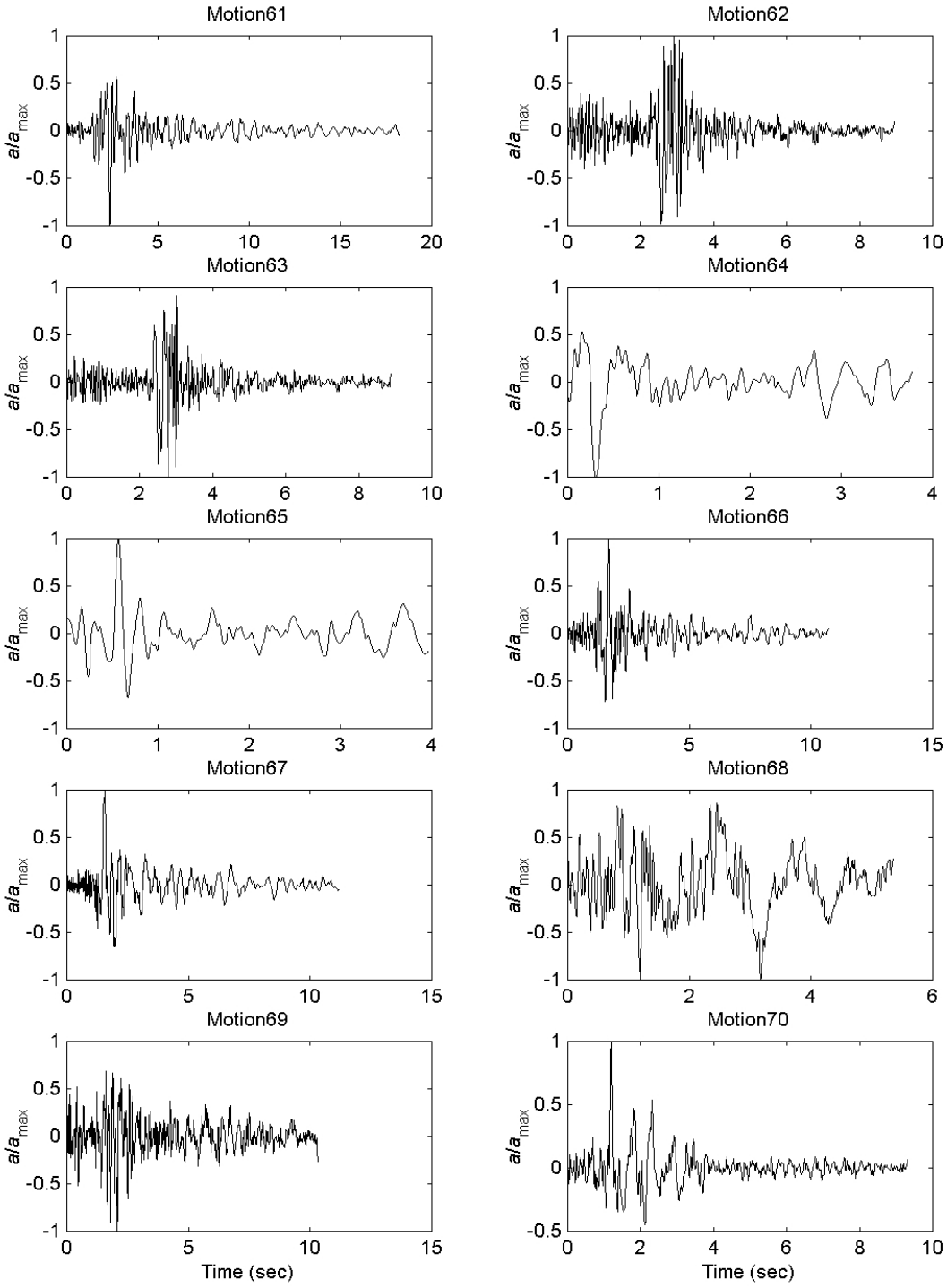

Figure A.7 Motions 61 through 70.

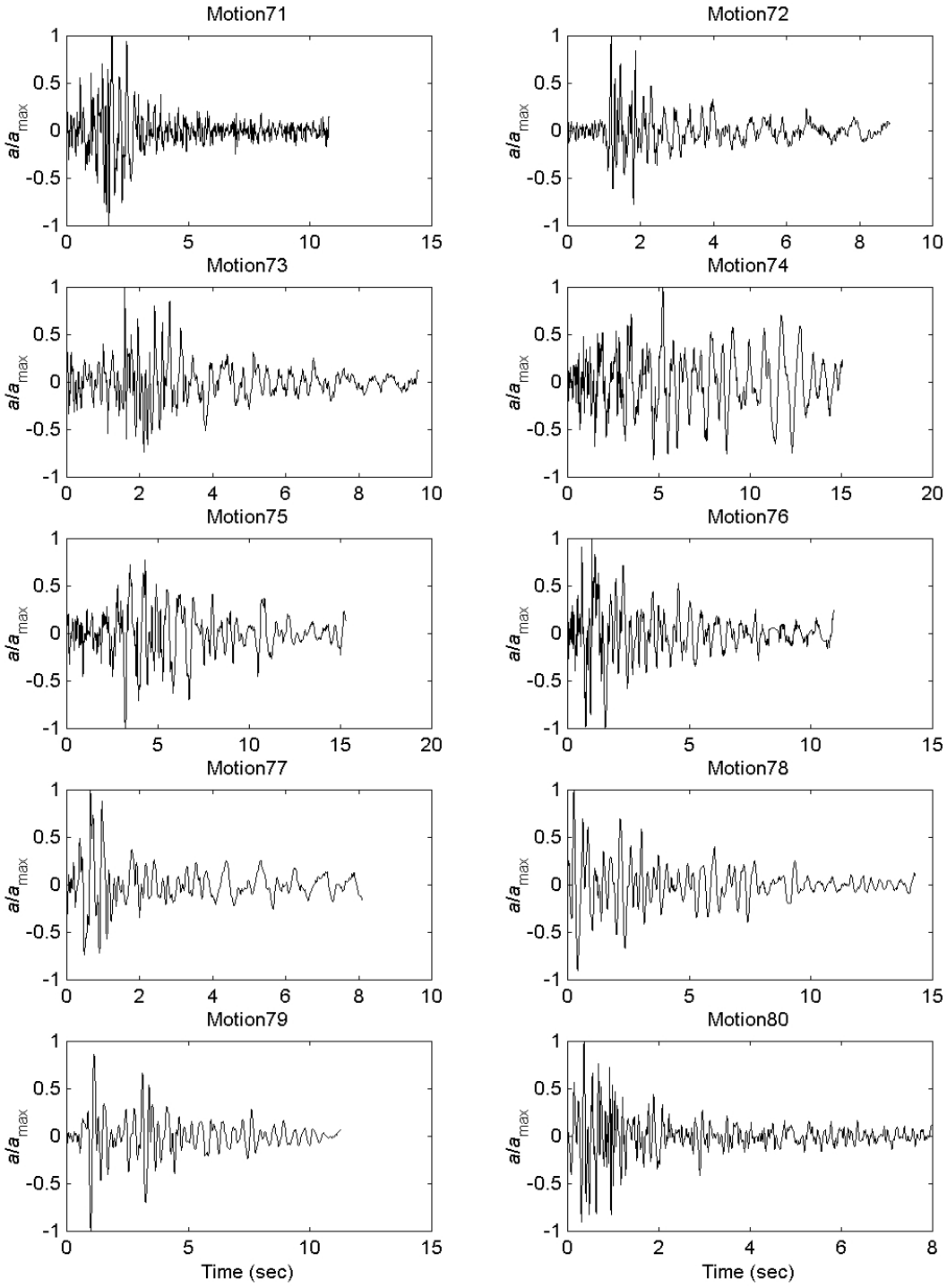

Figure A.8 Motions 71 through 80.

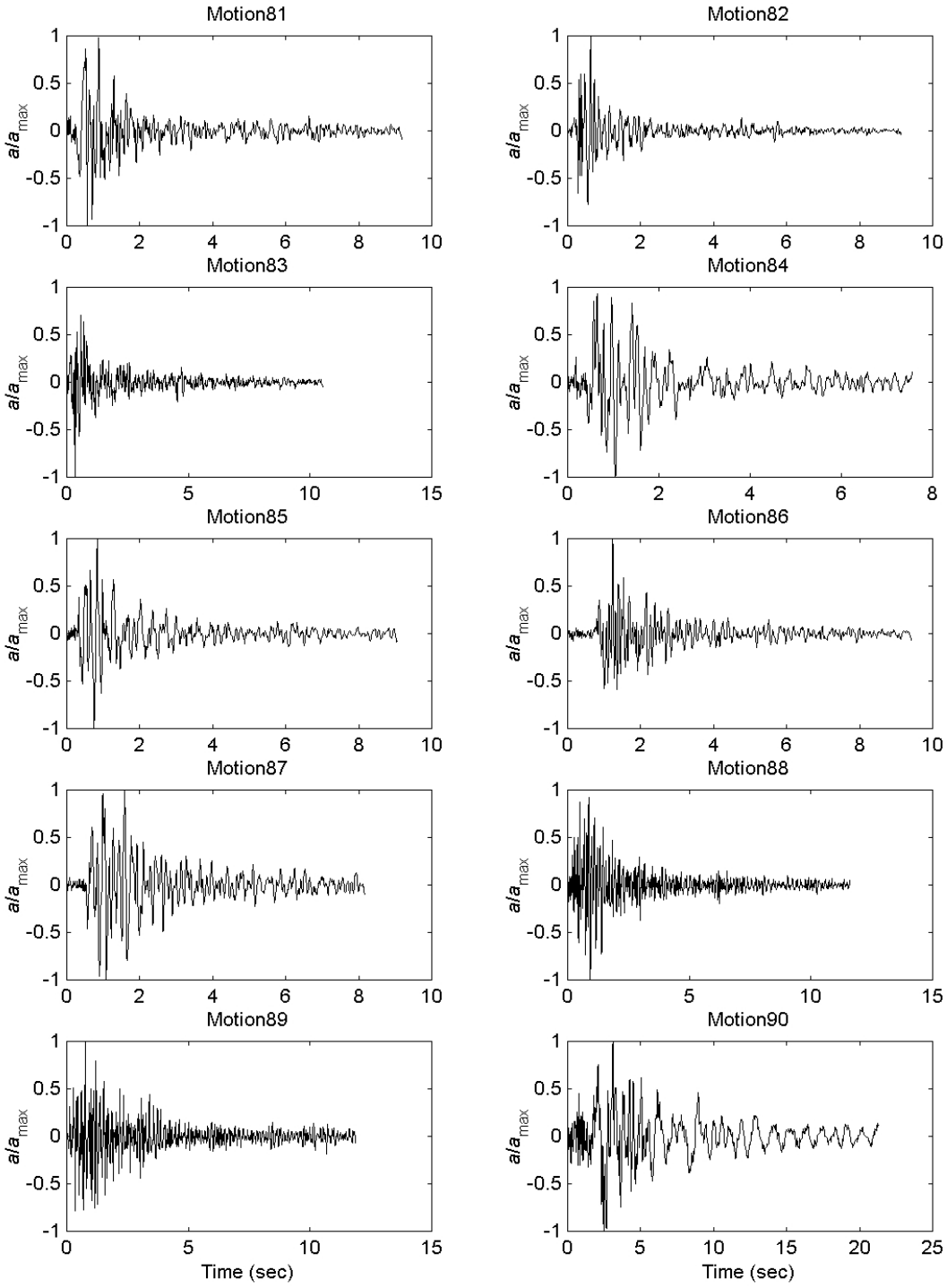

Figure A.9 Motions 81 through 90.

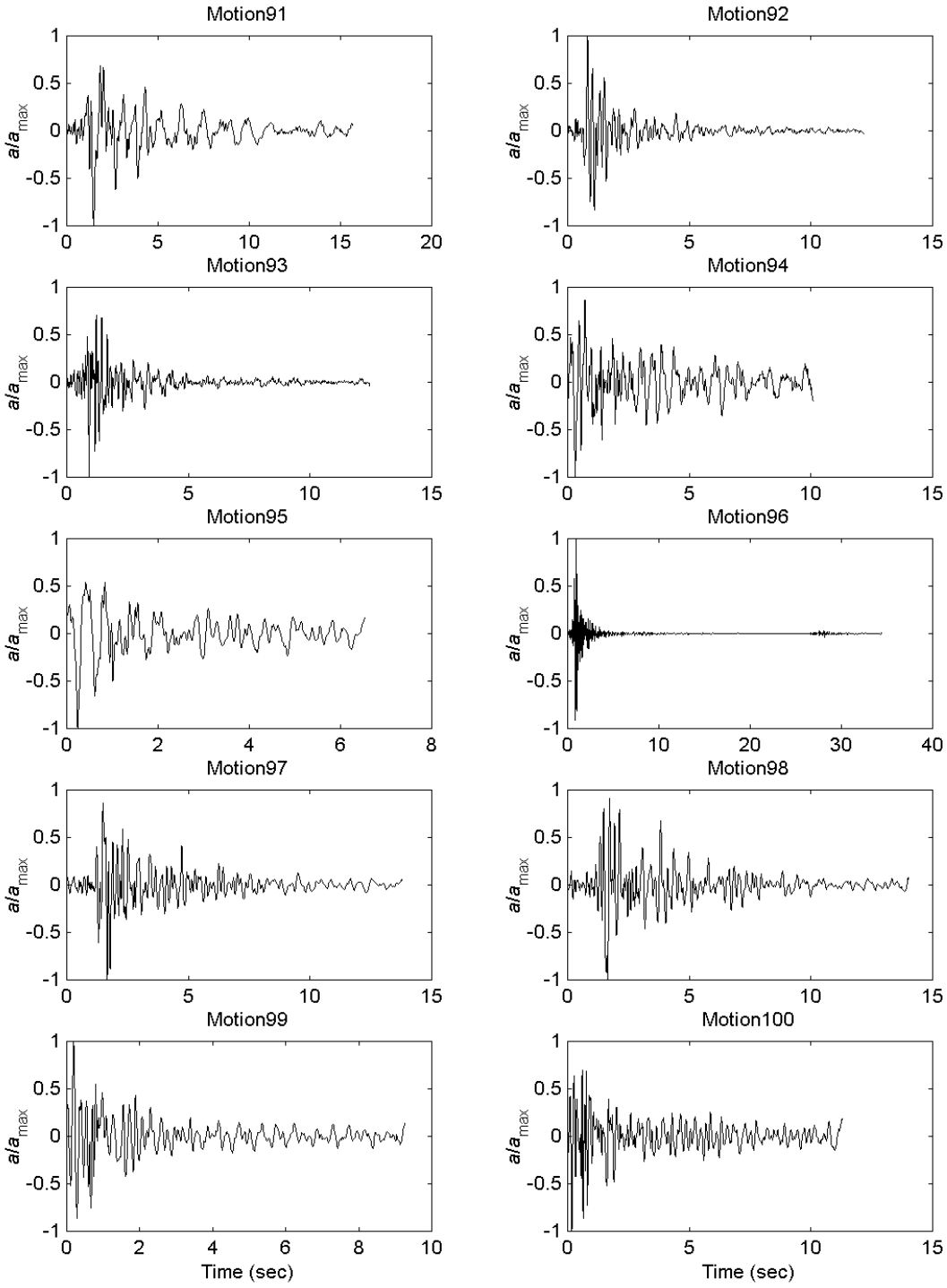

Figure A.10 Motions 91 through 100.

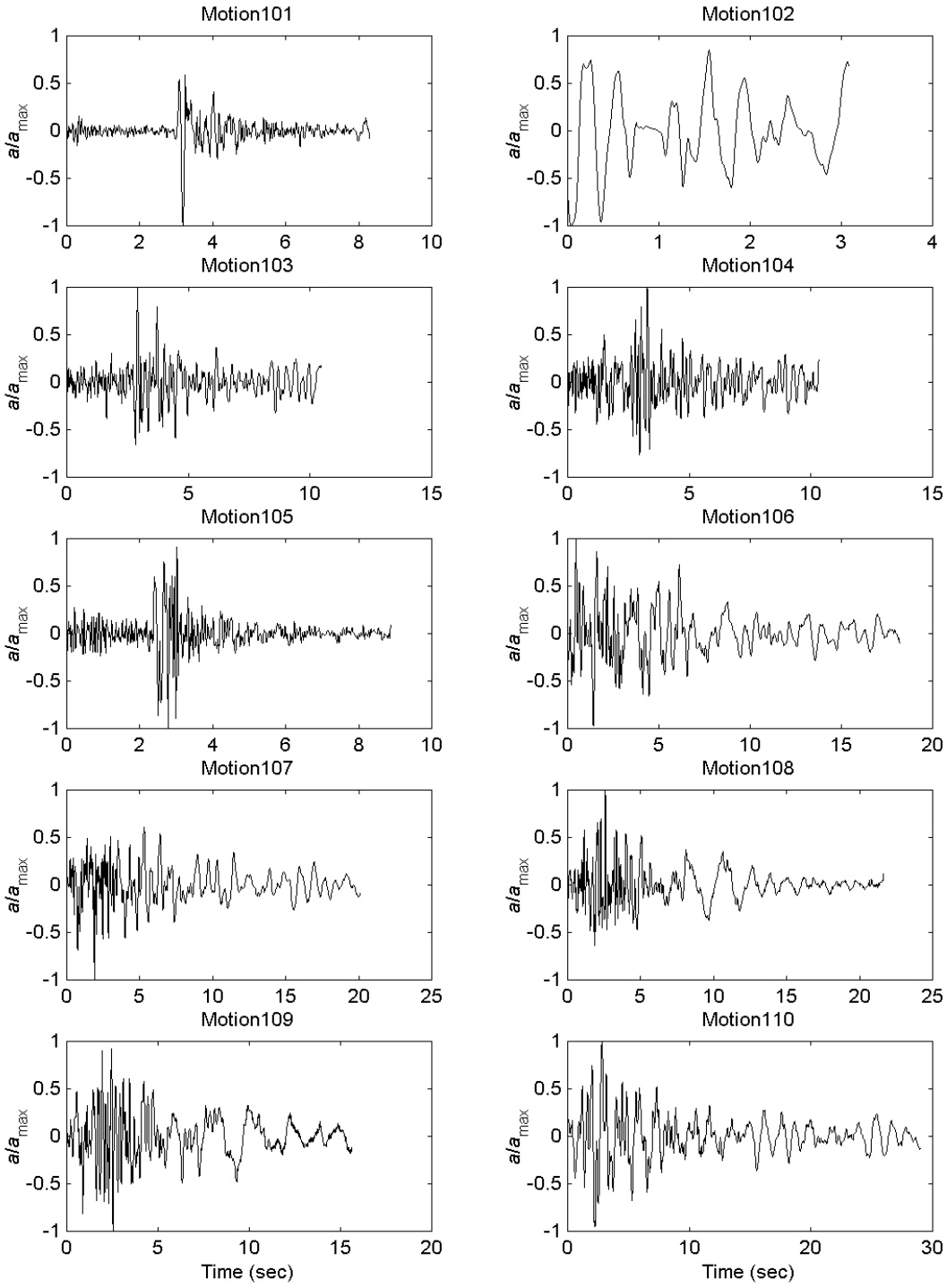

Figure A.11 Motions 101 through 110.

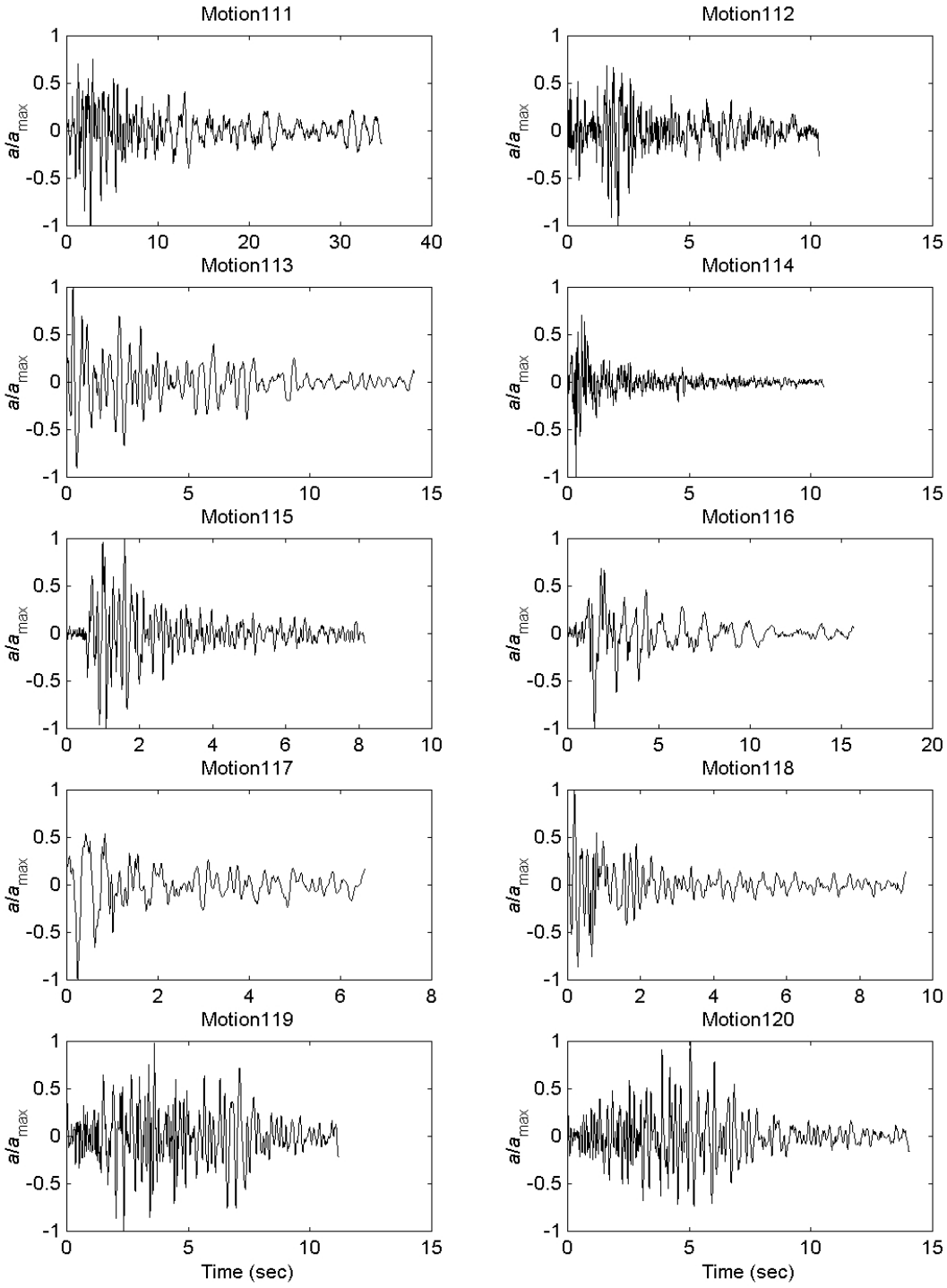

Figure A.12 Motions 111 through 120.

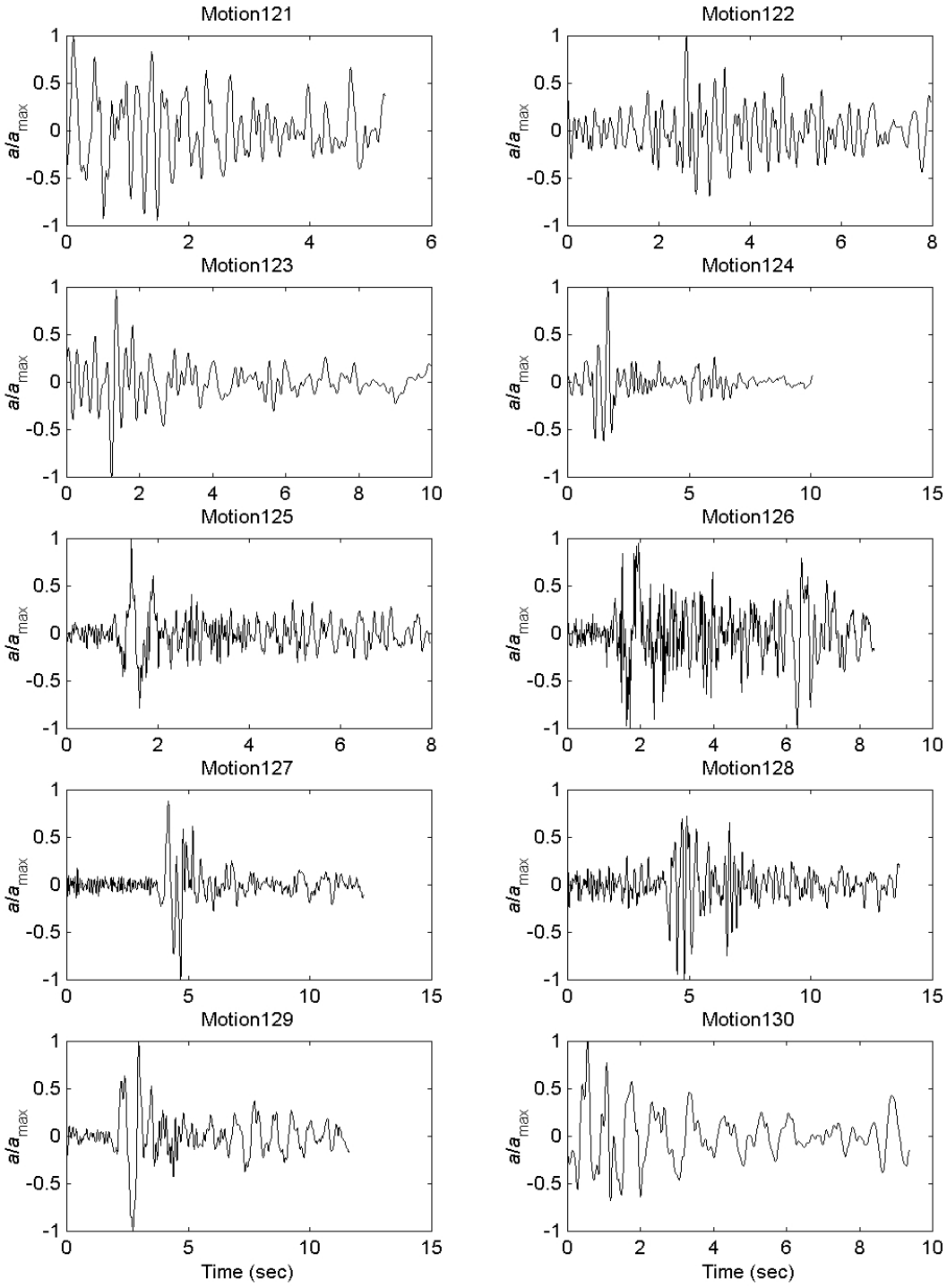

Figure A.13 Motions 121 through 130.

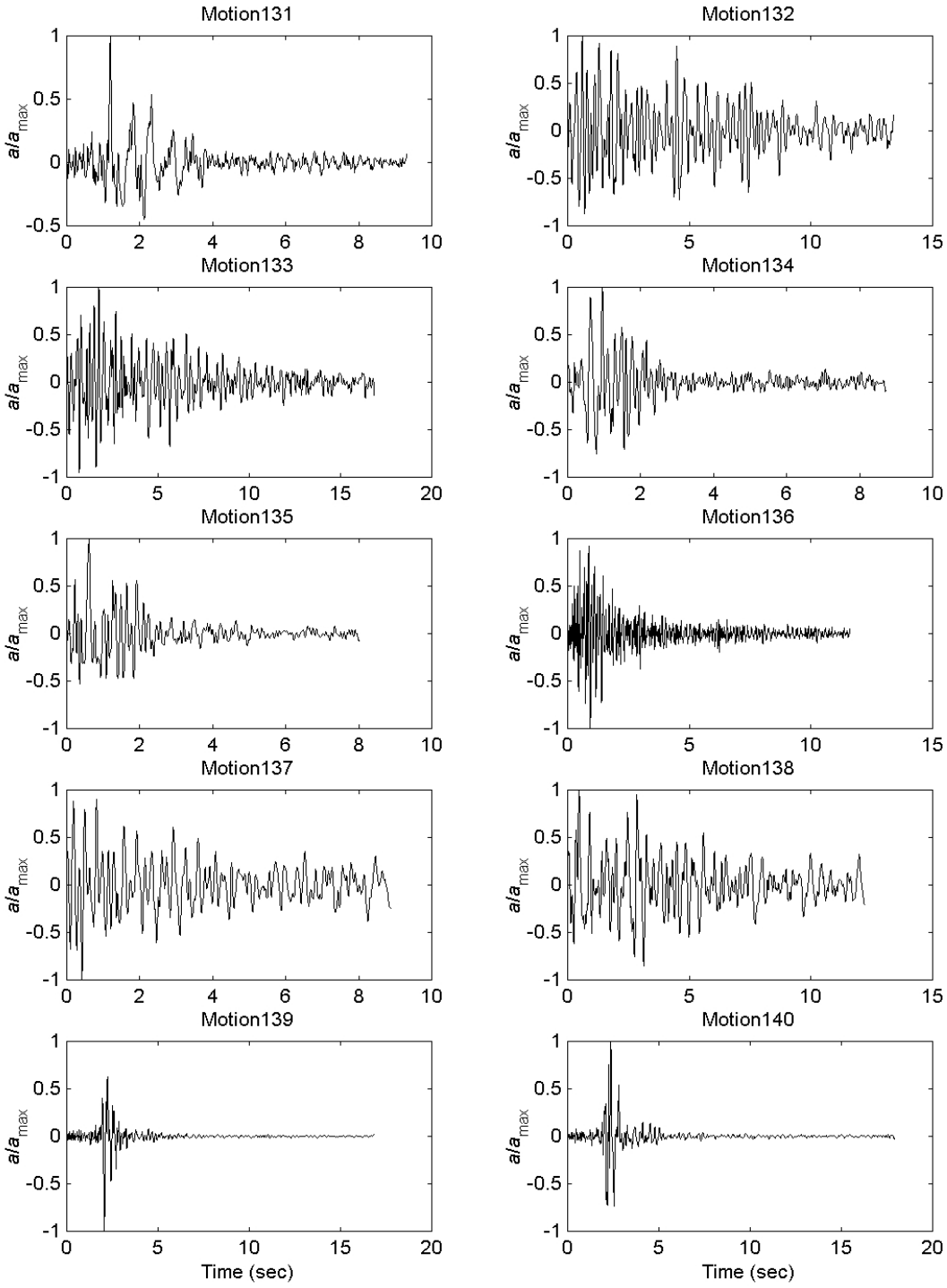

Figure A.14 Motions 131 through 140.

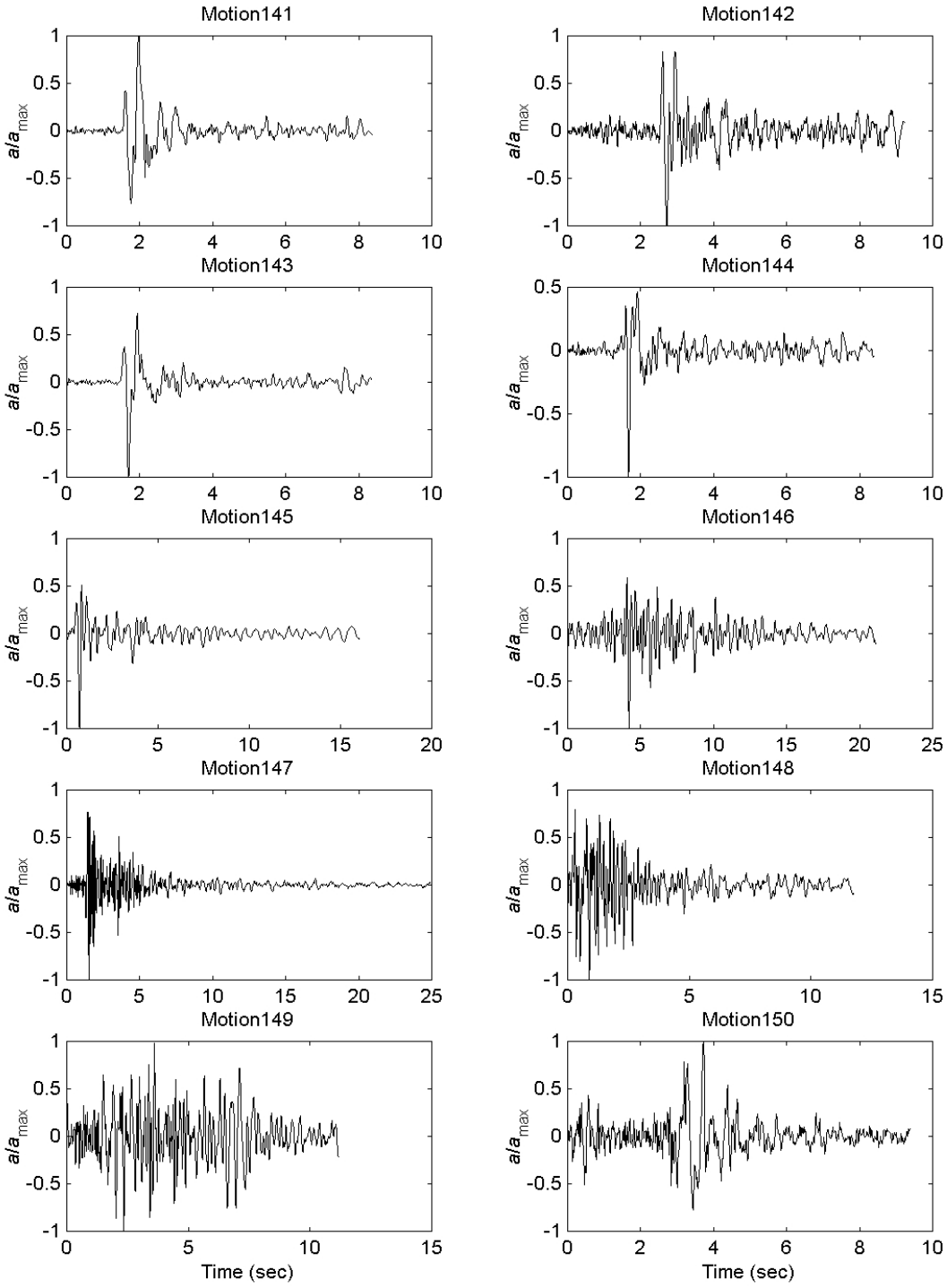

Figure A.15 Motions 141 through 150.

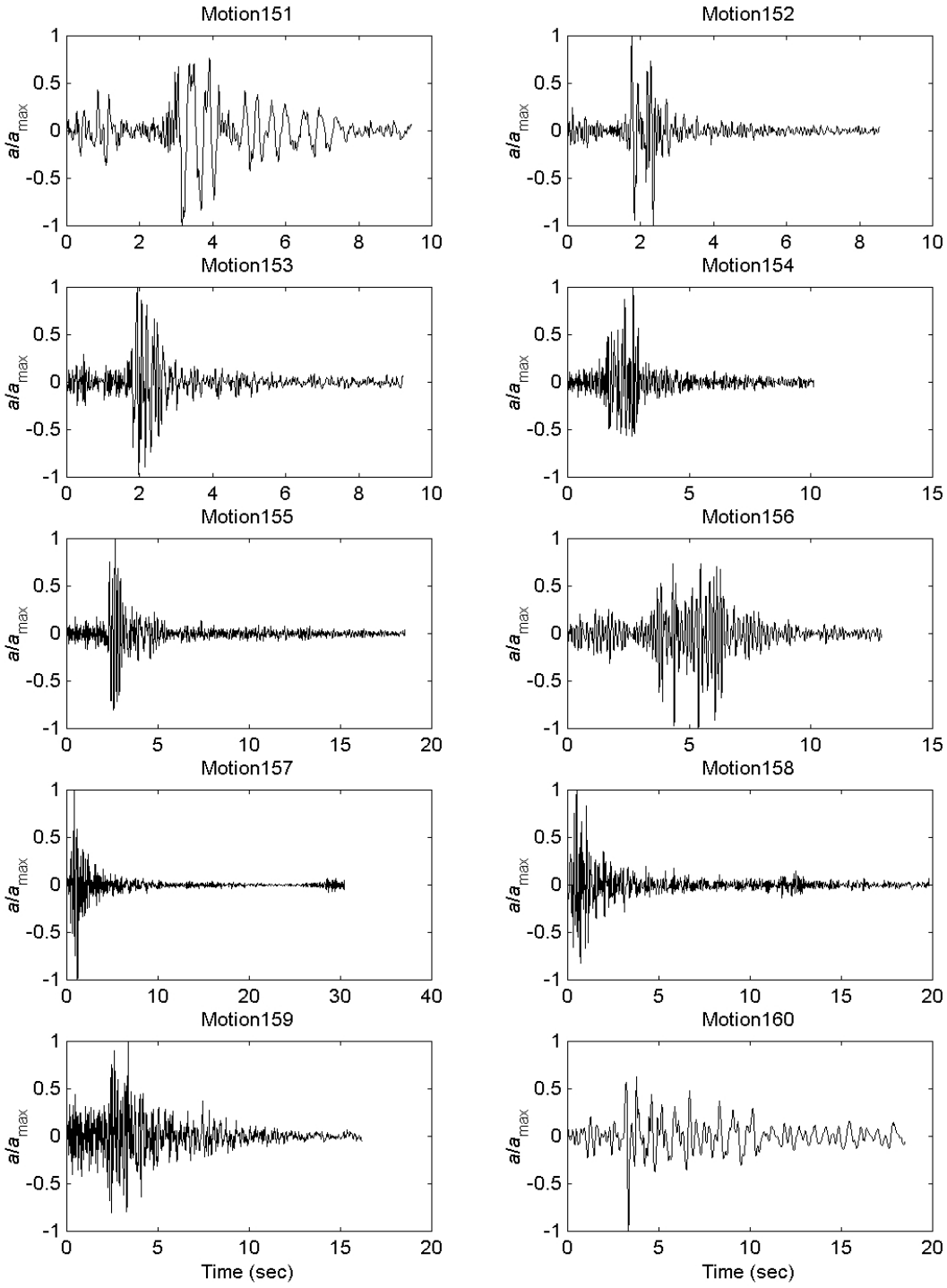

Figure A.16 Motions 151 through 160.

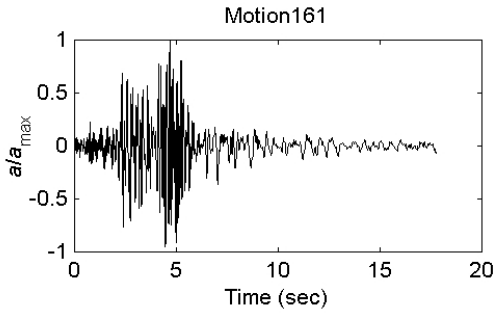

Figure A.17 Motion 161.

Appendix B

WAVE

Site response analyses were performed using one-dimensional, nonlinear, effective stress-based site response analyses as implemented in the computer program WAVE (Horne, 1996). WAVE uses a second-order accurate explicit finite difference scheme to compute the response of a horizontally layered soil deposit to vertically propagating shear waves.

The behavior of liquefiable soils is described in WAVE with the *UWsand* constitutive model (Kramer and Arduino, 1999; Arduino et al., 2001; 2002). The *UWsand* model is capable of representing the nonlinear, inelastic behavior of "typical" liquefiable sands, i.e., sands that behave in accordance with empirical observations of field liquefaction behavior. The *UWsand* model uses a Mohr-Coulomb yield function, a hardening rule that constrains nonlinearity to match that described by a particular modulus reduction curve (in this case, the Seed-Idriss upper bound curve (Seed and Idriss, 1970), the Cundall-Pyke hypothesis (Pyke, 1979) for determination of the plastic shear modulus upon stress reversal, and a non-associative flow rule that captures phase transformation behavior (i.e., alternative contractive-dilative response) at high stress ratios. *UWsand* was developed in a manner that would allow easy calibration – by combining empirical liquefaction resistance data (the *CRR* vs $(N_1)_{60}$ curves of Youd and Idriss (2001)) with a relationship between earthquake magnitude and equivalent numbers of cycles (Seed et al., 1975), the liquefaction curves shown as solid lines in Figure B.1 can be obtained. These curves, which are usually used to describe the pore pressure generation behavior of elements of liquefiable soil in laboratory (cyclic triaxial or cyclic simple shear) tests, can be interpreted as the apparent elemental behavior of typical liquefiable sands in the field. An advantage of this manner of expressing the liquefaction behavior is that it allows the pore pressure generation behavior to be characterized as a function of $(N_1)_{60}$. The *UWsand* model has been calibrated against these curves to produce pore pressure generation behavior that is consistent with that exhibited by typical

sands in past earthquakes; the *UWsand* predictions are shown as individual data points in Figure B.1. These results show that *UWsand* is capable of accurately predicting the onset of liquefaction exhibited by sands in the field.

To achieve its goal of describing the behavior of typical liquefiable sands with information that is commonly available to practicing geotechnical engineers, other parameters used in *UWsand* (e.g., maximum shear modulus, frictional angle, etc.) were also calibrated against $(N_1)_{60}$. While *UWsand* can be calibrated to match the behavior of individual liquefiable sands, it also has the option of being used to describe the behavior of typical sands, in which the only parameter required to describe the sand is $(N_1)_{60}$. When implemented into WAVE, the *UWsand* model has shown the ability to simulate liquefaction response that is consistent with field observations; more details on the development and validation of *UWsand* can be found in Arduino et al. (2002).

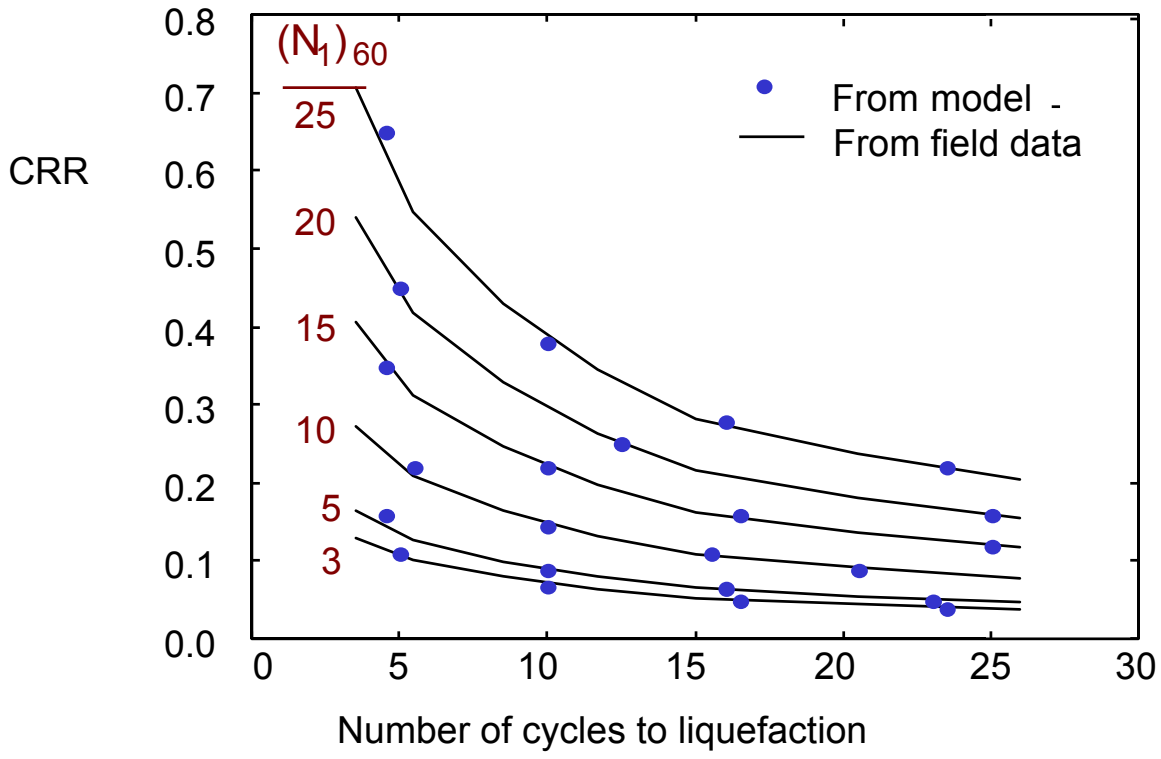

Figure B.1. Comparison of the number of cycles to liquefaction from field observations (solid lines) and *UWsand* model (discrete points).

Arduino, P., Kramer, S.L., and Baska D.B. (2002). “A practical constitutive model for typical liquefiable soils,” in preparation.

Horne, J.C., (1996), “Effects of liquefaction-induced lateral spreading on pile foundations,” Ph.D. Dissertation, University of Washington.

Kramer, S.L. and Arduino, P. (1999). “Constitutive modeling of cyclic mobility and implications for site response,” Earthquake Geotechnical Engineering, P. Seco e Pinto, ed., A.A. Balkema, Rotterdam, Vol. 3, pp. 1029-1034.

Seed, H.B. and Idriss, I.M. (1970). "Soil moduli and damping factors for dynamic response analyses," *Report No. EERC 70-10*, Earthquake Engineering Research Center, University of California, Berkeley.

Seed, H. B., Idriss, I. M., Makdisi, F., and Banerjee, N. (1975) "Representation of Irregular Stress Time Histories by Equivalent Uniform Stress Series in Liquefaction Analyses," EERC 75-29, Earthquake Engrg. Res. Ctr., Univ. of Calif., Berkeley.

Pyke, R.M. (1979). "Nonlinear soil models for irregular cyclic loadings," *Journal of the Geotechnical Engineering Division*, ASCE, Vol. 105, No. GT6, pp. 715-726.

Youd., T.L. and Idriss, I.M. (2001). “Liquefaction resistance of soils: Summary report from the 1996 NCEER and 1998 NCEER/NSF workshops on evaluation of liquefaction resistance of soils,” Journal of Geotechnical and Geoenvironmental Engineering. Vol. 127, No.4, pp 297-313.